

USING SOIL MOISTURE TRENDS
ACROSS TOPOGRAPHIC GRADIENTS
TO EXAMINE CONTROLS
ON SEMI-ARID ECOSYSTEM DYNAMICS

By

Toni Jo Smith

A thesis

submitted in partial fulfillment

of the requirements for the degree of

Master of Science in Hydrologic Sciences

Boise State University

May 2010

BOISE STATE UNIVERSITY GRADUATE COLLEGE

DEFENSE COMMITTEE AND FINAL READING APPROVALS

of the thesis submitted by

Toni Jo Smith

Thesis Title: Using Soil Moisture Trends Across Topographic Gradients to Examine Controls on Semi-arid Ecosystem Dynamics

Date of Final Oral Examination: 09 April 2010

The following individuals read and discussed the thesis submitted by student Toni Jo Smith, and they evaluated her presentation and response to questions during the final oral examination. They found that the student passed the final oral examination.

Shawn G. Benner, Ph.D. Chair, Supervisory Committee

Alejandro N. Flores, Ph.D. Member, Supervisory Committee

Molly M. Gribb, Ph.D. Member, Supervisory Committee

James P. McNamara, Ph.D. Member, Supervisory Committee

The final reading approval of the thesis was granted by Shawn G. Benner, Ph.D., Chair of the Supervisory Committee. The thesis was approved for the Graduate College by John R. Pelton, Ph.D., Dean of the Graduate College.

ACKNOWLEDGEMENTS

The author wishes to gratefully acknowledge the National Science Foundation, Decagon Devices, Inc., ExxonMobil Corporation, and the Geological Society of America for their generous support of this research. Genuine thanks to my thesis Supervisory Committee: Dr. Shawn Benner, Dr. Alejandro Flores, Dr. Molly Gribb, and Dr. James McNamara. Thank you to Dr. Nancy Glenn for your tireless guidance with the remote sensing work. Sincere thanks also go to the many people who offered thoughtful and patient counsel, support, and grueling physical assistance in the realization of this project: Pamela Aishlin, Montague Busbee, David Eiriksson, Chantell Everitt, Dr. Alejandro Flores, Ivan Geroy, Dr. Molly Gribb, Brian Hanson, Dr.-to-be Melvin Kunkel, Dr. James McNamara, Benjamin McVeigh, Daniella Morgos, Dr. Jennifer Pierce, Dr. Mark Seyfried, Nicholas Sutfin, and Ashley Zumwalt. Thanks to Dr. Karen Viskupic, Dr. David Wilkins, Cindy Busche and Christina Rivas for your enthusiasm, encouragement and guidance in my personal and professional development, particularly through the GK-12 program. Dr. Benner, you have been the most incredible advisor imaginable, and I am truly grateful for your patience, wisdom, care and commitment. I would also like to deeply thank my family for inspiring me to work conscientiously and live honestly. Your unyielding faith and love gives me the courage to keep trying as hard as I can.

ABSTRACT

This study investigated controls on soil water storage and its effect on vegetation cover in a semi-arid, mountainous environment characterized by warm-dry summers and wet-cold winters. Soil moisture and soil temperature were monitored over 286 days at eight sites spanning four elevations (approx. 1100, 1300, 1500, and 1800 m asl), and paired north and south exposures. These sites span an ecological gradient from grass and shrub land to conifer forest. Measurements of soil texture, soil depth, vegetation cover (normalized difference vegetation index, NDVI), and soil carbon content were made at the same sites. Variables that strongly influence the soil water distribution are topographically-driven and include: mean annual precipitation, which increases by a factor of 1.8, and mean annual temperature, which increases by a factor of 1.5, over the 700 m elevation increase; potential insolation, which is 1.5 to 1.9 times higher from north to south aspect, and by 1.1 to 1.4 times over the elevation gradient on north and south aspects, respectively; and soil depth, which is 1.1 to 2.3 times greater on a north aspect than south aspect at a given elevation, and is 1.4 to 2.3 times greater at higher relative to lower elevations on north and south aspects, respectively. North aspects store from 1.1 to 3.7 times as much water as south aspects at a given elevation, and higher elevations store up to 3 times more water than the lowest elevations at a given aspect; these trends are dictated by both higher average water content and deeper soils on higher elevations and on north facing slopes. Overall, soils are shallow, ranging from 34 to 92 cm deep and underlain by granodioritic bedrock. Due to the shallow profile and coarse texture of study

area soils, 6 to 16 cm of water infiltrated into dry soil can exceed the storage capacity and may be lost to vertical or lateral redistribution in one to four weeks. Filling of the soil water reservoir, as indicated by whole-profile hydraulic connectivity and attainment of field capacity at the soil-bedrock interface, was observed at all sites in response to both winter and spring precipitation, with north aspects and higher elevations experiencing longer periods of deep wetting.

Vegetation cover is typically greater on north relative to south aspects, and generally increases with increasing elevation. Maximum (peak) seasonal NDVI values are reached as much as seven weeks earlier on south aspects at a given elevation, and as much as 12 weeks earlier at lower elevations compared to higher elevations. North-facing soils hold 3.5 to 4.2 times as much organic carbon as south-facing soils at all but the highest elevation forested sites, where the south and north aspect soil carbon contents were similar. Both vegetation cover and soil carbon content are largest at sites that retain moisture for a longer portion of the summer period, consistent with a water limited ecosystem. The duration of wet soil conditions during the summer, when vegetation production peaks, is strongly influenced by the magnitude and duration of spring and summer precipitation. These observations suggest that vegetation productivity and soil carbon storage in this environment will be particularly sensitive to climatic changes that alter spring and summer precipitation, which is delivered near, or during, the growing season. In contrast, the ecosystem may be less sensitive to changes in the magnitude of winter precipitation, which recharges the relatively small soil reservoir in the winter

season and is generally lost from the soil early into the spring when productivity is depressed by lower temperatures and low insolation.

TABLE OF CONTENTS

ACKNOWLEDGEMENTS	iv
ABSTRACT	v
LIST OF TABLES	xi
LIST OF FIGURES	xiv
1. INTRODUCTION	1
2. STUDY AREA: THE DRY CREEK EXPERIMENTAL WATERSHED.....	9
3. METHODS	14
3.1. Soil Water and Soil Temperature.....	14
3.1.1. Soil Volumetric Water Content, Soil Temperature, Soil Depth	14
3.1.2 Soil Water Storage	18
3.1.3. Duration of Snow Cover	18
3.1.4. Soil Matric Potential	19
3.1.5. Approximate Wilting Point.....	21
3.1.6. Field Capacity	21
3.1.7. Storage Capacity	23
3.2. Potential Growing Season.....	23
3.3. Vegetation Distribution.....	24
3.3.1. Plant Area Index	24

3.3.2. Normalized Difference Vegetation Index.....	27
3.4. Soil Properties.....	29
3.5. Soil Carbon.....	31
4. RESULTS.....	33
4.1. Soil Water and Soil Temperature.....	33
4.2. Vegetation Distribution.....	39
4.3. Soil Properties.....	41
4.4. Soil Carbon Content.....	44
5. DISCUSSION.....	45
5.1. Water Balance.....	45
5.2. Implications for Ecologic Functioning and Carbon Cycling.....	47
6. Conclusions.....	58
REFERENCES.....	60
APPENDIX A.....	75
Tables	
APPENDIX B.....	92
Figures	
APPENDIX C.....	128
Protocol for Plant Area Index Sampling and Data Processing	
APPENDIX D.....	138
Protocol for NDVI Data Assembly and Processing	
APPENDIX E.....	144

Methodology for Particle Size Analysis by Sieving and Laser Diffraction	
APPENDIX F.....	151
Protocol for Preparation of Soil Samples for Analysis of Carbon Content	
APPENDIX G.....	154
Soil Texture Results by Laser Diffraction and Hydrometer/Sieve Conversion	
Methods	
APPENDIX H.....	167
Time Series of Soil Moisture and Soil Temperature at 10-minute Sampling	
Intervals	
APPENDIX I	176
Site-by-Site Description of Soil Moisture and Soil Temperature Observations	

LIST OF TABLES

Table A.1. Basic attributes and locations of soil moisture measurement stations. UTM coordinates are from Zone 11 N, in datum NAD83.....	76
Table A.2. Water contents associated with wilting point matric potential (-3 MPa), as well as field capacity water contents determined: a) using field data, and b) estimated from an assumed matric potential (-0.03 MPa) for each site. Also provided are parameter values used in determining water contents associated with matric potentials for each soil class. Parameters from Clapp et al. 1978 and Laio et al. 2001. Symbol Φ represents porosity and θ represents water content.	78
Table A.3. Important dates and values of soil water content, soil temperature, soil water storage, spatial variability, snow cover, and growing season initiation and end. Mean values derived from period of record common to all sites, 11/20/2008 to 9/1/2009; other values taken from entire measurement period.	79
Table A.4. Depth of soil to bedrock as measured in each pit dug for installation of soil moisture and temperature sensors. Bedrock was treated as the gravelly decomposed granite layer which was unsuitable for sensor installation.	83
Table A.5. Results of paired laser diffraction (A) and mechanical (hydrometer/sieve) analyses (B) used to develop a linear correlation to approximate mechanical results from laser diffraction results.	84

Table A.6. Bulk density approximations from soil samples. Site MLN, sample set “a” was excluded due to sampling error. Samples at the 0-5cm bgs interval are not believed to be reliable and are excluded. 86

Table A.7. Total carbon content of soil as percent by weight for intervals 0-5 cm (“5”), 5-10 cm (“10”), 10-15 cm (“15”), 15-20 cm (“20”), 20-25 cm (“25”), and 25-30 cm (“30”) bgs. Values reported are the averaged results of 2 field replicates and random lab replicates; replicates deviate less than 8% from the reported values. 88

Table A.8. Total carbon content in the upper 30 cm of soil at all sites. Values reported are the averaged results of 2 field replicates and random lab replicates; replicates deviate less than 8% from the reported values. 89

Table A.9. Values of the coefficient of determination (R^2) representing the degree to which variation in one variable is explained by another variable. Of the variables, “peak NDVI” was selected from monthly averages derived over a four year period; “soil carbon” was measured as total soil carbon in the uppermost 30 cm of the profile; mean soil water content, soil water storage, and soil temperature were calculated from the common period of record, 11/20/2008 to 9/1/2009; mean annual precipitation and mean annual air temperature were calculated based on elevation using the linear hypsometric relationship observed in the study area; and potential insolation was modeled as total annual insolation..... 90

Table A.10. Results of forward selection multiple regression analysis treating elevation (associated with gradients in precipitation and air temperature) and potential insolation as

independent variables, and treating soil carbon, peak NDVI, and mean soil water storage
as dependent variables. 91

LIST OF FIGURES

- Figure B.1. The Dry Creek Experimental Watershed study area, including study sites and meteorological (weather) stations. Ecological differences across topographic gradients are evident from lowest to highest elevations (lower left to upper right), and from south-facing to north-facing slopes at middle elevations (as at sites MHS and MHN). Aerial image courtesy of the National Agriculture Imagery Program (NAIP) 2004..... 93
- Figure B.2. Seasonal and topographic trends in precipitation and temperature at Dry Creek Experimental Watershed. Temperature as nine-year average at three meteorological stations (top) and precipitation as nine-year average at the same meteorological stations (bottom). Precipitation and temperature are out-of-phase in this environment. Higher elevations experience overall lower temperatures and greater precipitation. 94
- Figure B.3. Orographic trend of higher precipitation and lower temperature with increasing elevation in the study area. Values are nine-year average total annual precipitation and nine-year average annual mean temperature. Mean annual precipitation and mean annual temperature for each of the study sites were derived from the hypsometric equations shown. 95
- Figure B.4. Nine-year average seasonal precipitation compared with precipitation during the 2008-2009 season of study. During an average year, most of the annual

precipitation falls during the autumn and winter months (Oct-Mar) and the summer (Jun-Sep) is dry. During the 2008-2009 period of study, winter precipitation was relatively low, spring rains were relatively high, and the dry summer was punctuated by a large rain event in August..... 95

Figure B.5. Distribution of potential incident solar radiation (insolation) over the study area, modeled using the ArcGIS Solar Radiation tool. Values are total potential insolation modeled over the 2008 year, but they reflect the general distribution of potential insolation in any year. At a given elevation, a south-facing slope may receive nearly twice as much potential insolation as a complimentary north-facing slope..... 96

Figure B.6. Modeled values of total annual potential insolation at the study sites (squares and circles), with measured values from weather stations (diamonds) in the study area. The measured total annual potential insolation values confirm that the modeled values are realistic. Potential insolation increases slightly with increasing elevation, but the potential insolation difference across the aspect gradient is much larger than the difference across the elevation gradient..... 97

Figure B.7. Time series of mean daily temperature and total daily insolation measured from a weather station located at 1610 m elevation in the study area. Peak insolation occurs during the midsummer, around July. Air temperature lags slightly, reaching its peak around July to August. 97

Figure B.8. Modeled (potential) insolation relates positively with mean annual precipitation and negatively with mean annual temperature in the study area. The amount of radiation received is distinctly different for north and south aspects (north aspects receive much less radiation than south aspects).
..... 98

Figure B.9. Configuration of soil moisture stations and soil pits in this study. Each site is composed of four soil pits which are treated as replicates representing soil moisture and soil temperature at each site. In turn, each pit contains soil moisture and temperature sensors located at 2 cm, 15 cm, and 30 cm below ground surface. Most pits contain a fourth sensor located above the soil-bedrock interface, but at two sites (MLS and LS) soil was generally only about 30 cm deep..... 99

Figure B.10. General configuration of Plant Area Index (PAI) sampling transects at each soil moisture station. Three transects of 11 sampling points each were positioned around each station, allowing repeated measurement of 33 sample points per station during the 2009 growing season..... 99

Figure B.11. Basic distributions of soil water content (top) and soil temperature (bottom) time series over the common measurement period, 11/20/2008 to 9/1/2009. Sample sizes are $n = 286$ days for each site. The height of the boxplots represents variation in time. The separation of box plots suggests that overall, growing season soil moisture and soil temperature differ with aspect and, to a lesser degree, with elevation. An exception is soil

temperature at the highest elevation sites, which does not appear to differ significantly with aspect. 100

Figure B.12. Soil water content (top) and soil temperature (bottom) at the high elevation north facing (HN) and high elevation south-facing (HS) sites as profile- and site-averaged values. Error bars represent spatial variability as the standard deviation of profile-averaged values among the four pits at each site. Precipitation events (rain and snow) are plotted in the center graph. Dates of snow cover, inferred from dampened diurnal fluctuations in shallow soil temperature, are shown at top of the temperature plot. Dates of initial snow cover (marked by bold vertical dashes) are uncertain because the temperature trends may reflect snow cover or soil freezing, but dates of snow cover cessation are more certain. The north aspect has somewhat higher soil moisture, slightly lower soil temperature, and a slightly later snowmelt date than the south aspect. 101

Figure B.13. Soil water content (top) and soil temperature (bottom) at the mid-high elevation north facing (MHN) and mid-high elevation south-facing (MHS) sites as profile- and site-averaged values. Error bars represent spatial variability as the standard deviation of profile-averaged values among the four pits at each site. Precipitation events (rain and snow) are plotted in the center graph. Dates of snow cover, inferred from dampened diurnal fluctuations in shallow soil temperature, are shown at top of the temperature plot. Dates of initial snow cover (marked by bold vertical dashes) are

uncertain because the temperature trends may reflect snow cover or soil freezing, but dates of snow cover cessation are more certain. The north aspect generally has higher growing-season soil moisture, lower soil temperature, and a later snowmelt date than the south aspect..... 102

Figure B.14. Soil water content (top) and soil temperature (bottom) at the mid-low elevation north facing (MLN) and mid-low elevation south-facing (MLS) sites as profile- and site-averaged values. Error bars represent spatial variability as the standard deviation of profile-averaged values among the four pits at each site. Precipitation events (rain and snow) are plotted in the center graph. Dates of snow cover, inferred from dampened diurnal fluctuations in shallow soil temperature, are shown at top of the temperature plot. Dates of initial snow cover (marked by bold vertical dashes) are uncertain because the temperature trends may reflect snow cover or soil freezing, but dates of snow cover cessation are more certain. The north aspect generally has higher growing-season soil moisture, lower soil temperature, and a later snowmelt date than the south aspect..... 103

Figure B.15. Soil moisture (top) and soil temperature (bottom) at the low elevation north facing (LN) and low elevation south-facing (LS) sites as profile- and site-averaged values. Error bars represent spatial variability as the standard deviation of profile-averaged values among the four pits at each site. Precipitation events (rain and snow) are plotted in the center graph. Dates of snow cover, inferred from dampened diurnal fluctuations in shallow soil

temperature, are shown at top of the temperature plot. Dates of initial snow cover (marked by bold vertical dashes) are uncertain because the temperature trends may reflect snow cover or soil freezing, but dates of snow cover cessation are more certain. The north aspect generally has higher growing-season soil moisture, lower soil temperature, and a later snowmelt date than the south aspect. 104

Figure B.16. Relationship between elevation and soil temperature at all sites, with means calculated from the common period of measurement, 11/20/2008 to 9/1/2009. Soil temperature shows a strong relationship with elevation at both aspects. 105

Figure B.17. Soil temperature measured at 2 cm bgs closely tracks trends in spring, summer, and fall air temperatures over 2009 where a study site and a meteorological station are collocated. 105

Figure B.18. Differences in soil depth with aspect and elevation. Error bars show standard deviation of soil depths among the four pits at each site. At all but the highest elevation sites, soils are deeper on north aspects than on south aspects, and soil depth increases with elevation. 106

Figure B.19. Distributions of soil water stored in the profile over the common measurement period, 11/20/2008 to 9/1/2009. Sample size is $n = 286$ days at each site. The soil water storage calculation accounts for generally greater soil depths on north aspects and higher elevations. 106

Figure B.20. Relationship between elevation and mean soil water storage at all sites, with means calculated from the common period of measurement, 11/20/2008 to 9/1/2009. By accounting for generally increasing soil depth at increasing elevations, soil water storage values show a stronger relationship with elevation on south aspects than did soil water content..... 107

Figure B.21. Soil water content at different depths in the soil profile at site HN, the highest elevation north aspect. The green line indicates field capacity and orange line indicates approximate wilting point for the soil. 108

Figure B.22. Soil water content at different depths in the soil profile at site HS, the highest elevation south aspect. Green line indicates field capacity and orange line indicates approximate wilting point for the soil. 109

Figure B.23. Soil water content at different depths in the soil profile at site MHN, the mid-high elevation north aspect. Green line indicates field capacity and orange line indicates approximate wilting point for the soil. 110

Figure B.24. Soil water content at different depths in the soil profile at site MHS, the mid-high elevation south aspect. Green line indicates field capacity and orange line indicates approximate wilting point for the soil. Data gaps were linearly interpolated to approximate number of days the bottom boundary exceeded field capacity. 111

Figure B.25. Soil water content at different depths in the soil profile at site MLN, the mid-low elevation north aspect. Green line indicates field capacity and orange line indicates approximate wilting point for the soil. Data gaps were

	linearly interpolated to approximate number of days the bottom boundary exceeded field capacity.	112
Figure B.26.	Soil water content at different depths in the soil profile at site MLS, the mid-low elevation south aspect. Green line indicates field capacity and orange line indicates approximate wilting point for the soil. Data gaps were linearly interpolated to approximate number of days the bottom boundary exceeded field capacity.	113
Figure B.27.	Soil water content at different depths in the soil profile at site LN, the low elevation north aspect. Green line indicates field capacity and orange line indicates approximate wilting point for the soil.....	114
Figure B.28.	Soil water content at different depths in the soil profile at site LS, the low elevation south aspect. Green line indicates field capacity and orange line indicates approximate wilting point for the soil. Data gaps were linearly interpolated to approximate number of days the bottom boundary exceeded field capacity.	115
Figure B.29.	Vegetation canopy cover during the growing season approximated using the Normalized Difference Vegetation Index (NDVI) derived from remote sensing images collected by Landsat-5 TM. Values shown are monthly averages over the growing seasons of the four-year period from 2006 to 2009. The series for each site has been fit with a fifth-order polynomial to clarify patterns and infer relative timing of peak NDVI. Colored shapes mark the inferred peak NDVI for each site. Forested sites have the highest	

NDVI; below them, north-facing sites have greater NDVI than south-facing sites at the lowest, mid-low, and mid-high elevations; on a given aspect, NDVI generally increases with elevation (MHS is an exception), and the date of peak NDVI generally occurs later on north aspects and on higher elevation sites (MLS is an exception). 116

Figure B.30. Vegetation cover as Plant Area Index (PAI) measured during part of the 2009 growing season using a handheld AccuPAR LP-80 ceptometer. Measurements were taken on the ground to validate the NDVI values derived from remote sensing. As with NDVI, forested sites show the most dense canopy cover. Below them, north-facing sites have greater PAI than south-facing sites, and higher elevation sites have greater PAI on a given aspect. The date of peak PAI appears to occur later on north aspects and higher elevation sites relative to south aspects and lower elevation sites, but peak dates were not determined from the PAI dataset because early and late season measurements were prohibited by persistent cloudiness during the 2009 growing season. 117

Figure B.31. Correlation between Plant Area Index (measured at 1 m resolution on the ground) and NDVI (measured at 30 m resolution from Landsat 5-TM satellite) for the 2009 growing season. The two methods of estimating vegetation cover are strongly correlated, offering validation for using the NDVI as a measure of vegetation canopy cover in the study area. 118

Figure B.32. Results of soil textural analyses for samples taken from 2 cm below ground surface. Soils on north aspects generally plot in a finer textural class than those on south aspects. Silt is the chief determinant of the fine fraction (ranging from 9.0% to 39.8% silt by mass), whereas clay content varies little (from 7.4% to 10.5% clay by mass). The low elevation north facing site LN is distinctly high in silt relative to all other samples. HN n = 6; HS n = 5; MHN n = 6; MHS n = 8; MLN n = 6; MLS n = 7; LN n = 6; LS n = 13. Thank you to A. Gerakis and B. Baer for the plotting program..... 119

Figure B.33. Results of soil textural analyses for samples taken from 15 cm below ground surface. Soils on north aspects generally plot in a finer textural class than those on south aspects. Silt is the chief determinant of the fine fraction (ranging from 8.7% to 42.3% silt by mass), whereas clay content varies little (from 7.5% to 12.7% clay by mass). The low elevation north facing site LN is distinctly high in silt relative to all other samples. HN n = 4; HS n = 4; MHN n = 16; MHS n = 14; MLN n = 3; MLS n = 4; LN n = 16; LS n = 13. Thank you to A. Gerakis and B. Baer for the plotting program..... 120

Figure B.34. Results of soil textural analyses for samples taken from 30 cm below ground surface. Soils on north aspects generally plot in a finer textural class than those on south aspects. Silt is the chief determinant of the fine fraction (ranging from 4.6% to 42.2% silt by mass), whereas clay content varies little (from 7.2% to 11.5% clay by mass). The low elevation north facing site LN is distinctly high in silt relative to all other samples. HN n = 4; HS n

= 4; MHN n = 4; MHS n = 9; MLN n = 4; MLS n = 4; LN n = 4; LS n = 7.

Thank you to A. Gerakis and B. Baer for the plotting program..... 121

Figure B.35. Results of soil textural analyses for samples taken at the soil-bedrock interface, which occurred at varying depths. Soils on north aspects generally plot in a finer textural class than those on south aspects. Silt is the chief determinant of the fine fraction (ranging from 9.8% to 35.9% silt by mass), whereas clay content varies little (from 7.6% to 10.7% clay by mass). The low elevation north facing site LN is distinctly high in silt relative to all other samples. HN n = 4; HS n = 4; MHN n = 4; MHS n = 7; MLN n = 4; MLS n = 1; LN n = 8; LS n = 3. Thank you to A. Gerakis and B. Baer for the plotting program. 122

Figure B.36. Correlation between particle size fractions (excluding gravel) obtained using laser diffraction versus hydrometer/sieve methods. Linear relationships between the sand and silt fractions determined using both laser diffraction and mechanical analysis (hydrometer/sieve) were used to predict mechanical analysis results from laser diffraction results for soil samples. Because laser diffraction is a relatively new method in soil textural analysis, a converting results to the more traditional mechanical method allows us to relate our soil classifications with those in other studies. 123

Figure B.37. Soil sand content does not generally appear to change systematically with depth; an exception is site LN, which contains less sand in the upper 30 cm bgs. 123

Figure B.38. Soil silt content does not generally appear to change systematically with depth; an exception is site LN, which contains more silt in the upper 30 cm bgs. 124

Figure B.39. Soil clay content does not generally appear to change systematically with depth at the study sites, and is low in all soil samples. 124

Figure B.40. Spatial trends in the bulk density of soil averaged over 5 to 30 cm below ground surface. Soil was sampled as two replicates from each site except MLN; bars show bulk density results from each sample to display uncertainty in results. Bulk density is generally greater where soil carbon content is lower - on south aspects relative to north aspects, and in lower elevations relative to higher elevations. 125

Figure B.41. Total soil carbon content as percent by weight over the profile at each site. Results are averaged from two field replicates at each site and random laboratory replicates; replicate values lay within 8% of the mean value for each depth..... 125

Figure B.42. Lengths of the potential growing season for each study site with mean annual trends in air temperature and insolation. Potential growing season was defined as the time period beginning when the shallow soil (2cm bgs) surpassed 5°C for the season and ending when the soil profile dried below the approximate wilting point. We see denser peak plant cover and greater soil carbon content at locations which retain plant-available soil water for a longer period of the warm, sunny summer..... 126

Figure B.43. Comparison of mean annual precipitation, mean spring (April-May-June) precipitation, and soil water storage capacity (field capacity * soil depth) at each study site. The storage capacity of soils is small relative to annual precipitation. Average amounts of spring precipitation are sufficient to recharge the soil water reservoir, and the timing of spring precipitation allows it to be utilized in ecosystem functions..... 126

Figure B.44. Correlations between annual maximum, or “peak” vegetation cover (as Normalized Difference Vegetation Index, NDVI) and soil carbon content at study sites. The strength of the correlation between the variables is evidence that above and below ground carbon stocks respond to similar controlling factors..... 127

1. INTRODUCTION

The response of terrestrial ecosystems to the changing climate is a critical question in global change science because terrestrial carbon reservoirs may serve to mitigate, or to hasten, the rate of atmospheric CO₂ enrichment on human timescales (Jobbágy *et al.* 2000; Amundson 2001; Heimann *et al.* 2008). The fate of the sizeable carbon stocks held in terrestrial ecosystems and soils is uncertain given the current lack in understanding of the controls on vegetation productivity and associated soil carbon storage in different ecosystems (Schlesinger 1977; Amundson 2001; Davidson *et al.* 2006). Climate change is expected to produce changes in precipitation patterns around the world (Weltzin *et al.* 2003). If we are to successfully prepare for global changes in the terrestrial carbon and water cycles, we must first improve our understanding of how vegetation and soils in a variety of climates will respond to changing climate conditions, and particularly to changing precipitation patterns (Chapin *et al.* 2002; Weltzin *et al.* 2003; Foley *et al.* 2004; Xu, Baldocchi *et al.* 2004; Chou *et al.* 2008).

The impacts of a changing climate on ecosystem processes remain an area of uncertainty, particularly in semi-arid mountainous settings, where high sensitivity to changes in precipitation and temperature are coupled with complex topographically-driven climatic and ecologic gradients (Raich *et al.* 1992; Wigmosta *et al.* 1994; Weltzin *et al.* 2003; Williams 2005; Newman *et al.* 2006; Sole 2007; Caylor *et al.* 2009; Thomas *et al.* 2009; Vivoni *et al.* 2009). Integrative mathematical models will ultimately be

required to form quantitative predictions of changes in carbon stocks in these systems (Monteith 1981; Chen *et al.* 1999; Arora 2002; Rodríguez-Iturbe *et al.* 2004; Ivanov *et al.* 2008a). Long-term, field-based soil moisture datasets are lacking in steep, complex terrain at the watershed scale, prohibiting the calibration and validation results from hydrologic, ecologic, and climate models in many regions (Grayson *et al.* 1997; Salvucci 2001; Famiglietti *et al.* 2008; Ivanov *et al.* 2008b; Viola *et al.* 2008). A goal of this study is to generate field data that can help to constrain model development, and to build a conceptual understanding of how hydrologic drivers impact ecological function in semi-arid, mountainous environments.

The availability of soil water is a fundamental control on photosynthesis and associated ecosystem processes in semi-arid environments. Inversely, such ecosystems can influence the amount of water in soil (Noy-Meir 1973; Rodríguez-Iturbe *et al.* 1999; Orcutt *et al.* 2000; Rodríguez-Iturbe *et al.* 2001b; Arora 2002; Caylor *et al.* 2006). Soil water acts as the link between water, energy, and carbon budgets of a terrestrial ecosystem by partitioning climatic forces (i.e. precipitation, radiation) into ecosystem activity, latent and sensible heat fluxes, surface water runoff, and deep drainage (Rodríguez-Iturbe *et al.* 2001b; Arora 2002; Williams *et al.* 2009). Rodríguez-Iturbe (2000), Rodríguez-Iturbe *et al.* (2000; 2001b) and Ridolfi *et al.* (2003) model the vertically-integrated soil water balance at a point as shown in Equation 1,

$$nZ \frac{d\theta}{dt} = I(\theta, t) - E(\theta, t) - L(\theta, t) + \Phi_{lat} \quad (\text{Equation 1})$$

in which n represents soil porosity, Z_r represents the soil depth, s is relative soil moisture content ($0 \leq s(t) \leq 1$), t represents time, $I(s,t)$ represents infiltration of precipitation into soil, $E(s,t)$ is evapotranspiration loss, $L(s,t)$ is leakage loss, and Φ_{lat} represents a net lateral flux. In mountainous semi-arid systems, the source of soil water at a point can be rainfall, snowmelt, or lateral flows on or below the soil surface (Rodríguez-Iturbe *et al.* 2001b; Ridolfi *et al.* 2003). The water table is often too deep to interact with soil water via a capillary action (Rodríguez-Iturbe *et al.* 2004), although some studies suggest upward hydraulic gradients in deep arid to semi-arid soils (Walvoord *et al.* 2004). Precipitation may be prevented from reaching or infiltrating into the soil by canopy interception, runoff, and sublimation from the snowpack. Water may leave the soil vertically through evapotranspiration or leakage from the base of the soil profile into a deeper ground water reservoir. Soil texture, depth, composition, and structure influence infiltration, evapotranspiration, leakage, water availability, water retention capacity, albedo, carbon storage, and lateral flow rates, as well as mineralization rates and availability of soil nutrients such as nitrogen (Noy-Meir 1973; Aber *et al.* 1991; Famiglietti *et al.* 1998; Brady *et al.* 2002; Hillel 2004; Rodríguez-Iturbe *et al.* 2004; Seyfried *et al.* 2005; Plante *et al.* 2006).

Lateral redistribution of soil water toward or away from a given observation point can be influenced by topographic controls including slope gradient, curvature, and contributing area in regions of complex terrain (Rodríguez-Iturbe *et al.* 2001b; Rodríguez-Iturbe *et al.* 2004). Runoff and infiltration can also be influenced by topography (Famiglietti *et al.* 1998; Western *et al.* 1999). In mountainous terrain, both

the amount of precipitation and the air temperature are commonly influenced by elevation through the orographic effect (Dingman 2002). Slope aspect determines the amount of incident solar radiation (insolation), and thus potential evapotranspiration rates, with south aspects having higher rates of insolation and evaporation loss than north aspects in much of the northern hemisphere (Brady *et al.* 2002; Geiger *et al.* 2003).

Vegetation both influences and responds to soil water content (Rodriguez-Iturbe *et al.* 2001b; Hupet *et al.* 2002; Tromp-van Meerveld *et al.* 2006). Vegetation requires water from the soil to fix carbon from the air in photosynthesis (Taiz *et al.* 1998). Through photosynthesis, plants adjust the rate of transpiration by regulating their stomata in response to soil water availability (Taiz *et al.* 1998; Dingman 2002). The vegetation canopy intercepts precipitation (affecting infiltration) and shades the soil from insolation, protects soil from erosion, and changes the albedo and air turbulence at the land surface (affecting evaporation rate and soil temperature) in proportion to the density of coverage (Dingman 2002; Breshears *et al.* 2003). Vegetation protects the soil surface from wind and entrains windblown materials which may include loess and nutrients (Chadwick *et al.* 1990; Reheis *et al.* 1995; Goudie *et al.* 2006). Plants promote weathering and deposit organic materials containing carbon, nitrogen, phosphorous, and water onto the soil (affecting soil structure, composition, color, and water retention capacity), among other influences and feedbacks (Arora 2002; Brady *et al.* 2002; Gutierrez-Jurado *et al.* 2006). Organic materials in soil, contributed largely by vegetation, affect the soil structure, bulk density, composition, color, hydraulic conductivity, and nutrient content (Brady *et al.* 2002; Chapin *et al.* 2002; Wang *et al.* 2009).

Because it is such an important link between abiotic and biotic forces, soil moisture is a critical factor influencing large- and small- scale models of climate change, vegetation productivity, energy dynamics, and hydrologic processes. Although a clear understanding of soil moisture is important to the success of predicting and modeling the above processes, spatially and temporally detailed soil moisture data are lacking, and the controls on soil moisture distribution are highly variable in space and time (Hawley *et al.* 1983; Famiglietti *et al.* 1998; Grayson *et al.* 1998; Rodriguez-Iturbe *et al.* 1999; Salvucci 2001; Hupet *et al.* 2002; Porporato *et al.* 2002; Famiglietti *et al.* 2008). In prior work attempting to correlate soil moisture to its key physical predictors, some easily measured topographic factors, such as elevation and aspect, have been treated as controls (Beven *et al.* 1979; Gomez-Plaza *et al.* 2001; Wilson *et al.* 2005; Williams *et al.* 2009). However, topographic factors are often surrogates for other, more mechanistic controls on soil moisture. For example, elevation alone would be unlikely to affect soil moisture without the orographic trends in precipitation and air temperature, as well as changes in soil properties, which provide some physical explanation for ecological trends over elevation gradients (Daubenmire 1968; Whittaker *et al.* 1975). Likewise, slope aspect itself would provide little explanatory power if not for the different amounts of insolation received (Geiger *et al.* 2003; Ivanov *et al.* 2008b). Furthermore, factors other than topography can exert an important influence on the soil moisture distribution, such as soil properties and vegetation (Grayson *et al.* 1997; Western *et al.* 1999; Gomez-Plaza *et al.* 2001; Tromp-van Meerveld *et al.* 2006). Currently, our empirical understanding is insufficient to reliably identify the key physical controls on soil moisture distribution in a range of

environments, seasons and soil moisture states (Western *et al.* 1999; Gomez-Plaza *et al.* 2001; Western *et al.* 2004; Ivanov *et al.* 2008b; Williams *et al.* 2009).

Ecosystems located in mountainous or complex terrain can be useful for field studies because they capture climate gradients. Steep, mountainous terrain induces the development of microclimates induced by changing both elevation and aspect (Thornthwaite 1961; Geiger *et al.* 2003; Burnett *et al.* 2008). These induced climatic gradients have been applied over long timescales, making them useful natural settings in which to study the effects of different climate conditions on a single region while holding factors such as bedrock type and latitude constant (Geiger *et al.* 2003). Ecological transition zones commonly span these topographic gradients in response to the differing climate conditions (Smith *et al.* 2002; Geiger *et al.* 2003). Previous workers have used topographic gradients as a proxy for climate change to examine controls on weathering, soil formation, vegetation processes, soil moisture dynamics, and carbon cycling (Whittaker *et al.* 1975; Schulze *et al.* 1996; Wang *et al.* 2000; Smith *et al.* 2002; Caylor *et al.* 2006; Gutierrez-Jurado *et al.* 2006; Tromp-van Meerveld *et al.* 2006; Gutierrez-Jurado *et al.* 2007; Burnett *et al.* 2008).

The present study was conducted in a climate where precipitation and temperature occur out of phase, with alternating cold-wet and hot-dry seasons. This system resembles Mediterranean climates, which can be found in Greece, Turkey, Portugal, Spain, France, Italy, and Chile, as well as in North American in south-central Oregon, southern California, and south-central Arizona, among other locations (Henderson-Sellers *et al.* 1986; Vourlitis *et al.* 2007; Chou *et al.* 2008; Viola *et al.* 2008; Thomas *et al.* 2009;

Silver *et al.* 2010). While this system shares the characteristic summers typified by high temperatures and drought conditions with rare, sporadic precipitation, it is differentiated by much colder winters, which typically see freezing temperatures and development of a snowpack at the middle and upper elevations (McNamara *et al.* 2005; Thomas *et al.* 2009). During the transition from winter to summer in this environment, warming temperatures briefly coincide with high soil moisture, resulting in an episode of active water and carbon exchanges and transient soil moisture conditions (McNamara *et al.* 2005; Ladd *et al.* 2007). Changes in the amount and timing of precipitation and temperature, such as those which are expected to result from climate change, are anticipated to impact these out-of-phase, water-limited systems in complex, interrelated, but not yet predictable, ways (Smith *et al.* 2000; Weltzin *et al.* 2003; Xu and Baldocchi 2004; Chou *et al.* 2008; Viola *et al.* 2008).

Previous research in the mountainous American west has commonly emphasized the impacts that changes in snow amount and duration will have on discharge patterns downstream (Hamlet *et al.* 1999; Stewart *et al.* 2005). Observed and anticipated changes in winter precipitation include declining snowpack volume, earlier snowmelt, and an increase in the proportion of winter precipitation falling as rain rather than snow (Hamlet *et al.* 2005; Stewart *et al.* 2005; Knowles *et al.* 2006; Mote 2006; Hamlet *et al.* 2007). Less work has investigated the impacts of the amount and timing of spring and summer precipitation on upland hydrology and ecosystem functioning (Weltzin *et al.* 2003; Hamlet *et al.* 2007).

We have conducted an intensive field campaign examining soil conditions and ecosystem carbon stocks in the semi-arid Dry Creek Experimental Watershed, whose complex terrain captures gradients in elevation, aspect, climate and ecology. We have observed that the natural vegetation appears to be distributed in response to climatic gradients across the complex topography of the study area. In this study we examine whether measured differences in soil moisture across elevation and aspect gradients mimic the observed differences in vegetation cover. A temporally intensive (sub-hourly to daily) data series of soil moisture and soil temperature at eight study locations (four different elevations, each with paired sites on north and south aspects, and with measurements from multiple points and multiple soil depths at each study location) are compared to time series of vegetation cover at these sites. Our focus is on relatively shallow soil water (maximum depth 116 cm below ground surface, bgs), as the water table is very deep (24 to 130 m bgs) on hillslopes in the study area (Aishlin 2006). We use the topographic, climatologic, and ecologic gradients, and associated seasonal dynamics, to explore how changes in soil moisture may alter patterns in vegetation and soil. We analyze temporal trends in soil moisture and vegetation and propose that the semi-arid foothills ecosystem will be particularly sensitive to changes in the amount and timing of spring precipitation.

2. STUDY AREA: THE DRY CREEK EXPERIMENTAL WATERSHED

The Dry Creek Experimental Watershed (DCEW) is an approximately 27 km², northeast-southwest trending semi-arid basin located about 16 km northeast of Boise, Idaho in the mountain foothills region known as the Boise Front (McNamara *et al.* 2005). The watershed acts as a center of hydrologic research for several diverse groups at Boise State University, with instrumentation including three weather stations, seven stream gages, and multiple soil moisture monitoring stations (<http://earth.boisestate.edu/boisefront/boisefront/Index.html>). Figure B.1 shows the DCEW topography, vegetation, and instrumentation discussed in this study. Meteorological variables including precipitation, snow depth (from ground surface), air temperature, and shortwave radiation are recorded at three meteorological stations located in DCEW at elevations of 1151, 1610, and 1850 m. The three stations are maintained by Boise State University (BSU). Details regarding data collection and processing at the three sites are provided by Aishlin (2006). A fourth site, the Bogus Basin SNOTEL meteorological station, is maintained by the USDA Agricultural Research Service at an elevation of 1932 m, north of the DCEW upper boundary (<http://www.wcc.nrcs.usda.gov/nwcc/site?sitenum=978&state=id>). These meteorological stations provide a record extending from as early as 1998 until 2009.

The perennial Dry Creek drains the watershed from its headwaters in the Boise Front Range, at an elevation of about 2100 m, to its confluence with the Boise River west

of Boise at about 800 m of elevation (Williams 2005). The DCEW encompasses the upper portion of the basin, with its upper boundary located near the headwaters region, and the lower boundary located at about 1100 m elevation. The bedrock of DCEW consists of medium- to coarse-grained biotite granodiorite of the Idaho Batholith. Soils on hillslopes are typically shallow (< 2 m deep) gravelly loams to gravelly sands, developed in situ from weathering of bedrock (USDA 1997; Gribb *et al.* 2009; Tesfa *et al.* 2009). Slope gradients average about 29% on north-facing slopes, and about 21% on south-facing slopes (M. Poulos, personal communication October 2009), with an overall average slope gradient of about 25% (Tesfa *et al.* 2009). The topographically complex watershed spans gradients of elevation (1000 m) and slope aspect (north to south).

In addition to the topographic gradient, the DCEW spans a marked ecological gradient. In lower elevations of DCEW, grass and sagebrush shrublands dominate, while higher elevations support forest vegetation including fir, spruce, and pine (McNamara *et al.* 2005; Williams 2005). In mid-elevations of the watershed, a steep vegetation gradient from shrub lands to evergreen forest is observed at the same elevation from north to south aspect. These trends are evident in the aerial photograph shown in Figure B.1. Land use in the watershed includes grazing in the lower to middle elevations, logging in the upper elevations, and recreational uses throughout (hiking, biking, hunting) (Williams 2005). The watershed has been historically affected by fire and invasive species (cheat grass), but is representative of many semi-arid environments in the American west.

The climate of the DCEW is characterized by cold, wet winters and hot, dry summers, as well as a hypsometric effect of increasing precipitation and decreasing

temperature at higher elevations. The lower DCEW is classified as a steppe summer dry climate, and the upper DCEW as a moist continental climate with dry summers, using the Köppen climate classification system (Henderson-Sellers *et al.* 1986; McNamara *et al.* 2005). Precipitation and temperature are out-of-phase, with most precipitation falling during the cold winter months as snow in the higher elevations, and as rain and snow in the lower elevations (Figure B.2).

Yearly air temperatures range from -15°C to 33°C at lower elevations, and from -14°C to 26°C at higher elevations. Average daily temperatures above 5°C generally occur from April to November (Figure B.2). Most precipitation typically occurs from November through April, with average annual precipitation ranging from about 400 mm at lower elevations to about 700 mm in the headwater region (Figure B.3). Figure B.4 shows how precipitation patterns during the 2008-2009 season of study differ from average patterns. The most distinct deviations are unusually high precipitation falling in June and August 2009, and relatively low amounts of precipitation over winter. A hypsometric effect induces a gradient of greater mean precipitation and lower mean air temperature with increasing elevation (Figure B.3).

Insolation, or the amount of incident solar radiation reaching the surface, varies widely with aspect, and to a lesser degree with elevation, in the study area. Slope aspect, slope gradient, and elevation are the key long-term variables determining the amount of insolation received in the steep terrain of the DCEW (Geiger *et al.* 2003). Figure B.5 shows how insolation varies with topography in the study area. The total annual potential insolation was modeled for each site using the Solar Radiation tool in ArcGIS

Spatial Analyst (ESRI, Redlands, CA) in order to assess the energy received on slopes of different aspects and gradients (Huang *et al.* 2009). Generally clear sky conditions over the year were assumed in model parameters. Topographic inputs to the tool were provided as a 10 m resolution digital elevation model provided by the United States Geological Survey. The modeled results were compared to observed total annual solar radiation for 2000-2008 measured from Lower Weather and Treeline weather stations in DCEW, as well as mean annual solar radiation for 2000-2004 measured from the SNOTEL Bogus Basin station (Figure B.6). Henceforth, observed solar radiation will be termed “observed insolation” and modeled insolation will be termed “potential insolation.” As shown in Figure B.6, a positive linear relationship between annual potential insolation and elevation is apparent for north and south aspects. The amount of potential insolation received at a given elevation can be 2 times higher on the south aspect relative to the north aspect. In contrast, potential insolation at a given aspect increases by a factor of 1.1 (south aspects) and 1.4 (north aspects) over 700 m of elevation change in the watershed. Thus, potential insolation differs more between north and south aspects at a given elevation than across the 1000 m-elevation gradient at either aspect. The agreement of the observed and potential annual insolation is reflective of the generally low annual cloud cover at the study area, and suggests that the modeled values are a good approximation of actual insolation. Comparison of the annual timing of measured daily insolation and measured air temperature taken from a BSU meteorological station at 1610 m elevation in the DCEW shows that peak air temperature

(August) is delayed by about one month from peak insolation (July) in the summer (Figure B.7).

Potential insolation exhibits two orographic trends in the study area; there is a positive relationship between potential insolation and mean annual precipitation (and elevation), as well as a negative relationship between potential insolation and mean annual temperature (and elevation) (Figure B.8). The coefficients of determination are equal because both mean annual precipitation and mean annual temperature are derived from elevation using the orographic relationships shown in Figure B.3. The differences in energy received on different slopes may relate to processes such as snowpack duration and melt rate, weathering of rock and soil, evaporation from the soil, transpiration and productivity of plants, and respiration of roots and soil microbes, among others.

3. METHODS

We have observed that the distribution of vegetation relates to topography in the study area. This study seeks to examine whether measured differences in soil moisture across elevation and aspect gradients mimic the observed differences in vegetation cover. To address the study objective, study sites were located at four elevations on north- and south-facing slopes. Soil moisture and soil temperature were measured at multiple depths at multiple locations at sub-hourly to daily intervals over 286 days at the study sites. Vegetation cover was measured as an approximately bi-monthly time series at each study site using two independent light-based methods at different scales. Soil texture, soil depth, and soil carbon content were also determined at multiple depths at each site to investigate potential differences in water retention, storage capacity, and carbon storage properties at each site.

3.1. Soil Water and Soil Temperature

3.1.1. Soil Volumetric Water Content, Soil Temperature, Soil Depth

Soil moisture (as volumetric water content, henceforth “soil water content” or “soil moisture”) and soil temperature were monitored at eight sites in DCEW using 121 ECH₂O EC-TM sensors (Decagon Devices, Inc., Pullman WA). Volumetric water content is defined as the volume of water per total volume of soil according to Equation 2,

$$\theta = \frac{V_w}{V_T} \quad (\text{Equation 2})$$

where θ represents volumetric water content (dimensionless), V_w represents the volume of water (cm^3), and V_T represents the total volume of soil (cm^3) (Dingman 2002; Hillel 2004).

Study site locations are shown in Figure B.1, and station coordinates and characteristics are provided in Table A.1. The stations were placed on north- and south-facing aspects at four different elevations spanning a 700 m elevation gradient. The naming scheme for the stations, shown in Table A.1, is as follows: H indicates “High Elevation”, L indicates “Low Elevation,” and M modifies the elevations to “Mid-.” An N indicates a north-facing slope, while an S indicates a south-facing slope. For example, site MLN will be the Mid-Low elevation, North-facing slope in this study. The lowest and mid-lowest elevation sites (LN, LS, MLN, and MLS) are located in shrub/grass land ecology. The highest elevation sites (HN, HS) are placed in forest. At the mid-highest elevation sites, the north-facing site (MHN) is located in forest, while the south-facing site (MHS) is placed in shrub/grass land (Figure B.1). Each site was placed at the mid-slope position in a location which represented the vegetation characteristics of the overall slope; forested sites were placed in old-growth, unlogged locations. Care was taken to locate each north-south pair of sites on slopes of comparable gradient, and to avoid convexities or concavities in the topography. Each station was composed of four soil pits placed about 2 to 6 m apart, and in each pit EC-TM sensors monitored water content and temperature at up to four depths every 10 minutes (Figure B.9).

Sensors are placed at depths of 2, 15, and 30 cm below the mineral soil surface. In pits where soil depths exceed 30 cm (only LS and MLS have soils no deeper than 30 cm), a fourth sensor is installed above the soil-bedrock interface. Bedrock was identified as the depth at which the soil became dominated by gravelly decomposed granite which was unsuitable for installation of the EC-TM sensors. The depth to the soil-bedrock interface was measured from each soil pit, and the mean depth from the four pits was calculated to represent mean soil depth at each site. Estimates of mean annual precipitation and mean annual air temperature were calculated for the elevation of each study site in this project using the hypsometric relationship shown in Figure B.3, and assuming that elevation is the most important spatial factor which imposes a significant control on mean annual precipitation and air temperature.

In this study, the four pits at each site are generally treated as replicate samples; an average of the four pits is assumed to represent soil conditions typical of the hillslope upon which each site is located. As the chief objective of this study is to illustrate the differences in soil conditions across watershed-scale topographic gradients, we expect the four soil pits placed at mid-slope position at each study site to approximately capture the spatial variability and spatiotemporal contrasts at the hillslope scale, particularly at the fine temporal resolution of our sampling routine. The data reported in this thesis are based on daily averages calculated from the original 10 minute sampling interval. When discussing the results, “site average” refers to an average value across all four replicate pits and all soil depths monitored at a site. Unless otherwise stated, results are derived

from site averages. Results described as “profile-averaged” refer to the mean of all 3 to 4 depths measured in a profile.

The EC-TM sensors send electromagnetic energy along the prongs of the probe, and a measurable charge is built between the prongs which is proportional to the dielectric permittivity of the surrounding soil; the soil dielectric, in turn, is dominated by the water content (Hillel 2004; Decagon Devices 2007). The raw output signal from the sensors is converted into a water content value using a linear calibration equation for mineral soils derived by Decagon Devices, Inc., and validated for soils from the Dry Creek Experimental Watershed in the laboratory. The sensors measure temperature using a thermistor mounted adjacent to a prong, so the thermistor reads the average temperature along the length of the prong (5.2 cm). Error in the sensors in media comparable to the soils of DCEW has been reported as +/-3% VWC between sensors and per sensor and +/- 1°C between sensors (Decagon Devices 2007). The maximum sample volume represented by the sensor reading is roughly 400 cm³.

We used data over the entire period of record common to all sites for calculations in which we sought to compare the annual behavior of soil moisture and soil temperature at the different sites. The common period of record was 11/20/2008 to 9/1/2009, encompassing nearly an entire water year. In analyses where sites were compared, such as computations of statistics and the number of days potential bedrock flow days, data gaps were linearly interpolated to ensure that the time period was equally represented by all sites. To determine maximum and minimum values of soil water content or soil temperature, the entire period of record was used.

3.1.2 Soil Water Storage

Measured values of volumetric water content and soil depth were used to calculate the total water stored in the profile. Each soil pit contains 3 to 4 sensors measuring volumetric water content at depths spanning from 2 cm below ground surface (bgs) to near the soil-bedrock interface. From the measured depths the volumetric water content of the soil was interpolated at 1 cm increments from soil surface to bedrock depth. A line fitting the interpolated points was integrated to determine the total water stored in each soil pit. This total amount of water stored is reported as a depth of water. Both the interpolation and integration processes were performed using MATLAB R2008b software (The Mathworks, Inc., Natick, MA). The water storage values account for the different soil depths and water contents observed at different sites, reflecting the total volume of water present in a soil mantle at a given time.

3.1.3. Duration of Snow Cover

Measured values of soil temperature at the 2 cm soil depth were used to infer dates of snow cover formation and disappearance at each site. Periods of snow cover were interpreted as the period during which diurnal fluctuations of shallow soil temperature were strongly dampened and limited to approximately 0°C. The resulting inferences of snow cover periods agreed well with snow depth data recorded using Judd Ultrasonic Depth Sensors (Judd Communications LLC, Salt Lake City, UT) from weather stations located at similar elevations in the watershed.

3.1.4. Soil Matric Potential

In order to assess the amount of water available for dynamic processes such as evapotranspiration and deep drainage to bedrock fractures, it was necessary to account for the water retention properties of the different soils in the study area (Brady *et al.* 2002). Moist soil subjected to a vacuum (negative pressure, or tension) will lose water from pore spaces in a manner related to the pore distribution and strength of attractive forces among soil particles, soil capillaries, and pore water; the amount of water lost per unit drop in pressure will change over a drying period due to the changing matric (energy) potential of pore water (Clapp *et al.* 1978; Hillel 2004). The empirical relationship between the volume fraction of water in a soil and the matric potential of the pore water is known as a soil-moisture characteristic curve (Hillel 2004). Equation 3 relates matric potential to volumetric water content in a given soil textural class as,

$$\psi = \psi_s \left(\frac{\theta}{\theta_s} \right)^{-b} \quad (\text{Equation 3})$$

where ψ (MPa or cm) is the matric potential (“suction”), ψ_s (MPa or cm) is the suction when soil is saturated, θ (dimensionless) is the volumetric water content corresponding to ψ , θ_s (dimensionless) is the assumed saturated water content (the maximum limit of which is the soil porosity), and b (dimensionless) is an empirical fitting parameter. Values of ψ_s , θ_s , and b are unique to each USDA soil texture class and are provided by Clapp and Hornberger (1978). Numerous properties relate to the soil water retention characteristics of a soil, including texture, structure, carbon content, bulk density, topography, and antecedent moisture condition, among others (Famiglietti *et al.* 1998;

Brady *et al.* 2002; Rawls *et al.* 2003; Hillel 2004; Leij *et al.* 2004). In essence, two soils with the same water content may have a different amount of water available for redistribution due to the different amounts of absorptive force exerted on the pore water in each soil.

In this study we wanted to approximate the time at which each site reached a) a water content sufficiently high that soil water could redistribute vertically or laterally under the force of gravity, often referred to as “field capacity” (Brady *et al.* 2002; Hillel 2004), and b) a water content sufficiently low that plants would experience severe water stress and essentially go dormant, similar to the “permanent wilting point” concept often used in soil science (Veihmeyer *et al.* 1955; Hillel 2004). Both field capacity and permanent wilting point are physically imprecise concepts. For example, different plants have different extraction capabilities and water use efficiencies and thus wilt or cease to extract soil water at different matric potentials. Despite such shortcomings, field capacity and wilting point continue to be useful standard tools for approximately describing the range in soil moisture when water is available for dynamic processes such as redistribution and transpiration, respectively (Brady *et al.* 2002; Hillel 2004). We apply the field capacity and wilting point concepts in this study to define the matric potentials (and associated soil water contents) below which water is no longer appreciably available for redistribution and evapotranspiration, respectively. We acknowledge that, in the semi-arid environment of this study, many vegetation species have adapted to withstand long periods of very dry soil (very negative matric potentials) without permanently wilting, but that transpiration activity and extraction of soil water by plants does effectively cease

in the late growing season when soil water limitation inflicts severe plant stress in most native shrub and grass species (Noy-Meir 1973; Rodríguez-Iturbe *et al.* 2004; Seyfried *et al.* 2009).

3.1.5. Approximate Wilting Point

The approximate wilting point of soil at each site was estimated using parameters and relationships from the literature. Equation 3 was solved for θ at chosen values of ψ described below. Previous workers have concluded that plants in semi-arid environments reach a wilting point below values of -3 to -5 MPa (-30,591 to -50,986 cm H₂O), up to as low as -9 MPa (-76,500 cm H₂O) (Kappen *et al.* 1972; Scholes *et al.* 1993; Linton *et al.* 1998; Laio *et al.* 2001). A matric potential value of -3 MPa (-30,600 cm H₂O) was used here for ψ as the point at which soil water was effectively unavailable for appreciable evapotranspiration. Equation 3 was used to estimate the volumetric water content at the matric potential of field capacity and wilting point for the different soil textures encountered in the study (Clapp *et al.* 1978; Dingman 2002), although a more site-specific field capacity was then determined by an alternative method (below). Water retention characteristics are commonly approximated using soil textural properties (Laio *et al.* 2001). The volumetric water contents corresponding to the wilting point matric potentials at each site are provided in Results.

3.1.6. Field Capacity

The chief objective in identifying the field capacity water content at each site was to determine whether soils became sufficiently wetted at depth to create a potential for

bedrock flow, which could include one or both of vertical flow from the base of the soil profile into bedrock (deep drainage) and lateral flow at the soil-bedrock interface (McNamara *et al.* 2005). Thus, field capacity water content for each site was estimated from the soil water content data. Because we are primarily interested in the frequency with which field capacity is exceeded at the soil-bedrock interface, we focused on empirical determinations of field capacity at the bottom of the soil profile at each site. Because the USDA soil texture class differed slightly, if at all, over the soil profile, it is assumed that field capacity at the soil-bedrock interface is similar to field capacity over the soil profile. Time series plots of soil water content at each depth were generated for each study site. In each time series, soils were observed to reach a near-maximum water content at all depths in early winter following prolonged fall precipitation and the onset of snow pack; following the early winter peak, soil water content at all depths declined exponentially. According to common definitions, the field capacity water content at the soil-bedrock interface was chosen as the water content at which the rate of soil water decline approached horizontality (Brady *et al.* 2002).

This method of selection is qualified by the observation that the time at which a given depth of soil exceeds field capacity is closely associated with the timing of increase in soil water content at greater depths. Shallower soils must wet above field capacity before soil water redistribution can occur. In the study environment, there is effectively no capillary contribution of water from a shallow water table, so vertical and lateral redistribution are the most important sources for soil water at the soil-bedrock interface. Figures illustrating profile soil water time series and the results of this field capacity

selection method are presented in the results. Field capacity is often assumed to occur at a matric potential value of -0.03 MPa (-340 cm H₂O) of tension (Laio *et al.* 2001; Dingman 2002), but in this study the water content corresponding to that matric potential occurred at a higher water content than the empirically determined value of field capacity described above. Table A.2 provides the results of both methods to determine field capacity; the empirically determined field capacity values are reported in Results and Discussion.

3.1.7. Storage Capacity

A soil's capacity to store water is determined by a) the depth of soil available to hold water, and b) the amount of water a soil can store before added water drains out. We multiplied the average soil depth at a site by the field capacity determined for the bottom boundary of soil at the site (above) to approximate each site's potential for soil water storage, which we call the storage capacity.

3.2. Potential Growing Season

The potential growing season was bracketed for each site using our measured values of soil temperature and soil moisture, and our understanding that the growing season will be limited by temperature in spring and by water in summer. Growing season is defined somewhat widely depending on geographic location, climate, and crop type (Feng *et al.* 2004; Miller *et al.* 2005). In this study, we chose to use field observations to inform our definition of a natural growing season in the study environment. We defined

the onset of the potential growing season as the final date on which the surface (2 cm depth) soil warmed to above 5°C as a daily mean temperature, in keeping with some definitions of the onset of plant development (Monteith 1981; Feng *et al.* 2004). We defined the initiation of the potential growing season using the temperature of soil at 2 cm bgs, according to our observation that surface soil temperatures closely track seasonal air temperatures (Results). The conclusion of the growing season was defined as the date on which the soil profile reached a water content below the soil-texture-specific wilting point described above. Thus defined, the potential growing seasons of each site agreed well with our field observations of the duration of green vegetation, and with our measurements of vegetation cover, as well as with previous observations of the duration of active soil respiration in the study area (K. Ladd, personal communication, November 2009). We acknowledge again that not all vegetation wilts, dies, or browns when soil dries to the wilting point, but that general favorability for growth dramatically declines, effectively ending the potential growing season .

3.3. Vegetation Distribution

3.3.1. Plant Area Index

Plant area index (PAI), was measured at weekly to bimonthly intervals at 33 points surrounding each soil moisture station over April to October 2009. An AccuPAR LP-80 LAI/PAR ceptometer provided by Decagon Devices, Inc. (Pullman, WA), was used to conduct the measurements. The AccuPAR LP-80 contains 80 photosensors which detect photosynthetically active radiation (PAR), that portion of the electromagnetic

spectrum having wavelengths of 400-700 nm which can be used to manufacture carbohydrates in photosynthesis (Taiz *et al.* 1998; Decagon Devices 2006-2010). The fraction of PAR transmitted through the vegetation canopy is determined by measuring PAR above and below the vegetation canopy (Breda 2003; Decagon Devices 2006-2010). Leaf Area Index (LAI) is defined as the total one-sided leaf area per unit of ground area (Breda 2003). The fraction of transmitted PAR is used to indirectly approximate Leaf Area Index (LAI), according to Equation 4,

$$LAI = \frac{\left[\left(1 - \frac{1}{2K} \right) f_b - 1 \right] \ln \tau}{A(1 - 0.47 f_b)} \quad (\text{Equation 4})$$

where K (dimensionless) is the extinction coefficient for the canopy, f_b (dimensionless) is the beam fraction of incident PAR, τ (dimensionless) is the fraction of transmitted PAR (below-canopy/above-canopy PAR), and A (dimensionless) is a function of leaf absorptivity in the PAR waveband (Decagon Devices 2006-2010). The ceptometer method cannot distinguish green leaves from branches, stems, dead leaves, and other non-leafy vegetation components, and in many environments (such as semi-arid shrub lands), such materials may compose a significant portion of the canopy. In such environments, measurements of intercepted PAR may more accurately represent PAI than LAI (Chen *et al.* 1996; White *et al.* 2000; Breda 2003). Thus, values of vegetation cover measured using the AccuPAR ceptometer will be reported hereafter as PAI.

The goal of the PAI measurements was to capture trends in vegetation cover at a relatively fine time scale (weekly to bimonthly) and fine spatial scale (approximately 1

m). Figure B.10 shows the approximate configuration of PAI sampling locations around study stations. Although it is not a direct measurement of vegetation cover, the relatively simple ceptometer method allowed many measurements to be taken at the eight stations at approximately bimonthly intervals from April to October 2009. Direct measurements of leaf or plant area index are time- and labor-intensive, and so are typically limited to very low spatial and temporal resolution (Clark *et al.* 2001; Breda 2003; Duursma *et al.* 2003). The ceptometer made it possible to collect relatively high numbers of samples, allowing this study to infer relative differences in vegetation cover at different locations in spite of high spatial variability of vegetation. Furthermore the on-the-ground method provided a validation of trends observed using satellite data collected at a coarser spatial and temporal resolution (below).

Radiation-based measurements of plant cover are sensitive to the intensity of light incident upon the top of the vegetation canopy. This means that variables such as solar elevation (time of day, time of year) and cloud cover can strongly affect ceptometer measurements (Breda 2003; Decagon Devices 2006-2010). Whenever possible, ceptometer readings were taken between 9:00 AM and 3:00 PM on sunny or uniformly cloudy days to maintain consistency of solar angle. Each reading was taken as the average of a series of three readings. The sampling procedure was to place one's foot on a sample point flag, step directly upslope with the opposite foot, and measure PAR above and below the canopy in the undisturbed sampling region upslope of the transect flags. Care was taken to face the sun in order to prevent shading of the instrument, and the built-in bubble level was used to ensure a consistent incident angle of radiation. In low-

canopy shrub lands, incident PAR radiation was measured by holding the ceptometer above the vegetation canopy at each sampling point. At forested sites, incident PAR was read in a forest clearing at the beginning, middle, and end of each transect. A uniform leaf angle distribution parameter, χ , of 1 was selected in the LP-80 software for all sites to maintain consistency in measurement; the computed LAI is not very sensitive to χ , and more reliable values of χ for the vegetation being studied were not available. Due to an unusually cloudy spring and atypical summer storms, several weeks of PAI data collected in this study were considered to be invalid. In spite of this, a time series of PAI was measured at all sites late April until late September 2009. Complete details of the PAI sampling methodology are included in Appendix C.

3.3.2. Normalized Difference Vegetation Index

Remote sensing was used to determine the Normalized Difference Vegetation Index (NDVI) (Rouse *et al.* 1974; Jensen 2000) for all sampling locations over four growing seasons (April 1 through October 31). The goal of the four-year monthly average NDVI calculation was to incorporate longer-term trends in vegetation productivity than the single 2009 growing season of the PAI dataset discussed above. The Normalized Difference Vegetation Index (NDVI) is a commonly applied vegetation index which has been related to important vegetation characteristics such as type, health, LAI, primary productivity, phenology, and biomass (Paruelo *et al.* 1997; Turner *et al.* 1999; Elmore *et al.* 2000; Jensen 2000; Running *et al.* 2000; Pocewicz *et al.* 2004; Archibald *et al.* 2007; Butterfield *et al.* 2009; Santin-Janin *et al.* 2009). In general, vegetation indices exploit the fact that chlorophyll content causes green vegetation to reflect strongly in the near

infrared (NIR) portion of the electromagnetic spectrum and absorb in the red wavelengths. Thus, the NDVI is best described as a measure of “greenness” (Butterfield *et al.* 2009) The NDVI is calculated from remotely sensed reflectance data using Equation 5,

$$\text{NDVI} = \frac{\text{NIR} - \text{Red}}{\text{NIR} + \text{Red}} \quad (\text{Equation 5})$$

where NIR is the reflectance signal in the near-infrared radiometric band, and Red is reflectance in the red band (Rouse *et al.* 1974; Jensen 2000).

Images collected by Landsat-5 TM at 30 m spatial resolution, and made freely available by the United States Geological Survey (USGS), were radiometrically corrected to exoatmospheric reflectance using ENVI software and used to calculate NDVI across the study area at eight- to sixteen-day time intervals (depending on cloud cover) for 2006-2009 (Rouse *et al.* 1974; Turner *et al.* 1999; Chander *et al.* 2003). Images with greater than 10% cloud cover were not used. Landsat-5 TM has collected spectral data in six reflective bands since March 1, 1984, making Landsat data uniquely suited to relatively long-term, large-scale analysis of seasonal vegetation change. Values of NDVI for each sample site (resampled from the nine pixels nearest the site location) and each image date were sampled using the Extraction tool in ArcGIS 9.3, and the monthly average NDVI for each location was calculated for those months with multiple images. A four-year monthly-average NDVI was calculated by averaging each month’s NDVI over the four-year period analyzed; average monthly NDVI data for each study site were fit with a fifth-order polynomial trendline to allow inference of peak productivity dates. Values of

NDVI during the winter months (November through February) were rare because cloud cover is especially prevalent during that period; thus, values from Jan, Feb, Nov, and Dec may be weaker approximations of the winter-season NDVI. The maximum annual “peak” NDVI was chosen from the average monthly NDVI set as an objective estimate of the relative amount of vegetation cover at the study sites, which allowed us to avoid error associated with the early- and late- season images.

The two different indirect measures of vegetation cover, PAI and NDVI, were found to be suitable methods of assessing vegetation density at different spatial and temporal scales, and have been found to correlate well with each other (Running *et al.* 1986; Curran *et al.* 1992). However, each method measures a distinctly different property, and neither measures vegetation productivity or biomass directly. For example, when used to track phenology of annual grasses in a previous study, NDVI was shown to record peak “greenness” 40 days earlier than peak LAI and peak biomass were reached in annual grass species (Butterfield *et al.* 2009). Complete details of NDVI data assembly and processing are included in Appendix D.

3.4. Soil Properties

Soil textural analysis was performed on soil samples of approximately 300 g to 500 g from each of the 121 EC-TM sensor locations. Soils were classified using the USDA Textural Triangle classification system. Soil texture was determined using two methods, mechanical analysis (hydrometer/sieve method) and laser diffraction analysis. The two methods of particle size analysis, mechanical and laser diffraction, differ in

many aspects of how they measure particle size distributions of materials, but results from the methods are linearly correlated to one another (Konert *et al.* 1997; Beuselinck *et al.* 1998; Arriaga *et al.* 2006; Malvern Instruments Ltd. 2009). Laser diffractometry determines particle size fractions on a volume basis, while hydrometer and sieve analysis determine particle size fractions on a mass basis (Syvitski 1991; Beuselinck *et al.* 1998). The laser diffraction method is advantageous when numerous soil analyses must be conducted because it can determine the relative fractions of fine materials (fine sand, silt, and clay) more rapidly and precisely than the hydrometer method, albeit under a different set of assumptions (Konert *et al.* 1997; Arriaga *et al.* 2006).

Twenty unique soil samples, plus random replicates, were dry sieved to remove gravel (particles > 2 mm in diameter) and split into subsamples. One subsample was analyzed mechanically via hydrometer and wet-sieve methods according to ASTM D422-63 to determine mass fractions of sand, silt, and clay particles. The other subsample was dry-sieved to remove particles > 0.075 mm, soaked for ≥ 16 hours in a 4% solution of sodium hexametaphosphate dispersing agent, and was then analyzed using a Malvern Mastersizer 2000 laser diffractometer to determine volume percent of fine sand, silt, and clay in the < 0.075 mm fraction. The particle refractive index was assumed to be 1.5, and the particle absorption index was assumed to be 1 (Sperazza *et al.* 2004). The laser diffraction results were scaled to the whole < 2 mm fraction to determine the mass fractions of sand, silt, and clay. A linear correlation model between laser diffraction and hydrometer/sieve results, developed from 15 samples (replicates averaged where present) from four soil moisture sites, allowed particle size distribution results obtained via laser

diffraction to be converted to an estimation of the more traditional mechanical (hydrometer-sieve) results. Clay fractions were not sufficiently diverse among the soils tested to create a reliable linear relationship between the methods, so hydrometer - equivalent fractions of sand and silt were estimated from laser diffraction results using the linear correlation, while equivalent clay fractions were determined by difference. The remaining 101 soil samples were analyzed via wet sieving and laser diffraction to determine the sand, silt, and clay fractions, and the linear correlation model was used to convert the laser diffraction results to estimates of results via mechanical analysis which are reported in this paper. The goal of converting the results was to make our reported soil texture information readily relatable to other studies of soil texture which more commonly utilize mechanical methods of particle size analysis than the newer laser diffraction method. The USDA soil classification system was used to classify the sub-2 mm fraction of soil (USDA 1999). Complete details of the sieving and laser diffraction methodologies are provided in Appendix E.

3.5. Soil Carbon

Soil samples were collected in duplicate for analysis of total carbon and total nitrogen contents at all eight soil moisture stations during the summer of 2008. Samples were collected as soil cores 30 cm deep in 5 cm increments to examine both spatial and profile trends. An AMS Standard Core Sampler with Slide Hammer was used to collect the samples. Field samples were dried in an oven for 24 hr at 105°C and sieved to remove the fraction > 2 mm in diameter. The < 2 mm fraction of each sample was homogenized,

sub-sampled and disaggregated in a mortar and pestle. Bulk density was approximated for each 5 cm core by dividing the air-dried (24 hr) soil weight by the volume of the sampling chamber. Soils were stored at -5°C before and after processing. Complete details of the preparation methodologies are provided in Appendix F.

Total carbon (C) and nitrogen (N) contents were determined through the dry combustion method using a Thermo Scientific Flash EA 1112 Elemental Analyzer. During analysis triplicates were run randomly on every eighth sample, with laboratory blanks and aspartic acid standards run for quality assurance of the results. To determine respective fractions of organic and inorganic carbon, selected subsamples were pre-treated with 2-3 drops of 4 M HCl and allowed to effervesce to completion in a fume hood. Pre-treated samples were then oven-dried for 24 hr at 105°C and analyzed using dry combustion as described above. Inorganic carbon was determined as the difference between total and organic carbon fractions (Kunkel, personal communication, 2009).

4. RESULTS

4.1. Soil Water and Soil Temperature

An overview of general trends in daily mean soil water and soil temperature measured at eight sites, placed on north and south aspects at four elevations across the study area, is presented. Appendix I contains detailed descriptions of soil moisture and soil temperature observations at each site, as well as comparisons of behavior on paired north and south aspects and along the elevation gradient. Plots of soil moisture and soil temperature time series at the original 10 minute sampling intervals are provided in Appendix H, but are not discussed in this thesis. Results and parameters used to determine wilting point and field capacity water contents for each site are provided in Table A.2.

North-facing soils contained more water and had lower temperatures than south-facing soils at a given elevation, though the differences are minimal at the highest elevation sites (Figure B.11). At a given elevation, the north aspect had higher soil water content than the south aspect (Figure B.11). Over the common period of record, north aspects had higher mean profile-averaged water contents than south aspects at the highest, mid-high, mid-low, and lowest elevation sites, by 0.04, 0.03, 0.07, and 0.06 volumetric water content, respectively (Table A.3). The profile-averaged mean soil temperature over the same time period was 1.0°C, 4.7°C, 7.4°C, and 7°C higher on south

aspects relative to north aspects from highest to lowest elevations, respectively (Table A.3). The same trend is evident when looking at time series of the study sites (Figures B.12, B.13, B.14, and B.15); at a given elevation, the north aspect generally had higher water content than the complimentary south aspect, and was consistently cooler. Soil temperature varies with aspect and correlates negatively and very strongly with elevation on both aspects (Figures B.11, bottom and Figure B.16). The difference in soil water content and soil temperature between north and south aspects is smallest at the highest elevation sites (Figure B.11 and Figure B.16). Soil temperature at 2 cm bgs closely tracked seasonal air temperature trends (Figure B.17).

The average soil depth is 16 cm (mid-high elevations) to 50 cm (mid-low elevations) deeper on north aspects relative to south aspects at a given elevation, except at the highest elevation sites where the south aspect soil was somewhat deeper (7 cm) than that on the north aspect (Figure B.18, Table A.4). The spatial variability in soil depth is considerable; the range in soil depth among the four pits at a site (within about 3 to 4 m of each other) was as little as 7 cm (high elevation) and as large as 39 cm (mid-high) on north aspects, and as little as 3 cm (low elevation) and up to 25 cm (mid-low) on south aspects (Table A.4). This range is comparable to that observed by Tesfa *et al.* (2009) for soil depth determinations collected within 2-3 m of each other in the study area.

North aspects stored from 1.1 to 3.7 times as much water as south aspects at a given elevation and higher elevations stored up to 3 times more water than the lowest elevations at a given aspect (Table A.3). Mean water storage (over the common period of record) on the north aspect exceeded that on the south aspect by 1.5, 4.8, 11.2, and 8.4 cm

on the highest to lowest elevation sites, respectively (Table A.3). To recapitulate, soil water storage is the product of the soil depth and the site- and profile-averaged soil water content at a site (See Methods). Thus, the difference in soil water content between north and south aspects is amplified by the deeper north-facing soils, producing large differences in soil water stored on north and south aspects with the exception of the highest-elevation sites, which show similar soil water storage. The spatial distribution of soil water storage varies strongly by aspect (Figure B.19), and shares a positive correlation with elevation which is weak on north aspects ($R^2 = 0.54$), and strong on south aspects ($R^2 = 0.93$) (Figure B.20).

North-facing soils had soil water storage capacities 0.1 cm, 4.2 cm, 10.5 cm, and 6.1 cm greater than south aspects at the highest to lowest elevations, respectively (Table A.3). Soil water storage capacity increased with elevation on the south aspects, but did not change consistently with elevation on the north aspects (Table A.3). Soil water storage capacity reflects the mean soil depth and the field capacity of a soil; a soil's potential for storing water is only as great as the depth of soil available to store water in, and the amount of water that the soil can hold before added water is lost to drainage (See Methods). A ratio of mean annual precipitation to soil water storage capacity shows that north-facing soils at the mid-high to lowest elevations can store a greater proportion of the annual precipitation than south-facing soils at the same elevations; the ratio is very similar for both aspects at the highest elevation sites (Table A.3). The field capacity water content of each soil determined from field data at each site was from 0.02 to 0.08 (cm³/cm³) lower than that predicted assuming a matric potential of -0.03 MPa, implying

that gravitational drainage in natural soils of the study area actually occurs in drier soils than would be assumed using common laboratory-derived parameters (Clapp *et al.* 1978; Laio *et al.* 2001; Dingman 2002).

During winter and spring we observed evidence of migrating wetting fronts, hydraulic connectivity and drainage at the soil-bedrock interface at all sites. Migrating wetting fronts were inferred from the exceeding of field capacity at successive depths during fall wet-up at each site (Figures B.21, B.22, B.23, B.24, B.25, B.26, B.27, and B.28) (See Methods), recognizing that the only source of soil water at a given depth is precipitation or infiltration from above (Yenko 2003; McNamara *et al.* 2005; Seyfried *et al.* 2009). Once field capacity was exceeded at the soil-bedrock interface, it is likely that the soil water was able to drain vertically into the bedrock, or perhaps flow laterally along the soil-bedrock interface. Hydraulic connectivity was inferred from simultaneous peaks in soil moisture at all depths of the soil profile in response to input events (rainfall or snow melt). These observations provide evidence for vertical and potentially lateral flux and hydraulic connectivity over the soil profiles during the winter wet period.

Examination of the series of figures (B.21 through B.28) illustrates that the duration and timing of this period is unique to each site. Field observations confirm that vegetation growth was at a minimum during the winter wet period at each site, which in addition to the low temperatures indicates negligible evapotranspiration flux. Thus, during winter the soil water content was generally high, and fluxes were likely to occur as vertical or lateral redistribution in soil or as drainage to bedrock.

Soils began drying down after snow melted and soil temperatures began rising, but infiltration associated with spring rains returned the profiles to field capacity and reestablished hydraulic connectivity over the profile. The spring wet, high-flux period was previously observed by McNamara *et al.* (2005) in the study area. Figures B.12, B.13, B.14 and B.15 illustrate that soil water content generally declined after the snow pack disappeared, unless the timing of snow removal coincided with inputs from spring rain. At all sites, field capacity was exceeded at the soil-bedrock interface while snow pack was present. When the snow pack disappeared, soils exceeded field capacity at depth and then soon began drying. Spring rains then returned the profile to field capacity, even at the bedrock depth (Figures B.21, B.22, B.23, B.24, B.25, B.26, B.27 and B.28).

Snow melted and soil temperatures began rising earlier on south aspects and at lower elevations (Figures B.12, B.13, B.14, B.15). Snow melted from south aspects up to 66 days earlier than north aspects, and at a given aspect (south) snowmelt occurred up to 88 days earlier at the lowest elevation than the highest elevation sites (Table A.3). The soil surface (2 cm bgs) warmed above 5°C (our chosen threshold for initiation of favorable growth conditions) up to 28 days earlier in spring on the south aspect than on the north aspect at a given elevation, and at a given aspect (south) the lowest elevation warmed above 5°C up to 65 days earlier in spring than the highest elevation (Table A.3).

Soils became dry earlier on south aspects and at lower elevations. We used an estimated wilting point for each soil to represent a “dry” state in order to account for the different water retention properties of different soils at the study sites (See Methods). The date of dry down to wilting point water content is compared for each north-south aspect

pair in Figures B.12, B.13, B.14, and B.15. A given north-facing soil remained above the wilting point up to 53 days longer into the growing season than a south-facing soil at the same elevation, and at a given aspect, a high elevation soil retained plant available water up to 63 days longer than a lower elevation soil.

Summer rain wetted the soil-bedrock interface at some sites. An August rain event wetted the soil-bedrock interface at the highest elevations, and at south aspects at the mid-low and lowest elevations; mid-high sites and lower elevation north aspects did not wet up at depth in response to the August rain (Figures B.21, B.22, B.23, B.24, B.25, B.26, B.27, and B.28). Deep wetting induced by this rain was likely due to the unusually high intensity of the storm. Such large summer precipitation events are rare in the study environment (Figure B.4) (McNamara *et al.* 2005). The lack of response in deep soils at some sites offers evidence for the supposition that evapotranspiration generally removes soil water delivered as summer precipitation (McNamara *et al.* 2005).

Soil water was highly variable in space, while soil temperature showed much less spatial variability. Error bars on the time series shown in Figures B.12, B.13, B.14, and B.15 represent the standard deviations of profile-averaged values among the four pits at each site. In each figure, the error bars on the soil water content series are far larger than those on the soil temperature series, indicating the much higher spatial variability in soil moisture than in soil temperature. Soil water content appeared to become most spatially variable during wet periods, particularly during wet up from previously dry periods as occurs during spring and summer rain events. This is consistent with the conclusions of some previous workers (Hawley *et al.* 1983; Famiglietti *et al.* 1998; Western *et al.* 1999),

although others have found that soil water becomes most spatially variable during drying periods (Famiglietti *et al.* 1999; Hupet *et al.* 2002).

4.2. Vegetation Distribution

Vegetation is generally denser at higher elevations and on north-facing slopes. The date of peak canopy coverage occurs later in the growing season at higher elevations (Figures B.29, B.30). NDVI values were field checked against Plant Area Index (PAI) measurements collected at approximately equivalent dates over the 2009 growing season and were found to be strongly linearly correlated ($R^2 = 0.79$, Figure B.31). The strength of linear correlation of Leaf or Plant Area Index with remotely sensed spectral signals compares well to results of other studies in a variety of ecosystems, although some workers have reported that the relationship becomes asymptotic at PAI values above around five (Running *et al.* 1986; Running *et al.* 1989; Curran *et al.* 1992; Turner *et al.* 1999; Pocewicz *et al.* 2004). Generally, vegetation cover is greater, and peak canopy cover occurs later, on north aspects and at higher elevation in the study area. The NDVI will be discussed below, as it represents longer-term trends in vegetation patterns (four seasons) than the PAI (one season).

The highest elevation sites (HN and HS) are occupied by open forests of Douglas-fir (*Pseudotsuga menziesii*) and Ponderosa pine (*Pinus ponderosa*). The inferred peak of about 0.61 NDVI generally occurs in early August on the north aspect HN, and on the south aspect HS the peak of 0.64 NDVI occurs in July (Figure B.29). The duration of productivity and the coverage at peak is similar at both sites, although the south aspect

develops a higher NDVI at its peak. Trends captured by the NDVI data confirm visual observations of vegetation development and relative canopy cover at both sites.

Vegetation cover is approximately equal on the north and south aspects, and decline in cover might begin slightly earlier on the south aspect relative to the north aspect at the high elevation sites.

The mid-high elevation sites (MHN and MHS) are occupied by very different ecological communities. The mid-high north aspect, MHN, is vegetated with open forests of pine and fir, while the mid-high south aspect, MHS, is covered in sagebrush shrubs (*Artemisia* spp.) and grasses. The inferred peak of 0.55 NDVI occurs in mid-June on the north aspect, while the peak of 0.32 NDVI occurs in late May on the south aspect. It appears that the peak vegetation cover occurs around 20 days earlier on the south aspect than the north. The differences captured using the NDVI match well with trends in vegetation development and relative canopy cover at both sites. Vegetation cover on the south aspect begins declining about 20 days sooner than the north aspect, and the peak NDVI on the north aspect is greater than on the south aspect at the mid-high elevation sites.

The mid-low elevation sites (MLN and MLS) are occupied by sagebrush shrub and grass ecosystems, with a higher density of shrubs and grasses occurring on the north-facing slope. The inferred peak of 0.45 NDVI occurs in early June on the north aspect, MLN, while the peak of 0.37 NDVI occurs in mid-April on the south aspect, MLS (Figure B.29). Peak productivity occurs about 50 days earlier on the south aspect than on the north aspect. Trends in vegetation development and relative canopy cover seen in the

NDVI reflect those observed visually at the sites. Peak NDVI is greater on the north aspect, and canopy cover begins declining about 50 days earlier on the south aspect relative to the north aspect at the mid-low elevation sites.

The low-elevation sites (LN and LS) are inhabited by grass and sagebrush shrub communities, with more dense grass and shrub cover on the north aspect relative to the south. The inferred peak of 0.39 NDVI occurs in late May on the north aspect LN, and the peak of 0.30 NDVI occurs in late April on the south aspect LS. Peak vegetation cover occurs about 30 days earlier on the south aspect than on the north. Vegetation cover on the south aspect begins declining about 30 days sooner on the south aspect, and peak NDVI is greater on the north aspect at the low elevation sites.

4.3. Soil Properties

Soils on north aspects tend to occupy finer textural classes (using the USDA soil classification system) than those on south aspects (Figures B.32 through B.35). Table A.5 provides the size fraction results of paired laser diffraction and mechanical (hydrometer/sieve) analyses, and Figure B.36 displays the linear correlation between methods. Overall, north-facing soils are classified in the USDA classification system as gravelly sandy loams, while south-facing soils classify as gravelly loamy sands to gravelly sandy loams (Appendix G, Figures B.32 through B.35) (USDA 1999). An exception is the low elevation north-facing site LN, which classifies as a gravelly loam for depths from 2 cm to 30 cm bgs and contains a distinctly greater silt fraction than soils at the other sites (Figures B.32 through B.35). Soils with a greater fine fraction may hold

more water at complete saturation, and will retain more water as they dry (Table A.2). The following discussion will address soil textures as determined using only the sub-2 mm diameter fraction in accordance with the USDA soil classification system (USDA 1999).

The difference in soil texture on north aspects is determined largely by fraction of silt. While silt content ranges widely from 4.6% to 42.3% by mass across all samples, clay content varies to a lesser degree, from 7.2% to 12.7%. Increases in silt are primarily accommodated by decreases in the sand fraction. The distinctly high silt content at LN accounts for much of the range in silt content; when LN is excluded, the range in silt is from 4.6% to 29.7% and the range in clay is from 7.2% to 11.1% for all sites and depths. Averaged across all pits and depths, the silt content of soils on north aspects exceeds that of south aspects by 3.4% (highest elevation), 15.1% (mid-high elevations), 8.3% (mid-low elevations), and 24.8% (lowest elevation). Averaged across all pits and depths, the clay content of north-facing soils exceeds that of south aspects by 3.2% (lowest elevation), 1.9% (mid-high elevations), and 0.51% (mid-low elevation), while the average clay content at the highest elevation sites was actually 0.1% lower on north aspects relative to south aspects. Although clay contents are consistently very low in all soil samples, the amount of clay in soil is up to 41% greater on the north relative to south aspect at the lowest elevation sites, illustrating that the difference in clay content can be noteworthy, but is not as large as the differences in silt content.

Soil textures do not differ significantly with depth (Figures B.37 through B.39). Figures B.37 through B.39 show that soil texture does not change systematically with

depth, except at the low elevation north aspect which has increasing sand and decreasing silt with depth. Clay fraction changes very little at all sites except the lowest elevation north-facing site, where the clay fraction decreases by up to 44% (from 9% to 13% by mass) moving from 0 to 70 cm bgs over the profile; even at the lowest elevation north aspect, clay content is relatively small. Fractions of sand, silt, and clay (as mass percent) did not correlate significantly with depth over all samples (sand, $r = 0.017$, $p = 0.805$; silt, $r = -0.031$, $p = 0.653$; clay, $r = 0.095$, $p = 0.175$; $n = 206$, where r is the correlation coefficient, and p is the probability of the observed r given the null hypothesis of no correlation, $r = 0$). The mass percent of gravel did correlate significantly and positively with depth, but the relationship was not strong ($r = 0.366$, $p = < 0.0001$, $n = 206$).

Soils on north aspects have lower bulk densities than those on south aspects (Figure B.40, Table A.6). Bulk density, the ratio of the mass of solids to the total soil volume, reflects the porosity, texture, structure, and organic content of a soil (Brady *et al.* 2002; Hillel 2004). Bulk density is higher on the south aspect at all four elevations sampled, although the difference is small at the high elevation sites; the high elevation south aspect has a bulk density about 0.07 g/cm^3 greater than the north aspect, while the mid-high elevation south aspect bulk density is 0.39 g/cm^3 greater, the mid-low elevation south aspect is 0.14 g/cm^3 greater, and the low elevation south aspect is 0.23 g/cm^3 greater than the north aspect at the complimentary elevation. The difference in bulk density at different aspects does not appear to change systematically with elevation.

4.4. Soil Carbon Content

Soil carbon content is generally higher at higher elevations, north aspects, and shallower portions of the soil profile. Figure B.41 shows the trends in percent by weight soil carbon content over the 0 to 30 cm profile at each site. Table A.7 presents the results of percent carbon by weight for the 5 cm increments over a profile from 0-30 cm bgs at each site and Table A.8 presents results for total carbon in the upper 30 cm of soil at each site, in $\text{kg}/(30 \text{ cm} \cdot \text{m}^2)$. Inorganic carbon was found to be a negligible ($< 1\%$) component of the total carbon content; thus, the total carbon values represent organic carbon in all samples (M. Kunkel, personal communication, March 2010). The highest elevation sites contain the greatest total carbon content in the upper 30 cm of soil (HS = $5.47 \text{ kg}/\text{m}^2$, HN = $4.27 \text{ kg}/\text{m}^2$) followed by the north-facing soils at mid-low, mid-high, and low elevations (MLN = $3.95 \text{ kg}/\text{m}^2$, MHN = $3.87 \text{ kg}/\text{m}^2$, LN = $3.42 \text{ kg}/\text{m}^2$), and then the south-facing soils at mid-high, mid-low, and low elevations (MHS = $1.09 \text{ kg}/\text{m}^2$, MLS = $0.94 \text{ kg}/\text{m}^2$, LS = $0.81 \text{ kg}/\text{m}^2$). Over the 30 cm profile sampled, north aspects hold 3.5 to 4.2 times as much carbon as complimentary south aspects at similar elevation, except at the high elevation sites where the south aspect contains 28% more carbon than the north aspect. Soil carbon content differs most among all the sites within the shallow portion of the soil profile, ranging from $0.41 \text{ kg}/\text{m}^2$ to $3.86 \text{ kg}/\text{m}^2$ carbon in the 0-10 cm depth increment as shown in Figure B.41 and Table A.8. Carbon content generally declines with depth, converging toward low values of between 0.20 to $1.17 \text{ kg}/\text{m}^2$ carbon at 30 cm bgs.

5. DISCUSSION

5.1. Water Balance

The spatial distribution of soil water storage is strongly related to aspect and elevation, indicating that the primary physical mechanisms controlling soil water are those which are topographically distributed (Figure B.20, Table A.9). However, aspect and elevation are not in themselves physical mechanisms controlling soil water distribution; rather, they are proxies for other mechanistic variables. Among those mechanistic variables are precipitation (which increases moving up the elevation gradient), air temperature (which decreases moving up the elevation gradient) (Figure B.3), and potential insolation (which increases moving from north to south aspects, and increases to a lesser degree with higher elevations) (Figures B.5 and B.6). Precipitation varies monotonically with air temperature because each was estimated from the elevation of each study site using the orographic relationship provided in Figure B.3. The correlations of soil water with precipitation, air temperature, and potential insolation indicate a dual importance of water input (precipitation) and energy (insolation) in dictating soil moisture conditions and vegetation growth, an observation that has been made by many others (Table A.9) (Noy-Meir 1973; Monteith 1981).

The narrow timing of wet and warm soil conditions indicates that hydrologic processes in the study environment are sensitive to spring precipitation. Our findings

indicate that conditions for hydraulic connectivity and one or both of vertical redistribution and lateral flow at the soil-bedrock interface are met during winter and spring at all sites, and in response to large summer precipitation events at some sites (Figures B.21 through B.28). This evidence indicates that the potential for deep drainage and lateral flow along the bedrock interface occurred for 125 to 225 days at different study sites between 11/20/2008 and 9/1/2009; these conditions were triggered by both snow melt and spring rain. Because a chloride mass balance study has suggested that groundwater recharge across the watershed may be small ($\leq 11\%$ annual precipitation), wetting at the bedrock interface may be more likely to produce lateral flow, rather than deep drainage to groundwater, at all but the highest elevations where groundwater recharge may be higher ($\leq 22\%$ annual precipitation) (Aishlin 2006).

The duration of soil water into the spring and summer is strongly influenced by spring rains. Without spring rains, soils would have dried much sooner in the summer. By visually projecting the dry-down curve following snowmelt in Figures B.12 through B.15 it is evident that soils would have dried down weeks or months sooner if not for spring precipitation. Winter precipitation is important in recharging the soil reservoir, but once field capacity is exceeded, further soil water inputs from winter precipitation are lost from the soil reservoir by surface runoff, deep drainage, or lateral flow. According to our calculations of storage capacity (field capacity * soil depth) at the study sites, an empty soil reservoir can be fully recharged by water inputs ranging from as little as 6 cm to as much as 16 cm (Table A.3). As shown in Figure B.43, mean annual precipitation at each study site is much larger than the water storage capacity of the soil. If approximately half

of the annual precipitation falls as snow in the study area (McNamara *et al.* 2005), it appears that much of the snow melt water would be lost from the soil due to the small storage capacity and the early time of snow melt during a period of low temperatures, low insolation, and inactive evapotranspiration. Regardless of whether winter precipitation arrives as rain or snow, the soil water storage capacity is quickly satisfied in late winter and early spring, and the low temperatures and dormant vegetation limit drawdown of the soil reservoir. Much of the winter precipitation, then, is expected to drain from the soils as excess water. In contrast, spring precipitation reaches unsaturated soil at a time when evapotranspiration is more active and a given precipitation input can be lost from the soil profile over a period of about one to four weeks. It is only through repeated spring rain events that elevated moisture conditions are maintained into the summer. Average spring (April-May-June) precipitation is sufficient to recharge the soil water reservoir at the ecologically important time of warming temperatures, rising insolation, and active evapotranspiration (Figure B.43). The re-establishment of hydraulic connectivity and bedrock flow at all of the study sites in response to spring precipitation provides evidence of the capacity of spring rains to recharge the soil water reservoir. Thus, the magnitude and frequency of spring precipitation is important in determining the duration of soil water into the summer.

5.2. Implications for Ecologic Functioning and Carbon Cycling

In semi-arid environments, soil moisture dictates vegetation productivity through photosynthesis and transpiration (Noy-Meir 1973; Rodríguez-Iturbe *et al.* 2004); our

observations of vegetation cover and soil moisture distributions are consistent with this paradigm. Table A.9 presents values of the coefficient of determination, R^2 , in correlations between variables including vegetation cover (peak NDVI), soil carbon, mean soil water content, mean soil water storage, mean soil temperature, precipitation, air temperature, and potential insolation. Soil water and vegetation distributions are correlated, which is consistent with the importance of soil water in driving primary productivity, particularly in water-limited environments (Noy-Meir 1973). Vegetation and soil carbon are also strongly correlated ($R^2 = 0.87$) (Table A.9). Furthermore, the correlations of vegetation distribution with the primary controls on soil water (precipitation, air temperature and potential insolation), supports the concept that biomass in the study environment is closely linked to the spatial distribution of insolation, and the elevation-driven gradients in precipitation and air temperature.

The distribution of mean soil moisture, vegetation cover, and soil carbon are negatively correlated to potential insolation and air temperature and positively correlated to precipitation, consistent with trends observed in water-limited environments (Noy-Meir 1973; Ivanov *et al.* 2008b). When soil carbon content, peak NDVI, and mean soil water storage were modeled by forward selection linear regression with precipitation (which varies monotonically with air temperature because each was calculated from elevation as shown in Figure B.3) or potential insolation as the single most significant independent variable, the model explained 38%, 64%, and 34% of the spatial variability in each dependent variable, respectively. However, when precipitation (or air temperature) and potential insolation were both included as independent variables in the

multiple regression, the model was able to explain 70%, 84%, and 85% of the spatial variation in soil carbon, peak NDVI, and soil water storage, respectively. The results of the forward regression are provided in Table A.10. This exercise is not intended to produce a full predictive model for ecosystem carbon distribution, but rather shows that using the distributions of both precipitation (or air temperature) and potential insolation improves the degree to which spatial variability in vegetation cover, soil carbon, and soil water is explained.

The seasonal timing of precipitation, air temperature, and insolation are important in controlling vegetation productivity. The densest vegetation cover is observed where wet soils, warm temperatures, and high insolation coincide in time; the confluence of these environmental conditions is limited to the spring and early summer months. Figure B.42 shows the relative growing season lengths and their timing in relation to the annual observed insolation and temperature curves, where peak insolation and peak temperature can be viewed as approximating the height of summer. In spite of the earlier timing of snow melt and soil warming on south aspects, the growing season at a given elevation is longer on north aspects than on south aspects by up to 43 days (Table A.3). At a given aspect, the potential growing season is longest at the lowest elevations. Because vegetation cover is least dense at the lowest elevations, growing season length alone does not appear to explain why vegetation is denser at higher elevations. Instead, the distribution of vegetation may relate more strongly to the timing of the potential growing season in relation to peak summer temperature and insolation. Sites at which plant-available soil water endures further into summer are the sites which show relatively high

vegetation cover. Vegetation is most sparse at sites where soil is dry when peak temperatures and insolation occur. At the lowest elevation sites it appears that although the potential growing season is relatively long, it occurs early in the year when temperature and insolation are too low to allow rapid vegetation growth. Thus, the importance of growing season length may be dependent upon the position of the growing season relative to seasonal temperature and insolation trends (Figure B.42).

From another perspective, the vegetation distribution may also depend on the length of “lost time” during the growing season, perhaps more so than the period of optimal growth conditions (Monteith 1981). For example, Rodriguez-Iturbe *et al.* (2001a; 2004) describe plant water stress as comprising three components of soil water content in relation to a threshold water content, including the frequency, duration, and intensity of the plant water stress period. The stress period represents a time during which soil is in an ecologically unfavorable state of high water stress caused by dry soil, intense heat and high insolation. In this study, the south-facing and lower elevation sites experience the annual equivalent of greater total plant water stress, including greater frequency, duration, and intensity of stress (Figures B.12 through B.15). Growth on south aspects is brought to an early end by high evapotranspiration demands (high temperature and insolation) acting on a relatively small water storage capacity, resulting in a prolonged episode of severe water stress which shuts productivity off early in the summer. The water stress regime may explain the distribution of vegetation type as well as density, as summer water stress is likely to prohibit establishment of trees, which develop slowly and germinate later in spring. In contrast, grasses germinate in fall and develop root systems

which can respond rapidly to shallow soil water when temperatures rise in spring (Daubenmire 1968). Growth on south aspects may be further inhibited by intense radiation leading to higher evaporation rates, early soil dry down and possibly additional heat stress due to high leaf temperatures (Taiz *et al.* 1998). On north-facing slopes, insolation is moderated, which favors productivity by reducing evaporative demand at the soil surface (Ivanov *et al.* 2008b). Furthermore, the deeper, more finely-textured and more organic carbon-rich soils on north aspects provide a greater water retention capacity, and a deeper potential rooting zone.

An August rain event wetted the soil-bedrock interface at the highest elevations, and at south aspects at the mid-low and lowest elevations, while mid-high sites and lower elevation north aspects did not respond at depth (Figures B.21, B.22, B.23, B.24, B.25, B.26, B.27, and B.28). Deep wetting was loosely associated with sites having shallow soils and low water storage capacities, but neither appears to be the sole explanation for this trend. For example, the highest elevation sites (which did wet at depth) have soil depths and storage capacities similar to other sites (such as LN and MHS) which did not wet up at bedrock. Instead, assuming that summer precipitation was evenly distributed throughout the watershed, the lack of deep wetting at mid-high sites and lower elevation north aspects may reflect rapid uptake of shallow soil water through evapotranspiration by “intensive exploiter” type vegetation such as grasses, which are abundant at these sites (Ehleringer *et al.* 1991; Rodriguez-Iturbe *et al.* 2001a; McNamara *et al.* 2005; Archibald *et al.* 2007). In August, grasses are dormant on the lower elevation south-facing aspects (MLS and LS), while on the lower elevation north aspects (MLN and LN), grasses were

more dense and remain active (Figure B.29). Active grasses on the lower-elevation north aspects may have taken up infiltrating sporadic summer rain, preventing water from infiltrating to the soil-bedrock interface as occurred on the complimentary south aspects. At the highest elevations, trees did not take up shallow soil moisture and summer rains reached the soil-bedrock interface, as could be expected from a plant functional group which responds to deeper water supplied over winter and early spring (Ehleringer *et al.* 1991; Rodriguez-Iturbe *et al.* 2001a; Archibald *et al.* 2007).

Although climate change is anticipated to impact many characteristics of the environment in southwest Idaho and elsewhere, this study indicates that some predicted changes are likely to cause more severe responses than others. In the region, air temperature is expected to rise, especially winter temperatures (Christensen *et al.* 2007; Field *et al.* 2007). Mean annual precipitation in the region may increase, but is anticipated to decrease in summer (Christensen *et al.* 2007). Snow pack is expected to decrease, and snow melt is expected to occur increasingly early in the year (Hamlet *et al.* 2005; Stewart *et al.* 2005; Mote 2006). Furthermore, many locations in the mountainous American west record that rain now composes a higher fraction of annual precipitation than snow relative to historic records (Knowles *et al.* 2006). Earlier spring warming has produced a longer growing season in several US and Canada locations (Cayan *et al.* 2001; Feng *et al.* 2004; Field *et al.* 2007). Annual evapotranspiration appears to have increased as well (Field *et al.* 2007; Hamlet *et al.* 2007). Of the anticipated changes, those which are most likely to affect the soil moisture and vegetation distributions will be changes to insolation, precipitation, and air temperature, according to our results. In the

study environment, changes to insolation are not anticipated (unless cloud cover changes considerably). Summertime increases in temperature will potentially produce an increase in rates of soil dry down. Increases in air temperature may have mild to moderate effects on vegetation in winter due to low insolation and may result in delivery of more winter precipitation as rain rather than snow (Knowles *et al.* 2006). However, our observations suggest that this significant phase change may not have a dramatic impact on soil moisture dynamics, especially with respect to the amount of moisture available during the growing season. Due to the relatively small size of the soil water reservoir, the impact of predicted increases in precipitation will be highly dependent on timing.

Although snow accumulation and melt strongly influence stream discharge in the study area (McNamara *et al.* 2005; Williams *et al.* 2009), our results indicate that the duration of soil water within the watershed, which in turn dictates the length of the growing season, relies heavily on the amount and timing of spring precipitation. Although winter precipitation is important in recharging the soil water reservoir, our findings suggest that the form of winter precipitation as rain or snow may not be critical because storage capacity is small and evapotranspiration demands are minimal; once the soils are recharged to field capacity, additional water does not contribute appreciably to water storage (Figure B.43). Spring precipitation, on the other hand, is essential in recharging soil water while evapotranspiration withdraws water from the reservoir. Spring precipitation arrives when soils are warm and insolation is sufficiently high to support rapid evapotranspiration and respiration. Thus, the amount and timing of spring precipitation exerts an important influence on water and carbon fluxes in this

environment. The importance of warm season precipitation to hydrologic and ecologic systems has been suggested by modeling experiments (Gordon *et al.* 2004; Vivoni *et al.* 2009) and in some empirical studies (Chou *et al.* 2008).

Regardless of whether a shift in climate leads to earlier or later snow melt dates, the observations made here underscore the importance of the timing and amount of spring precipitation in impacting the duration of the growing season, the duration and severity of the water stress period, and, by extension, the amount of vegetation productivity. The strong correlations we observe in the distributions of vegetation cover and soil carbon content (Figure B.44) indicate that the changes which impact vegetation productivity may have serious implications for soil carbon storage as well. Modelers seeking to predict the response of water-limited, seasonally out-of-phase (temperature and precipitation are asynchronous) ecosystems will benefit from focusing on changes to the amount and timing of warm season precipitation.

We have attempted to simplify the system in order to identify its most important characteristic controls, and in doing so we have made a number of assumptions. For example, we have assumed that the single year of soil water measurements can represent spatiotemporal trends operating over longer time periods, allowing us to compare them with variables which reflect multi-year to decadal time scales such as soil carbon content, NDVI, and average annual precipitation. While the precipitation received during the study year was above average for spring and summer (Figure B.4), we have unequivocally observed that the system is highly sensitive to that precipitation. While this study identifies key sensitivities and controls in the study environment, we acknowledge

that the distribution and timing of precipitation, air temperature, and insolation are not the only factors determining the spatial distribution of soil moisture and carbon at every scale, and that the system includes important complexities and feedback mechanisms not addressed in this study. An additional complication is that the study area has been influenced by disturbances including logging, grazing, and fire which have potentially altered productivity and soil carbon storage for the past century. However, the lack of tree stumps in the shrub lands, and the age of trees at the forested sites provide evidence that the general trend in greater vegetation cover with elevation and north aspects has not been substantially impacted by disturbances. The long-term trends in vegetation and carbon distribution appear to be well represented by the study sites. As the ecology transitions from shrub and grasslands at the lower elevations to forests at the upper elevations, it is both responding to and producing changes in the primary drivers of soil water distribution through biological activity, sediment erosion and deposition, soil shading, rain interception, and evapotranspiration, among others (Dingman 2002; Breshears *et al.* 2003; Rodríguez-Iturbe *et al.* 2004; Caylor *et al.* 2006; Gutierrez-Jurado *et al.* 2006). Climate itself undergoes a considerable change over the elevation gradient, and the observed ecological shift may reflect a change in the degree to which ecosystem processes are dominated by seasonal water limitation.

If the topographic gradients represented in this study can be used as a proxy for climatic shifts, we can conjecture about the effects of a shift in seasonal temperature and precipitation patterns. It has been predicted that climate change will cause the mountainous American northwest to grow warmer, with shorter-lived snow pack, earlier

spring, earlier vegetation greening, and hotter, drier summers (Knowles *et al.* 2006; Field *et al.* 2007; Mix *et al.* 2010). If these changes occur, we might expect more of the study area to assume soil water dynamics like those observed on south aspects and lower elevations, where earlier snow melt, earlier peak vegetation cover, and more rapid soil dry down lead to loss of soil water prior to the peak summer and to extended periods of plant water stress. These trends would in turn be expected to reduce the potential for vegetation productivity (Daubenmire 1968; Boyer 1982; Istanbulluoglu *et al.* 2006; Niu *et al.* 2008), or cause a shift in the predominant vegetation species (Ehleringer *et al.* 1991; Tilman 1994; Rodriguez-Iturbe *et al.* 2001a; Caylor *et al.* 2009). Such changes may initiate a positive feedback, with declines in vegetation cover causing greater exposure to insolation and erosional forces (Okin *et al.* 2001; Breshears *et al.* 2003; Istanbulluoglu *et al.* 2006). Biological weathering and inputs of soil organic materials could be reduced, leading to degradation of soil aggregates, accelerated removal of fine soil particles by erosion, and diminution of soil water retention properties (Orcutt *et al.* 2000). In time, the deeper, finer, more organic-rich soils of north aspects in the study area could evolve to resemble the coarser, shallower soils on south aspects. If snow were removed from all locations earlier in the year but spring precipitation were maintained or increased (Field *et al.* 2007), the period of warm, wet soils might be prolonged. Such conditions might inspire greater productivity, but could also increase the relative importance of soil respiration on the soil carbon reservoir, especially at sites with greater soil carbon content (Xu, Baldocchi *et al.* 2004; Monson *et al.* 2005; Chou *et al.* 2008).

The responses of ecosystems to climatic change are complex and difficult to predict, as are the climate perturbations themselves. We acknowledge that change in one climatic variable, such as the timing and amount of spring precipitation, is certain to occur in concert with myriad other climatic changes, such as mean annual precipitation and mean annual temperature, summer drought, snow, cloud cover, atmospheric composition, and others. The array of climatic changes will instigate further changes in hydrology, vegetation productivity, phenology, nutrient cycling, soil depth and texture, organism distributions and behaviors, and countless others on various spatial and temporal scales, and through complex and unpredictable feedback mechanisms. Quantification and prediction of complex ecosystem dynamics requires comprehensive physically-based models. This research provides empirical evidence to inform and constrain such models and underscores the importance of coordinating field studies with modeling efforts. Furthermore, the observations discussed here offer an important insight into targeting key areas of sensitivity when attempting to model ecosystem responses to climate change in a mountainous, seasonally water-limited environment.

6. CONCLUSIONS

Overall, the distribution of vegetation follows the distribution of soil water in the study area, consistent with previous work in water-limited ecosystems (Noy-Meir 1973; Monteith 1981). North-facing slopes and higher elevations were generally the locations of greater water storage and higher vegetation cover. North aspects and higher elevations also tended to have deeper, more finely textured soils and higher soil carbon content than south aspects and lower elevations. Differences in soil water storage, vegetation cover, and soil depth were minimal at the highest elevation pair of study sites (HN and HS).

The duration of coinciding wet, warm soil conditions was used to delineate a potential growing season for natural vegetation in the study area. The season was defined as beginning when the profile-averaged soil temperature remained above 5°C in the spring, and ending when the profile-averaged soil moisture dried below an approximate wilting point specific to the soil texture class. The potential growing season was generally longer, and occurred later in the summer, on north aspects. Growing season length and timing resembled the seasonal behavior of vegetation cover, which was greater and reached maximum (peak) cover earlier on the north aspect in all four pairs of study sites. Comparison of vegetation cover and growing season timing indicates that growing season length may not be the most important driver of productivity; rather, the timing of the growing season relative to peak summer temperature and radiation may be important in determining the amount of vegetation growth at a location. If so, the late portion of the

growing season, which is here defined by the duration of soil moisture into the summer, may have particular importance in determining the amount of vegetation growth.

The duration of soil moisture into the summer is influenced strongly by the amount and timing of summer precipitation in the study area. Due to the small water storage capacity of coarse-grained, shallow soils across the study area, there is a limit to the contribution snow melt can make to the soil water reservoir. Snow melt occurs in early spring, when low temperatures and low insolation prohibit soil water losses through evapotranspiration; thus, much of the water delivered by snow melt in the early spring is lost as drainage. Evidence for water loss includes the prolonged observation of hydraulic connectivity and bedrock flow at all study sites in response to snow melt. In contrast, spring precipitation arrives at an ecologically important time when evapotranspiration processes create space in the soil water reservoir, and precipitation inputs can be taken up and used by vegetation. During the study period, hydraulic connectivity and bedrock flow were re-established at all sites by spring rain events, indicating that spring rains were sufficient to satisfy the soil water storage capacities (ranging from 6 to 16 cm water). Even in a year of average precipitation, spring rains deliver sufficient water to largely recharge the soil water storage capacity near the time of ecologically favorable summer temperature and insolation conditions.

REFERENCES

- Aber, J. D., J. M. Melillo, *et al.* (1991). "Factors Controlling Nitrogen Cycling and Nitrogen Saturation in Northern Temperate Forest Ecosystems." Ecological Applications **1**(3): 303-315.
- Aishlin, P. S. (2006). Groundwater recharge estimation using chloride mass balance, Dry Creek experimental watershed. Department of Geosciences, Hydrologic Sciences. Boise, ID, Boise State University. **Masters of Science**: 111.
- Amundson, R. (2001). "The carbon budget in soils." Annual Review of Earth and Planetary Sciences **29**: 535-562.
- Archibald, S. and R. J. Scholes (2007). "Leaf green-up in a semi-arid African savanna - separating tree and grass responses to environmental cues." Journal of Vegetation Science **18**(4): 583-594.
- Arora, V. (2002). "Modeling vegetation as a dynamic component in soil-vegetation-atmosphere transfer schemes and hydrological models." Reviews of Geophysics **40**(2): 26.
- Arriaga, F. J., B. Lowery, *et al.* (2006). "A fast method for determining soil particle size distribution using a laser instrument." Soil Science **171**(9): 663-674.
- Beuselinck, L., G. Govers, *et al.* (1998). "Grain-size analysis by laser diffractometry: comparison with the sieve-pipette method." Catena **32**(3-4): 193-208.
- Beven, K. J. and M. J. Kirkby (1979). "A physically based, variable contributing area model of basin hydrology." Hydrological Sciences Journal-Journal Des Sciences Hydrologiques **24**(1): 43-69.
- Boyer, J. S. (1982). "Plant Productivity and Environment." Science **218**(4571): 443-448.

- Brady, N. C. and R. R. Weil (2002). The nature and properties of soils. Upper Saddle River, N.J., Prentice Hall.
- Breda, N. J. J. (2003). "Ground-based measurements of leaf area index: a review of methods, instruments and current controversies." Journal of Experimental Botany **54**(392): 2403-2417.
- Breshears, D. D., J. J. Whicker, *et al.* (2003). "Wind and water erosion and transport in semi-arid shrubland, grassland and forest ecosystems: Quantifying dominance of horizontal wind-driven transport." Earth Surface Processes and Landforms **28**(11): 1189-1209.
- Burnett, B. N., G. A. Meyer, *et al.* (2008). "Aspect-related microclimatic influences on slope forms and processes, northeastern Arizona." Journal of Geophysical Research-Earth Surface **113**(F3): 18.
- Butterfield, H. S. and C. M. Malmstrom (2009). "The effects of phenology on indirect measures of aboveground biomass in annual grasses." International Journal of Remote Sensing **30**(12): 3133-3146.
- Cayan, D. R., S. A. Kammerdiener, *et al.* (2001). "Changes in the onset of spring in the western United States." Bulletin of the American Meteorological Society **82**(3): 399-415.
- Caylor, K. K., P. D'Odorico, *et al.* (2006). "On the ecohydrology of structurally heterogeneous semiarid landscapes." Water Resources Research **42**(7): 13.
- Caylor, K. K., T. M. Scanlon, *et al.* (2009). "Ecohydrological optimization of pattern and processes in water-limited ecosystems: A trade-off-based hypothesis." Water Resources Research **45**: 15.
- Chadwick, O. A. and J. O. Davis (1990). "Soil-Forming Intervals Caused by Eolian Sediment Pulses in the Lahontan Basin, Northwestern Nevada." Geology **18**(3): 243-246.

- Chander, G. and B. Markham (2003). "Revised Landsat-5 TM radiometric calibration procedures and postcalibration dynamic ranges." IEEE Transactions on Geoscience and Remote Sensing **41**(11): 2674-2677.
- Chapin, F. S., P. A. Matson, *et al.* (2002). Principles of terrestrial ecosystem ecology. New York, Springer.
- Chen, J. M. and J. Cihlar (1996). "Retrieving leaf area index of boreal conifer forests using landsat TM images." Remote Sensing of Environment **55**(2): 153-162.
- Chen, J. M., J. Liu, *et al.* (1999). "Daily canopy photosynthesis model through temporal and spatial scaling for remote sensing applications." Ecological Modelling **124**(2-3): 99-119.
- Chou, W. W., W. L. Silver, *et al.* (2008). "The sensitivity of annual grassland carbon cycling to the quantity and timing of rainfall." Global Change Biology **14**(6): 1382-1394.
- Christensen, J. H., B. Hewitson, *et al.* (2007). "Regional Climate Projections." Climate Change 2007: The Physical Science Basis. Contribution of Working Group I to the Fourth Assessment Report of the Intergovernmental Panel on Climate Change Retrieved April 3, 2008, from <http://www.ipcc.ch/pdf/assessment-report/ar4/wg1/ar4-wg1-chapter11.pdf>.
- Clapp, R. B. and G. M. Hornberger (1978). "Empirical Equations for Some Soil Hydraulic-Properties." Water Resources Research **14**(4): 601-604.
- Clark, D. A., S. Brown, *et al.* (2001). "Measuring net primary production in forests: Concepts and field methods." Ecological Applications **11**(2): 356-370.
- Curran, P. J., J. L. Dungan, *et al.* (1992). "Seasonal Lai in Slash Pine Estimated with Landsat Tm." Remote Sensing of Environment **39**(1): 3-13.
- Daubenmire, R. (1968). "Soil Moisture in Relation to Vegetation Distribution in Mountains of Northern Idaho." Ecology **49**(3): 431-&.

- Davidson, E. A., I. A. Janssens, *et al.* (2006). "On the variability of respiration in terrestrial ecosystems: moving beyond Q(10)." Global Change Biology **12**(2): 154-164.
- Decagon Devices (2006-2010). AccuPAR PAR/LAI ceptometer model LP-80, Operator's Manual. Pullman, WA, Decagon Devices, Inc.: 89.
- Decagon Devices (2007). ECH2O-TE/EC-TM Water Content, EC and Temperature Sensors; Operator's Manual. Pullman WA, Decagon Devices, Inc.: 38.
- Dingman, S. L. (2002). Physical hydrology. Upper Saddle River, New Jersey, Prentice Hall.
- Duursma, R. A., J. D. Marshall, *et al.* (2003). "Leaf area index inferred from solar beam transmission in mixed conifer forests on complex terrain." Agricultural and Forest Meteorology **118**(3-4): 221-236.
- Ehleringer, J. R., S. L. Phillips, *et al.* (1991). "Differential Utilization of Summer Rains by Desert Plants." Oecologia **88**(3): 430-434.
- Elmore, A. J., J. F. Mustard, *et al.* (2000). "Quantifying vegetation change in semiarid environments: Precision and accuracy of spectral mixture analysis and the Normalized Difference Vegetation Index." Remote Sensing of Environment **73**(1): 87-102.
- Famiglietti, J. S., J. A. Devereaux, *et al.* (1999). "Ground-based investigation of soil moisture variability within remote sensing footprints during the Southern Great Plains 1997 (SGP97) Hydrology Experiment." Water Resources Research **35**(6): 1839-1851.
- Famiglietti, J. S., J. W. Rudnicki, *et al.* (1998). "Variability in surface moisture content along a hillslope transect: Rattlesnake Hill, Texas." Journal of Hydrology **210**(1-4): 259-281.
- Famiglietti, J. S., D. R. Ryu, *et al.* (2008). "Field observations of soil moisture variability across scales." Water Resources Research **44**(1): 16.

- Feng, S. and Q. Hu (2004). "Changes in agro-meteorological indicators in the contiguous United States: 1951-2000." Theoretical and Applied Climatology **78**(4): 247-264.
- Field, C. B., L. D. Mortsch, *et al.* (2007, 2010). "North America. Climate Change 2007: Impacts, Adaptation and Vulnerability." Contribution of Working Group II to the Fourth Assessment Report of the Intergovernmental Panel on Climate Change Retrieved February 2010, 2010, from http://www.ipcc.ch/publications_and_data/ar4/wg2/en/ch14.html.
- Foley, J. A. and N. Ramankutty (2004). A primer on the terrestrial carbon cycle: what we don't know but should. The global carbon cycle. C. B. Field and M. R. Raupach. Washington, Island Press. **62**: 279-294.
- Geiger, R., R. H. Aron, *et al.* (2003). The Climate Near the Ground. Lanham, MD, USA, Rowman and Littlefield Publishers, Inc.
- Gomez-Plaza, A., M. Martinez-Mena, *et al.* (2001). "Factors regulating spatial distribution of soil water content in small semiarid catchments." Journal of Hydrology **253**(1-4): 211-226.
- Gordon, W. S. and J. S. Famiglietti (2004). "Response of the water balance to climate change in the United States over the 20th and 21st centuries: Results from the VEMAP Phase 2 model intercomparisons." Global Biogeochemical Cycles **18**(1).
- Goudie, A. and N. Middleton (2006). Desert dust in the global system. Berlin; New York, Springer.
- Grayson, R. B. and A. W. Western (1998). "Towards areal estimation of soil water content from point measurements: time and space stability of mean response." Journal of Hydrology **207**(1-2): 68-82.
- Grayson, R. B., A. W. Western, *et al.* (1997). "Preferred states in spatial soil moisture patterns: Local and nonlocal controls." Water Resources Research **33**(12): 2897-2908.
- Gribb, M. M., I. Forkutsa, *et al.* (2009). "The Effect of Various Soil Hydraulic Property Estimates on Soil Moisture Simulations." Vadose Zone Journal **8**(2): 321-331.

- Gutierrez-Jurado, H. A., E. R. Vivoni, *et al.* (2006). "Ecohydrology of root zone water fluxes and soil development in complex semiarid rangelands." Hydrological Processes **20**(15): 3289-3316.
- Gutierrez-Jurado, H. A., E. R. Vivoni, *et al.* (2007). "Ecohydrological response to a geomorphically significant flood event in a semiarid catchment with contrasting ecosystems." Geophysical Research Letters **34**(24).
- Hamlet, A. F. and D. P. Lettenmaier (1999). "Effects of climate change on hydrology and water resources in the Columbia River Basin." Journal of the American Water Resources Association **35**(6): 1597-1623.
- Hamlet, A. F., P. W. Mote, *et al.* (2005). "Effects of temperature and precipitation variability on snowpack trends in the western United States." Journal of Climate **18**(21): 4545-4561.
- Hamlet, A. F., P. W. Mote, *et al.* (2007). "Twentieth-century trends in runoff, evapotranspiration, and soil moisture in the western United States." Journal of Climate **20**(8): 1468-1486.
- Hawley, M. E., T. J. Jackson, *et al.* (1983). "Surface Soil-Moisture Variation on Small Agricultural Watersheds." Journal of Hydrology **62**(1-4): 179-200.
- Heimann, M. and M. Reichstein (2008). "Terrestrial ecosystem carbon dynamics and climate feedbacks." Nature **451**(7176): 289-292.
- Henderson-Sellers, A. and P. J. Robinson (1986). Contemporary climatology. London; New York, Longman Scientific & Technical ; Wiley.
- Hillel, D. (2004). Introduction to Environmental Soil Physics. San Diego CA, Elsevier Academic Press.
- Huang, S. and P. Fu (2009) "Modeling Small Areas Is a Big Challenge." ESRI ArcUser Online Volume, 28-31 DOI:

- Hupet, F. and M. Vanclooster (2002). "Intraseasonal dynamics of soil moisture variability within a small agricultural maize cropped field." Journal of Hydrology **261**(1-4): 86-101.
- Istanbulluoglu, E. and R. L. Bras (2006). "On the dynamics of soil moisture, vegetation, and erosion: Implications of climate variability and change." Water Resources Research **42**(6).
- Ivanov, V. Y., R. L. Bras, *et al.* (2008a). "Vegetation-hydrology dynamics in complex terrain of semiarid areas: 1. A mechanistic approach to modeling dynamic feedbacks." Water Resources Research **44**(3).
- Ivanov, V. Y., R. L. Bras, *et al.* (2008b). "Vegetation-hydrology dynamics in complex terrain of semiarid areas: 2. Energy-water controls of vegetation spatiotemporal dynamics and topographic niches of favorability." Water Resources Research **44**(3).
- Jensen, J. R. (2000). Remote Sensing of the Environment; An Earth Resource Perspective. Upper Saddle River, NJ, Prentice-Hall, Inc.
- Jobbágy, E. G. and R. B. Jackson (2000). "The vertical distribution of soil organic carbon and its relation to climate and vegetation." Ecological Applications **10**(2): 423-436.
- Kappen, L., O. L. Lange, *et al.* (1972). "Extreme Water Stress and Photosynthetic Activity of Desert Plant *Artemisia-Herba-Alba* Asso." Oecologia **10**(2): 177-&.
- Knowles, N., M. D. Dettinger, *et al.* (2006). "Trends in snowfall versus rainfall in the Western United States." Journal of Climate **19**(18): 4545-4559.
- Konert, M. and J. Vandenberghe (1997). "Comparison of laser grain size analysis with pipette and sieve analysis: A solution for the underestimation of the clay fraction." Sedimentology **44**(3): 523-535.
- Ladd, K., G. Murgel, *et al.* (2007). Identifying controls on surface carbon dioxide efflux in a semi-arid ecosystem. Environmental Sensing Symposium Boise, Idaho, Boise State University.

- Laio, F., A. Porporato, *et al.* (2001). "Plants in water-controlled ecosystems: active role in hydrologic processes and response to water stress - II. Probabilistic soil moisture dynamics." Advances in Water Resources **24**(7): 707-723.
- Leij, F. J., N. Romano, *et al.* (2004). "Topographical attributes to predict soil hydraulic properties along a hillslope transect." Water Resources Research **40**(2).
- Linton, M. J., J. S. Sperry, *et al.* (1998). "Limits to water transport in *Juniperus osteosperma* and *Pinus edulis*: implications for drought tolerance and regulation of transpiration." Functional Ecology **12**(6): 906-911.
- Malvern Instruments Ltd. (2009). "Mastersizer 2000." Retrieved April 5, 2009, from <http://www.malvern.com/LabEng/products/Mastersizer/MS2000/mastersizer2000.htm>.
- McNamara, J. P., D. Chandler, *et al.* (2005). "Soil moisture states, lateral flow, and streamflow generation in a semi-arid, snowmelt-driven catchment." Hydrological Processes **19**(20): 4023-4038.
- Miller, P., M. Mitchell, *et al.* (2005). "Climate change: Length of growing-season in the US Corn Belt, 1911-2000." Physical Geography **26**(2): 85-98.
- Mix, K., W. Rast, *et al.* (2010). "Increases in Growing Degree Days in the Alpine Desert of the San Luis Valley, Colorado." Water Air and Soil Pollution **205**(1-4): 289-304.
- Monson, R. K., J. P. Sparks, *et al.* (2005). "Climatic influences on net ecosystem CO₂ exchange during the transition from wintertime carbon source to springtime carbon sink in a high-elevation, subalpine forest." Oecologia **146**(1): 130-147.
- Monteith, J. L. (1981). "Climatic Variation and the Growth of Crops." Quarterly Journal of the Royal Meteorological Society **107**(454): 749-774.
- Mote, P. W. (2006). "Climate-driven variability and trends in mountain snowpack in western North America." Journal of Climate **19**(23): 6209-6220.

- Newman, B. D., B. P. Wilcox, *et al.* (2006). "Ecohydrology of water-limited environments: A scientific vision." Water Resources Research **42**(6): 15.
- Niu, S. L., M. Y. Wu, *et al.* (2008). "Water-mediated responses of ecosystem carbon fluxes to climatic change in a temperate steppe." New Phytologist **177**(1): 209-219.
- Noy-Meir, I. (1973). *Desert Ecosystems: Environment and Producers*. **4**: 25-51.
- Okin, G. S. and D. A. Gillette (2001). "Distribution of vegetation in wind-dominated landscapes: Implications for wind erosion modeling and landscape processes." Journal of Geophysical Research-Atmospheres **106**(D9): 9673-9683.
- Orcutt, D. M. and E. T. Nilsen (2000). The physiology of plants under stress : soil and biotic factors. New York; Chichester, Wiley.
- Paruelo, J. M., H. E. Epstein, *et al.* (1997). "ANPP estimates from NDVI for the Central Grassland Region of the United States." Ecology **78**(3): 953-958.
- Plante, A. F., R. T. Conant, *et al.* (2006). "Impact of soil texture on the distribution of soil organic matter in physical and chemical fractions." Soil Science Society of America Journal **70**(1): 287-296.
- Pocewicz, A. L., P. Gessler, *et al.* (2004). "The relationship between effective plant area index and Landsat spectral response across elevation, solar insolation, and spatial scales in a northern Idaho forest." Canadian Journal of Forest Research-Revue Canadienne De Recherche Forestiere **34**(2): 465-480.
- Porporato, A., P. D'Odorico, *et al.* (2002). "Ecohydrology of water-controlled ecosystems." Advances in Water Resources **25**(8-12): 1335-1348.
- Raich, J. W. and W. H. Schlesinger (1992). "The Global Carbon-Dioxide Flux in Soil Respiration and Its Relationship to Vegetation and Climate." Tellus Series B-Chemical and Physical Meteorology **44**(2): 81-99.

- Rawls, W. J., Y. A. Pachepsky, *et al.* (2003). "Effect of soil organic carbon on soil water retention." Geoderma **116**(1-2): 61-76.
- Reheis, M. C., J. C. Goodmacher, *et al.* (1995). "Quaternary Soils and Dust Deposition in Southern Nevada and California." Geological Society of America Bulletin **107**(9): 1003-1022.
- Ridolfi, L., P. D'Odorico, *et al.* (2003). "Stochastic soil moisture dynamics along a hillslope." Journal of Hydrology **272**(1-4): 264-275.
- Rodriguez-Iturbe, I. (2000). "Ecohydrology: A hydrologic perspective of climate-soil-vegetation dynamics." Water Resources Research **36**(1): 3-9.
- Rodriguez-Iturbe, I., P. D'Odorico, *et al.* (1999). "On the spatial and temporal links between vegetation, climate, and soil moisture." Water Resources Research **35**(12): 3709-3722.
- Rodríguez-Iturbe, I. and A. Porporato (2004). Ecohydrology of water-controlled ecosystems : soil moisture and plant dynamics. Cambridge, UK; New York, NY, USA, Cambridge University Press.
- Rodriguez-Iturbe, I., A. Porporato, *et al.* (2001a). "Intensive or extensive use of soil moisture: plant strategies to cope with stochastic water availability." Geophysical Research Letters **28**(23): 4495-4497.
- Rodriguez-Iturbe, I., A. Porporato, *et al.* (2001b). "Plants in water-controlled ecosystems: active role in hydrologic processes and response to water stress - I. Scope and general outline." Advances in Water Resources **24**(7): 695-705.
- Rouse, J. W., R. H. Haas, *et al.* (1974). Monitoring Vegetation Systems in the Great Plains with ERTS. Third Earth Resources Technology Satellite-1 Symposium, NASA.
- Running, S. W., R. R. Nemani, *et al.* (1989). "Mapping Regional Forest Evapotranspiration and Photosynthesis by Coupling Satellite Data with Ecosystem Simulation." Ecology **70**(4): 1090-1101.

- Running, S. W., D. L. Peterson, *et al.* (1986). "Remote-Sensing of Coniferous Forest Leaf-Area." Ecology **67**(1): 273-276.
- Running, S. W., P. E. Thornton, *et al.* (2000). Global Terrestrial Gross and Net Primary Productivity from the Earth Observing System. Methods in Ecosystem Science. O. E. Sala, R. B. Jackson, H. A. Mooney and R. W. Howarth. New York, Springer-Verlag: 44-55.
- Salvucci, G. D. (2001). "Estimating the moisture dependence of root zone water loss using conditionally averaged precipitation." Water Resources Research **37**(5): 1357-1365.
- Santin-Janin, H., M. Garel, *et al.* (2009). "Assessing the performance of NDVI as a proxy for plant biomass using non-linear models: a case study on the Kerguelen archipelago." Polar Biology **32**(6): 861-871.
- Schlesinger, W. H. (1977). "Carbon Balance in Terrestrial Detritus." Annual Review of Ecology and Systematics **8**: 51-81.
- Scholes, R. J. and B. H. Walker (1993). An African savanna : synthesis of the Nylsvley study. Cambridge [England]; New York, Cambridge University Press.
- Schulze, E. D., H. A. Mooney, *et al.* (1996). "Rooting depth, water availability, and vegetation cover along an aridity gradient in Patagonia." Oecologia **108**(3): 503-511.
- Seyfried, M. S., L. E. Grant, *et al.* (2009). "Simulated soil water storage effects on streamflow generation in a mountainous snowmelt environment, Idaho, USA." Hydrological Processes **23**(6): 858-873.
- Seyfried, M. S., S. Schwinning, *et al.* (2005). "Ecohydrological control of deep drainage in arid and semiarid regions." Ecology **86**(2): 277-287.
- Silver, W. L., R. Ryals, *et al.* (2010). "Soil Carbon Pools in California's Annual Grassland Ecosystems." Rangeland Ecology & Management **63**(1): 128-136.

- Smith, J. L., J. J. Halvorson, *et al.* (2002). "Soil properties and microbial activity across a 500 m elevation gradient in a semi-arid environment." Soil Biology & Biochemistry **34**(11): 1749-1757.
- Smith, S. D., T. E. Huxman, *et al.* (2000). "Elevated CO₂ increases productivity and invasive species success in an arid ecosystem." Nature **408**(6808): 79-82.
- Sole, R. (2007). "Ecology - Scaling laws in the drier." Nature **449**(7159): 151-153.
- Sperazza, M., J. N. Moore, *et al.* (2004). "High-resolution particle size analysis of naturally occurring very fine-grained sediment through laser diffractometry." Journal of Sedimentary Research **74**(5): 736-743.
- Stewart, I. T., D. R. Cayan, *et al.* (2005). "Changes toward earlier streamflow timing across western North America." Journal of Climate **18**(8): 1136-1155.
- Syvitski, J. P. M. (1991). Principles, methods, and application of particle size analysis. Cambridge; New York, Cambridge University Press.
- Taiz, L. and E. Zeiger (1998). Plant physiology. Sunderland, Mass., Sinauer Associates.
- Tesfa, T. K., D. G. Tarboton, *et al.* (2009). "Modeling soil depth from topographic and land cover attributes." Water Resources Research **45**: 16.
- Thomas, C. K., B. E. Law, *et al.* (2009). "Seasonal hydrology explains interannual and seasonal variation in carbon and water exchange in a semiarid mature ponderosa pine forest in central Oregon." Journal of Geophysical Research-Biogeosciences **114**: 22.
- Thornthwaite, C. W. (1961). "The Task Ahead." Annals of the Association of American Geographers **51**(4): 345-356.
- Tilman, D. (1994). "Competition and Biodiversity in Spatially Structured Habitats." Ecology **75**(1): 2-16.

- Tromp-van Meerveld, H. J. and J. J. McDonnell (2006). "On the interrelations between topography, soil depth, soil moisture, transpiration rates and species distribution at the hillslope scale." Advances in Water Resources **29**(2): 293-310.
- Turner, D. P., W. B. Cohen, *et al.* (1999). "Relationships between leaf area index and Landsat TM spectral vegetation indices across three temperate zone sites." Remote Sensing of Environment **70**(1): 52-68.
- USDA (1997). Soil survey of the Boise Front: Interim and supplemental report. Boise, Idaho, United States Department of Agriculture, National Resource Conservation Service.
- USDA (1999). Soil taxonomy : a basic system of soil classification for making and interpreting soil surveys. N. R. C. Service. Washington, DC, U.S. Dept. of Agriculture, Soil Survey Staff, United States Government Printing Office. **436**: 869.
- Veihmeyer, F. J. and A. H. Hendrickson (1955). "Rates of evaporation from wet and dry soils and their significance." Soil Sci **80**((1)): 61-67.
- Viola, F., E. Daly, *et al.* (2008). "Transient soil-moisture dynamics and climate change in Mediterranean ecosystems." Water Resources Research **44**(11).
- Vivoni, E. R., C. A. Aragon, *et al.* (2009). "Semiarid watershed response in central New Mexico and its sensitivity to climate variability and change." Hydrology and Earth System Sciences **13**(6): 715-733.
- Vourlitis, G. L., G. Zorba, *et al.* (2007). "Carbon and nitrogen storage in soil and litter of southern Californian semi-arid shrublands." Journal of Arid Environments **70**(1): 164-173.
- Walvoord, M. A. and F. M. Phillips (2004). "Identifying areas of basin-floor recharge in the Trans-Pecos region and the link to vegetation." Journal of Hydrology **292**(1-4): 59-74.

- Wang, T., D. Wedin, *et al.* (2009). "Field evidence of a negative correlation between saturated hydraulic conductivity and soil carbon in a sandy soil." Water Resources Research **45**.
- Wang, Y., R. Amundson, *et al.* (2000). "Seasonal and altitudinal variation in decomposition of soil organic matter inferred from radiocarbon measurements of soil CO₂ flux." Global Biogeochemical Cycles **14**(1): 199-211.
- Weltzin, J. F., M. E. Loik, *et al.* (2003). "Assessing the response of terrestrial ecosystems to potential changes in precipitation." Bioscience **53**(10): 941-952.
- Western, A. W., R. B. Grayson, *et al.* (1999). "Observed spatial organization of soil moisture and its relation to terrain indices." Water Resources Research **35**(3): 797-810.
- Western, A. W., S. L. Zhou, *et al.* (2004). "Spatial correlation of soil moisture in small catchments and its relationship to dominant spatial hydrological processes." Journal of Hydrology **286**(1-4): 113-134.
- White, M. A., G. P. Asner, *et al.* (2000). "Measuring fractional cover and leaf area index in arid ecosystems: Digital camera, radiation transmittance, and laser altimetry methods." Remote Sensing of Environment **74**(1): 45-57.
- Whittaker, R. H. and W. A. Niering (1975). "Vegetation of Santa Catalina Mountains, Arizona .5. Biomass, Production, and Diversity Along Elevation Gradient." Ecology **56**(4): 771-790.
- Wigmosta, M. S., L. W. Vail, *et al.* (1994). "A Distributed Hydrology-Vegetation Model for Complex Terrain." Water Resources Research **30**(6): 1665-1679.
- Williams, C. J. (2005). Characterization of the spatial and temporal controls on soil moisture and streamflow generation in a semi-arid headwater catchment. Department of Geology. Boise, Idaho, Boise State University. **Master of Science**: 204.

- Williams, C. J., J. P. McNamara, *et al.* (2009). "Controls on the temporal and spatial variability of soil moisture in a mountainous landscape: the signature of snow and complex terrain." Hydrology and Earth System Sciences **13**(7): 1325-1336.
- Wilson, D. J., A. W. Western, *et al.* (2005). "A terrain and data-based method for generating the spatial distribution of soil moisture." Advances in Water Resources **28**(1): 43-54.
- Xu, L. K. and D. D. Baldocchi (2004). "Seasonal variation in carbon dioxide exchange over a Mediterranean annual grassland in California." Agricultural and Forest Meteorology **123**(1-2): 79-96.
- Xu, L. K., D. D. Baldocchi, *et al.* (2004). "How soil moisture, rain pulses, and growth alter the response of ecosystem respiration to temperature." Global Biogeochemical Cycles **18**(4).
- Yenko, M. K. (2003). Hydrometric and geochemical evidence of streamflow sources in the Upper Dry Creek Experimental Watershed, southwestern Idaho.

APPENDIX A

Tables

Table A.1. Basic attributes and locations of soil moisture measurement stations. UTM coordinates are from Zone 11 N, in datum NAD83.

Site ID	Site Description	Easting	Northing	Elevation (m)	Slope (°)	Aspect (°)	Dominant Vegetation	Mean Annual Precipitation (mm)	Mean Annual Temperature (°C)	Mean Annual Potential Insolation (MJ/m ²)	Period of Record	Data Gaps
HN	High North-Facing	570973	4843448	1812	23	0	Douglas-fir, Ponderosa Pine	682	7.3	3888	8/7/2008 - 10/22/2009	9/17/2009-10/15/2009
HS	High South-Facing	571202	4843273	1835	25	193	Douglas-fir, Ponderosa Pine	692	7.2	5789	8/6/2008 - 10/22/2009	2/2/2009-2/20/2009
MHN	Mid-High North-Facing	570460	4840830	1472	28	5	Douglas-fir, Ponderosa Pine	533	9.1	3365	7/16/2008 - 10/5/2009	10/15/2008-10/18/2008
MHS	Mid-High South-Facing	570421	4841202	1457	33	170	Sagebrush Shrub, Grasses	527	9.2	5440	8/16/2008 - 10/5/2009	1/18/2009-1/23/2009
MLN	Mid-Low North-Facing	568613	4839073	1288	33	3	Sagebrush Shrub, Grasses	453	10.1	3333	6/15/2008 - 10/8/2009	12/7/2008-12/22/2008; 2/2/2009-3/9/2009; 5/31/2009-6/11/2009; 8/13/2009 - 8/17/2009

Site ID	Site Description	Easting	Northing	Elevation (m)	Slope (°)	Aspect (°)	Dominant Vegetation	Mean Annual Precipitation (mm)	Mean Annual Temperature (°C)	Annual Potential Insolation (MJ/m ²)	Period of Record	Data Gaps
MLS	Mid-Low South-Facing	568506	4839457	1298	25	178	Grasses, Sagebrush Shrub	457	10.0	5163	10/15/2008 - 10/5/2009	9/30/2008-10/15/2008; 11/14/2008-12/22/2008; 2/2/2009-3/9/2009; 3/14/2009-3/24/2009; 4/6/2009-4/18/2009
LN	Low North-Facing	566916	4837694	1120	24	9	Sagebrush Shrub, Grasses	379	10.9	2702	9/1/2008 - 9/1/2009	9/2/2009-11/2/2009
LS	Low South-Facing	566939	4837869	1139	27	188	Grasses, Sagebrush Shrub	388	10.8	5250	11/20/08 - 10/22/2009	12/26/2008 - 1/16/2009

Table A.2. Water contents associated with wilting point matric potential (-3 MPa), as well as field capacity water contents determined: a) using field data, and b) estimated from an assumed matric potential (-0.03 MPa) for each site. Also provided are parameter values used in determining water contents associated with matric potentials for each soil class. Parameters from Clapp et al. 1978 and Laio et al. 2001. Symbol Φ represents porosity and θ represents water content.

Site	USDA Soil Texture Classification (Bottom of Soil Profile)	Porosity, ϕ (-), or $\theta_{\text{saturation}}$	Air Entry Tension (cm)	b (-)	θ_{WP} (-)	θ_{FC} (-), from data	θ_{FC} (-), estimated at -0.03 MPa
HN	Sandy Loam	0.44	21.80	4.90	0.10	0.19	0.25
HS	Sandy Loam	0.44	21.80	4.90	0.10	0.17	0.25
MHN	Sandy Loam	0.44	21.80	4.90	0.10	0.17	0.25
MHS	Loamy Sand	0.41	9.00	4.38	0.06	0.15	0.18
MLN	Sandy Loam	0.44	21.80	4.90	0.10	0.19	0.25
MLS	Loamy Sand	0.41	9.00	4.38	0.06	0.16	0.18
LN	Sandy Loam	0.44	21.80	4.90	0.10	0.18	0.25
LS	Loamy Sand (80%)-Sandy Loam (20%)	0.42	15.40	4.64	0.08	0.17	0.22

Table A.3. Important dates and values of soil water content, soil temperature, soil water storage, spatial variability, snow cover, and growing season initiation and end. Mean values derived from period of record common to all sites, 11/20/2008 to 9/1/2009; other values taken from entire measurement period.

Site ID	HN	HS	MHN	MHS	MLN	MLS	LN	LS
Soil Water Content and Soil Temperature								
Maximum Profile-Averaged Θ (Date)	0.33 (4/22/2009)	0.27 (3/21/2009, 4/8/2009, 4/13/2009, 4/20/2009)	0.24 (3/19/2009 and 3/22/2009)	0.20 (3/16/2009)	0.28 (3/16/2009)	0.21 (4/2/2009)	0.29 (4/9/2008); 0.28 (3/15/2009)	0.21 (12/23/2009, 4/2/2009 - 4/10/2009)
Minimum Profile-Averaged Θ (Date)	0.03 (9/18/2008); 2009 uncertain due to failure	0.02 (9/14/2008, 10/3/2009)	0.03 (8/24/2008, 9/30/2009)	0.00 (pre- 8/16/2008, 9/22/2009)	0.03 (9/1/2008, 10/2/2009)	0.03 (9/1/2008, 10/1/2009)	0.04 (9/12/2008); 2009 uncertain due to failure	0.06 (6/1/2009)
Mean Profile-Averaged Θ (cm)	0.24	0.20	0.16	0.13	0.18	0.11	0.20	0.14
Maximum Profile-Averaged Soil Temperature ($^{\circ}\text{C}$) (Date)	13.39 (8/4/2009)	14.22 (8/29/2009)	17.88 (8/3/2009, 8/5/2009)	28.73 (8/4/2009)	20.77 (8/3/2009)	30.99 (8/3/2009)	22.03 (8/3/2009)	34.64 (8/3/2009)
Minimum Profile-Averaged Soil Temperature ($^{\circ}\text{C}$) (Date)	1.18 (4/21/2009)	1.70 (4/14/2009)	1.24 (3/1/2009)	1.8 (2/13/2009, 2/15/2009)	0.68 (3/16/2009)	1.13 (2/1/2009)	1.13 (2/21/2009)	1.36 (1/27/2009)
Mean Profile-Averaged Soil Temperature ($^{\circ}\text{C}$)	5.3	6.3	7.2	11.9	8.9	16.3	9.0	16.0

Site ID	HN	HS	MHN	MHS	MLN	MLS	LN	LS
# Days Profile Bottom Exceeded Field Capacity	225	218	162	137	[56]	[48]	125	175
Spatial Variability Over Replicate Pits								
Spatial Variability: Mean Standard Deviation of Soil Moisture Among Pits (cm ³ /cm ³)	0.02	0.02	0.03	0.02	0.02	0.02	0.02	0.03
Spatial Variability: Mean Standard Deviation of Soil Temperature Among Pits (°C)	0.28	0.53	0.32	0.62	0.52	0.46	0.40	0.91
Variability Over Soil Profile								
Mean Standard Deviation of Soil Moisture Over Profile (cm ³ /cm ³)	0.04	0.01	0.03	0.04	0.05	0.05	0.05	0.07
Mean Standard Deviation of Soil Temperature Over Profile (°C)	0.76	0.66	0.96	1.81	1.62	1.64	1.61	1.23

Site ID	HN	HS	MHN	MHS	MLN	MLS	LN	LS
Approximate Temperature Difference Over Profile	1°C (winter) and 3°C (summer)	1°C (winter) and 3°C (summer)	2°C (winter) and 4.5°C (summer)	2°C (winter) and 7°C (summer)	2.5 to 3°C (winter) and 7-8°C (summer)	4°C in winter, 7-8°C in summer	3°C in winter, 8°C in summer	3°C in winter, 5°C in summer
Soil Water Storage								
Maximum Water Storage (cm) (Date)	21.5 (4/22/2009)	19.6 (4/8/2009, 4/13/2009, 4/20/2009)	21.7 (3/19/2009)	15.6 (3/16/2009)	24.8 (3/16/2009)	7.9 (4/2/2009)	18.6 (3/16/2009)	7.1 (4/3/2009)
Minimum Water Storage (cm) (Date)	1.9 (9/7/2008); 2009 uncertain due to failure	1.42 (9/14/2008); 1.47 (10/3/2009)	2.90 (9/18/2008); 3.0 (10/3/2009)	1.26 (11/1/2008); 1.57 (10/2/2009)	2.57 (9/18/2008); 3.01 (10/3/2009)	0.99 (9/13/2008); 1.09 (10/3/2009)	2.95 (9/15/2008); 5.61 (8/5/2009)	2.12 (6/1/2009)
Mean Water Storage (cm)	15.7	14.3	14.6	9.8	15.4	4.2	13.1	4.7
Water Storage Capacity (cm)	12.5	12.4	15.6	11.4	16.5	6.1	11.9	5.8
Mean Annual Precipitation/ Storage Capacity	5.4	5.6	3.4	4.6	2.7	7.5	3.2	6.7
Potential Growing Season								
Dates of Snow Cover (continuous or intermittent)	12/5/2008 - 4/20/2009; continuous	12/5/2008 - 4/15/2009; continuous	12/5/2008 - 4/6/2009; intermittent	12/11/2008 - 3/13/2009; intermittent	Approx. 12/4/2008 - 4/1/2009; intermittent	Approx. 12/4/2008 - 1/26/2009; intermittent	Approx. 12/4/2008 - 3/13/2009; intermittent	12/13/2008 to 1/18/2009; continuous
Date 2 cm Soil Temperature Surpassed 5°C	5/15/2009	5/15/2009	5/2/2009	4/4/2009	4/7/2009	4/4/2009	4/7/2009	3/11/2009

Site ID	HN	HS	MHN	MHS	MLN	MLS	LN	LS
Date Profile Dried Below Wilting Point Water Content	7/27/2009	7/23/2009	7/19/2009	5/27/2009	7/7/2009	5/22/2009	7/9/2009	5/21/2009
# Potential Growing Days (5°C surface soil to wilting point)	73	70	78	53	91	48	93	71

Table A.4. Depth of soil to bedrock as measured in each pit dug for installation of soil moisture and temperature sensors. Bedrock was treated as the gravelly decomposed granite layer which was unsuitable for sensor installation.

Site-Pit	Depth to Bedrock (cm)	Site-Pit	Depth to Bedrock (cm)
HN-1	67	HS-1	65
HN-2	64	HS-2	70
HN-3	63	HS-3	80
HN-4	70	HS-4	77
HN-Avg	66	HS-Avg	73
MHN-1	90	MHS-1	80
MHN-2	116	MHS-2	66
MHN-3	77	MHS-3	87
MHN-4	85	MHS-4	70
MHN-Avg	92	MHS-Avg	76
MLN-1	100	MLS-1	32
MLN-2	96	MLS-2	31
MLN-3	70	MLS-3	56
MLN-4	83	MLS-4	31
MLN-Avg	87	MLS-Avg	38
LN-1	62	LS-1	35
LN-2	65	LS-2	32
LN-3	62	LS-3	35
LN-4	73	LS-4	32
LN-Avg	66	LS-Avg	34

Table A.5. Results of paired laser diffraction (A) and mechanical (hydrometer/sieve) analyses (B) used to develop a linear correlation to approximate mechanical results from laser diffraction results.

A. Laser Diffraction Results							
Site ID	Pit	Depth (cm)	Method	Sample ID	%Sand	%Silt	%Clay
LN	1	15	LaserDiffraction	LN-Pit1-15cm	41.0	54.4	4.6
LN	2	15	LaserDiffraction	LN_Pit2-15cm_5Reps	39.2	56.1	4.7
LN	3	15	LaserDiffraction	LN-Pit3-15cm	36.9	58.4	4.7
LN	4	15	LaserDiffraction	LN-Pit4-15cm	39.0	56.5	4.4
LS	1	2	LaserDiffraction	LS-Pit1-2cm-3Reps	83.1	16.1	0.8
LS	1	15	LaserDiffraction	LS-Pit1-15cm-3Reps	85.3	13.8	0.9
LS	1	30	LaserDiffraction	LS-Pit1-30cm	95.2	4.6	0.2
LS	2	15	LaserDiffraction	LS-Pit2-15cm	89.0	10.4	0.6
LS	3	2	LaserDiffraction	LS-Pit3-2cm	80.4	18.3	1.3
LS	3	15	LaserDiffraction	LS-Pit3-15cm	78.0	20.5	1.5
LS	4	15	LaserDiffraction	LS-Pit4-15cm	79.6	19.0	1.4
MHN	1	15	LaserDiffraction	MHN-Pit1-15cm	62.7	34.5	2.8
MHN	2	15	LaserDiffraction	MHN-Pit2-15cm-3Reps	58.7	38.7	2.6
MHN	3	15	LaserDiffraction	MHN-Pit3-15cm	56.7	40.3	3.0
MHN	4	15	LaserDiffraction	MHN-Pit4-15cm-3Reps	58.8	38.6	2.5
MHS	1	15	LaserDiffraction	MHS-Pit1-15cm-3Reps	84.7	14.5	0.9
MHS	2	2	LaserDiffraction	MHS-Pit2-2cm	86.8	12.4	0.8
MHS	2	15	LaserDiffraction	MHS-Pit2-15cm-3Reps	85.6	13.6	0.8
MHS	2	30	LaserDiffraction	MHS-Pit2-30cm-2Reps	86.1	13.0	0.9
MHS	2	60	LaserDiffraction	MHS-Pit2-59cm	86.5	12.7	0.8

B. Hydrometer/Sieve Results

Site ID	Pit	Depth (cm)	Method	Sample ID	%Sand	%Silt	%Clay
LN	1	15	Hydrometer	LN-Pit1-15cm-2Reps	47.0	37.7	15.3
LN	2	15	Hydrometer	LN-Pit2-15cm-2Reps	48.1	40.7	11.1
LN	3	15	Hydrometer	LN-Pit3-15cm	44.4	42.4	13.2
LN	4	15	Hydrometer	LN-Pit4-15cm	46.2	42.7	11.2
LS	1	2	Hydrometer	LS-Pit1-2cm-3Reps	81.1	12.3	6.6
LS	1	15	Hydrometer	LS-Pit1-15cm-2Reps	81.2	10.0	8.9
LS	1	30	Hydrometer	LS-Pit1-30cm-2Reps	86.9	5.4	7.7
LS	2	15	Hydrometer	LS-Pit2-15cm	79.0	9.1	11.9
LS	3	2	Hydrometer	LS-Pit3-2cm-2Reps	80.5	13.3	6.1
LS	3	15	Hydrometer	LS-Pit3-15cm-2Reps	75.0	13.7	11.3
LS	4	15	Hydrometer	LS-Pit4-15cm-2Reps	75.3	13.6	11.1
MHN	1	15	Hydrometer	MHN-Pit1-15cm	64.4	28.6	7.0
MHN	2	15	Hydrometer	MHN-Pit2-15cm	68.2	26.8	5.1
MHN	3	15	Hydrometer	MHN-Pit3-15cm	67.3	26.2	6.5
MHN	4	15	Hydrometer	MHN-Pit4_15cm	63.1	32.4	4.5
MHS	1	15	Hydrometer	MHS-Pit1-15cm-2Reps	82.0	12.4	5.6
MHS	2	2	Hydrometer	MHS-Pit2-2cm	91.1	8.5	0.4
MHS	2	15	Hydrometer	MHS-Pit2-15cm-2Reps	81.2	12.9	5.8
MHS	2	30	Hydrometer	MHS-Pit2-30cm	80.1	10.3	9.6
MHS	2	60	Hydrometer	MHS-Pit2-59cm-2Reps	82.8	9.7	7.5

Table A.6. Bulk density approximations from soil samples. Site MLN, sample set “a” was excluded due to sampling error. Samples at the 0-5cm bgs interval are not believed to be reliable and are excluded.

Sample ID	Depth interval (cm)	Bulk Density (g/cm ³)	Sample ID	Depth interval (cm)	Bulk Density (g/cm ³)
HN-1a	5	0.47	HN-1b	5	0.54
HN-2a	10	0.79	HN-2b	10	1.13
HN-3a	15	0.95	HN-3b	15	1.07
HN-4a	20	1.21	HN-4b	20	1.23
HN-5a	25	1.02	HN-5b	25	1.08
HN-6a	30	1.46	HN-6b	30	1.16
HS-1a	5	0.30	HS-1b	5	0.51
HS-2a	10	1.03	HS-2b	10	1.15
HS-3a	15	0.98	HS-3b	15	0.81
HS-4a	20	1.34	HS-4b	20	1.31
HS-5a	25	1.06	HS-5b	25	1.26
HS-6a	30	1.31	HS-6b	30	1.51
LN-1a	5	0.84	LN-1b	5	1.24
LN-2a	10	1.19	LN-2b	10	1.23
LN-3a	15	0.82	LN-3b	15	0.80
LN-4a	20	1.21	LN-4b	20	1.50
LN-5a	25	1.15	LN-5b	25	1.36
LN-6a	30	1.48	LN-6b	30	1.09
LS-1a	5	1.15	LS-1b	5	1.39
LS-2a	10	1.22	LS-2b	10	1.61
LS-3a	15	0.72	LS-3b	15	1.64
LS-4a	20	1.42	LS-4b	20	1.27
LS-5a	25	1.44	LS-5b	25	1.59
LS-6a	30	1.62	LS-6b	30	1.58
MHN-1b	5	0.67	MHN-1c	5	0.87
MHN-2b	10	1.21	MHN-2c	10	1.10
MHN-3b	15	1.09	MHN-3c	15	0.87
MHN-4b	20	1.28	MHN-4c	20	1.21
MHN-5b	25	1.05	MHN-5c	25	1.11
MHN-6b	30	1.27	MHN-6c	30	1.35
MHS-1a	5	1.38	MHS-1b	5	1.63
MHS-2a	10	1.45	MHS-2b	10	1.40
MHS-3a	15	1.36	MHS-3b	15	1.39
MHS-4a	20	1.34	MHS-4b	20	1.49
MHS-5a	25	1.95	MHS-5b	25	1.87
MHS-6a	30	1.55	MHS-6b	30	1.68

Sample ID	Depth interval (cm)	Bulk Density (g/cm ³)	Sample ID	Depth interval (cm)	Bulk Density (g/cm ³)
MLN-1b	5	1.13			
MLN-2b	10	1.57			
MLN-3b	15	1.25			
MLN-4b	20	1.22			
MLN-5b	25	1.29			
MLN-6b	30	1.38			
MLS-1a	5	1.32	MLS-1b	5	1.27
MLS-2a	10	1.28	MLS-2b	10	1.46
MLS-3a	15	1.33	MLS-3b	15	1.30
MLS-4a	20	1.49	MLS-4b	20	1.36
MLS-5a	25	1.89	MLS-5b	25	1.37
MLS-6a	30	1.56	MLS-6b	30	1.82

Table A.7. Total carbon content of soil as percent by weight for intervals 0-5 cm (“5”), 5-10 cm (“10”), 10-15 cm (“15”), 15-20 cm (“20”), 20-25 cm (“25”), and 25-30 cm (“30”) bgs. Values reported are the averaged results of 2 field replicates and random lab replicates; replicates deviate less than 8% from the reported values.

Depth (cm bgs)	Site, North Aspect	Sample ID	Weight % C	Site, South Aspect	Sample ID	Weight % C
5.00	HN	HN1	12.37	HS	HS1	18.73
10.00		HN2	7.42		HS2	6.55
15.00		HN3	3.35		HS3	3.90
20.00		HN4	1.74		HS4	2.79
25.00		HN5	1.54		HS5	2.30
30.00		HN6	1.55		HS6	1.60
5.00	MHN	MHN1	7.13	MHS	MHS1	2.00
10.00		MHN2	5.85		MHS2	1.44
15.00		MHN3	4.01		MHS3	1.04
20.00		MHN4	3.01		MHS4	0.93
25.00		MHN5	3.00		MHS5	1.05
30.00		MHN6	2.39		MHS6	0.68
5.00	MLN	MLN1	6.00	MLS	MLS1	1.82
10.00		MLN2	4.60		MLS2	1.22
15.00		MLN3	4.04		MLS3	1.04
20.00		MLN4	3.59		MLS4	0.78
25.00		MLN5	4.17		MLS5	0.69
30.00		MLN6	3.49		MLS6	0.63
5.00	LN	LN1	4.52	LS	LS1	2.03
10.00		LN2	4.19		LS2	0.68
15.00		LN3	4.06		LS3	0.58
20.00		LN4	3.41		LS4	0.52
25.00		LN5	3.39		LS5	0.56
30.00		LN6	2.83		LS6	0.92

Table A.8. Total carbon content in the upper 30 cm of soil at all sites. Values reported are the averaged results of 2 field replicates and random lab replicates; replicates deviate less than 8% from the reported values.

Site	Depth Interval (cm)	Total C (kg/(30cm*m ²))
HN	0 - 10	3.02
	10 - 20	0.78
	20 - 30	0.47
	Total	4.27
HS	0 - 10	3.86
	10 - 20	1.02
	20 - 30	0.59
	Total	5.47
MHN	0 - 10	1.98
	10 - 20	1.07
	20 - 30	0.82
	Total	3.87
MHS	0 - 10	0.53
	10 - 20	0.30
	20 - 30	0.26
	Total	1.09
MLN	0 - 10	1.62
	10 - 20	1.16
	20 - 30	1.17
	Total	3.95
MLS	0 - 10	0.46
	10 - 20	0.28
	20 - 30	0.20
	Total	0.94
LN	0 - 10	1.33
	10 - 20	1.14
	20 - 30	0.95
	Total	3.42
LS	0 - 10	0.41
	10 - 20	0.17
	20 - 30	0.23
	Total	0.81

Table A.9. Values of the coefficient of determination (R^2) representing the degree to which variation in one variable is explained by another variable. Of the variables, “peak NDVI” was selected from monthly averages derived over a four year period; “soil carbon” was measured as total soil carbon in the uppermost 30 cm of the profile; mean soil water content, soil water storage, and soil temperature were calculated from the common period of record, 11/20/2008 to 9/1/2009; mean annual precipitation and mean annual air temperature were calculated based on elevation using the linear hypsometric relationship observed in the study area; and potential insolation was modeled as total annual insolation.

	Peak NDVI	Soil Carbon	Mean Soil Water Content	Mean Soil Water Storage	Mean Soil Temperature	Mean Annual Precipitation (or Air Temperature, or Elevation)
North Aspects						
Peak NDVI						
Soil Carbon	0.87					
Mean Soil Water Content	0.55	0.64				
Mean Soil Water Storage	0.64	0.8	0.58			
Mean Soil Temperature	0.87	0.89	0.63	0.88		
Mean Annual Precipitation (or Air Temperature, or Elevation)	0.92	0.81	0.28	0.54	1	
Potential Insolation	0.83	0.98	0.16	0.83	0.92	0.9
South Aspects						
Peak NDVI						
Soil Carbon	0.87					
Mean Soil Water Content	0.55	0.64				
Mean Soil Water Storage	0.64	0.8	0.58			
Mean Soil Temperature	0.87	0.89	0.74	0.85		
Mean Annual Precipitation (or Air Temperature, or Elevation)	0.84	0.85	0.62	0.93	0.98	
Potential Insolation	0.79	0.85	0.79	0.97	0.84	0.88

Table A.10. Results of forward selection multiple regression analysis treating elevation (associated with gradients in precipitation and air temperature) and potential insolation as independent variables, and treating soil carbon, peak NDVI, and mean soil water storage as dependent variables.

	Model R²	Model Significance, p	Model Coefficients
Soil Carbon Content, C			
Elevation, e	0.3789	0.1042	$C = 0.0091e - 1.7028$
Elevation, e, and Insolation, i	0.7048	0.0473	$C = 0.0118e - 0.0009i + 0.8933$
Peak NDVI, N			
Elevation, e	0.6447	0.0164	$N = 0.0009e + 0.0021$
Elevation, e, and Insolation, i	0.8421	0.0099	$N = 0.0011e - 0.00005i + 0.16025$
Mean Soil Water Stored, S			
Insolation, i	0.3405	0.1289	$S = 23.7778 - 0.0026i$
Insolation, i and Elevation, e	0.8471	0.0091	$S = 0.033e - 0.0037i + 11.2573$

APPENDIX B

Figures

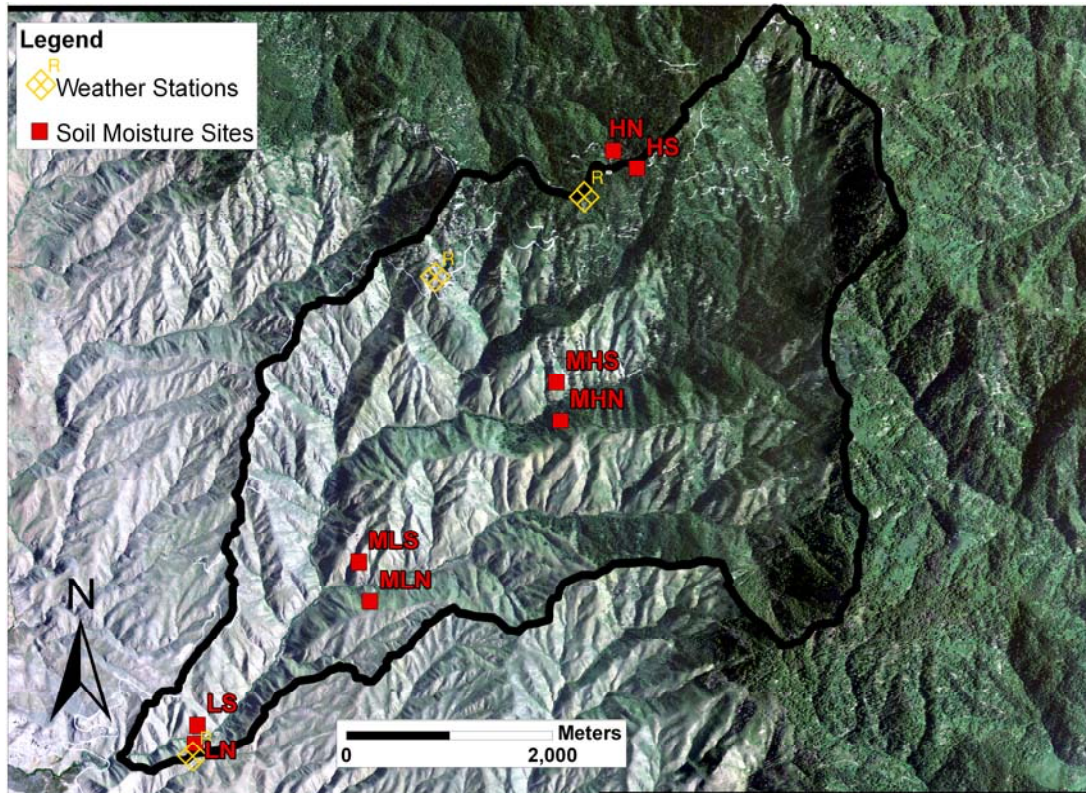


Figure B.1. The Dry Creek Experimental Watershed study area, including study sites and meteorological (weather) stations. Ecological differences across topographic gradients are evident from lowest to highest elevations (lower left to upper right), and from south-facing to north-facing slopes at middle elevations (as at sites MHS and MHN). Aerial image courtesy of the National Agriculture Imagery Program (NAIP) 2004.

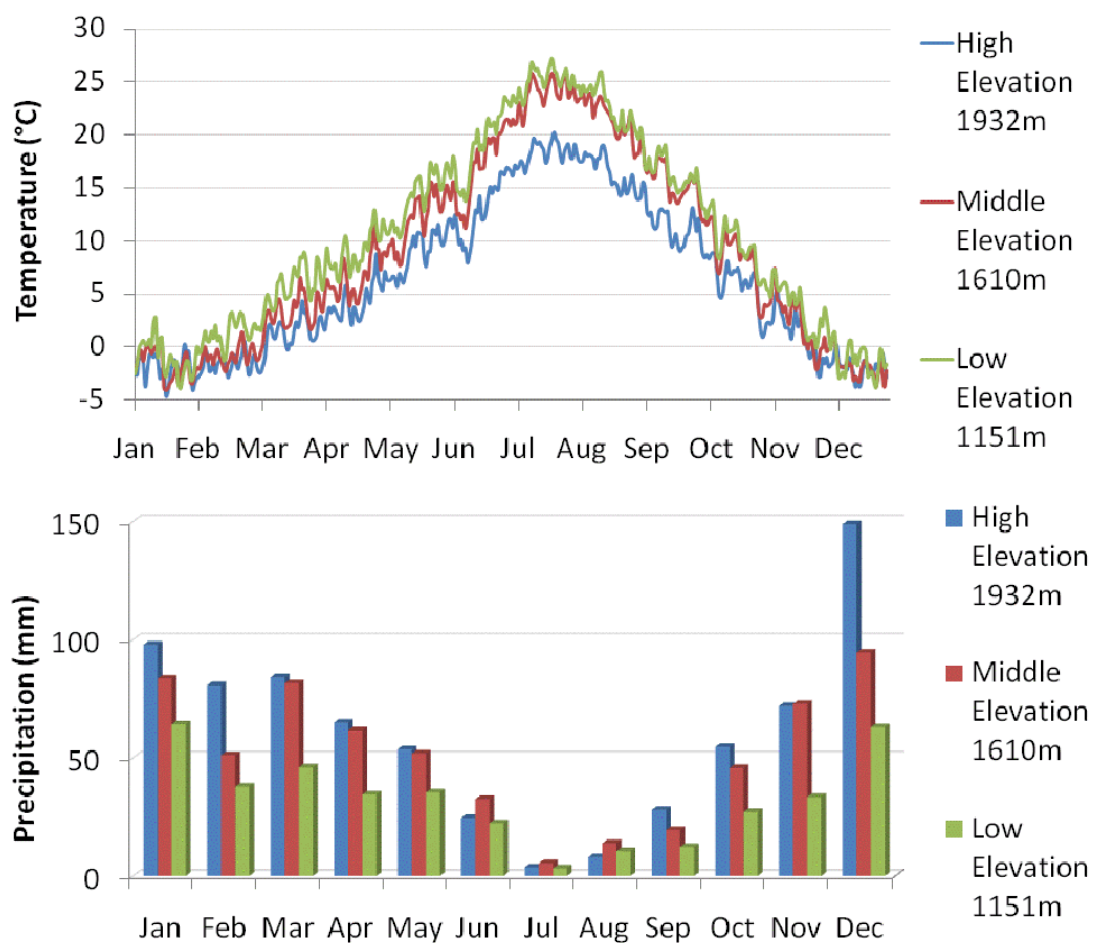


Figure B.2. Seasonal and topographic trends in precipitation and temperature at Dry Creek Experimental Watershed. Temperature as nine-year average at three meteorological stations (top) and precipitation as nine-year average at the same meteorological stations (bottom). Precipitation and temperature are out-of-phase in this environment. Higher elevations experience overall lower temperatures and greater precipitation.

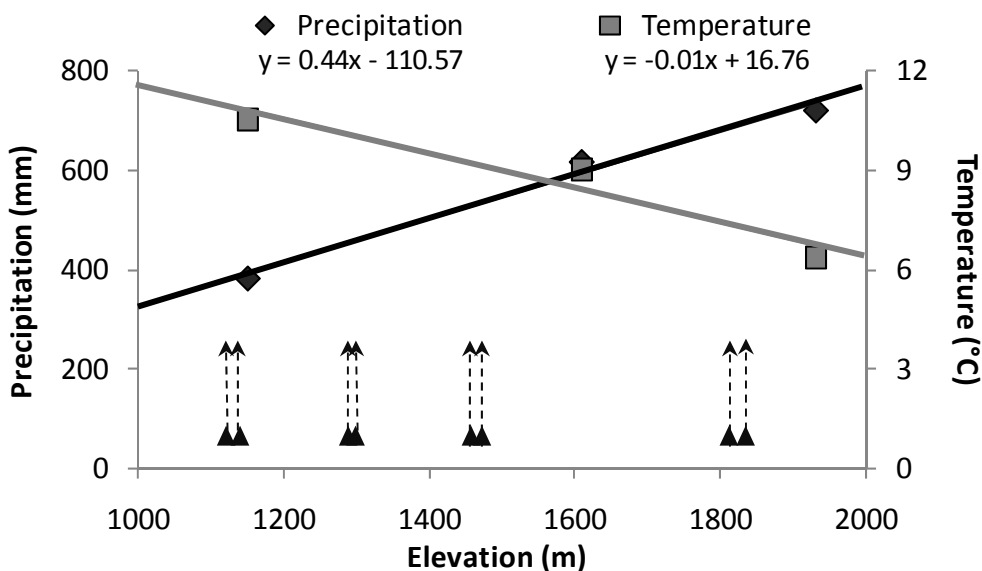


Figure B.3. Orographic trend of higher precipitation and lower temperature with increasing elevation in the study area. Values are nine-year average total annual precipitation and nine-year average annual mean temperature. Mean annual precipitation and mean annual temperature for each of the study sites were derived from the hypsometric equations shown.

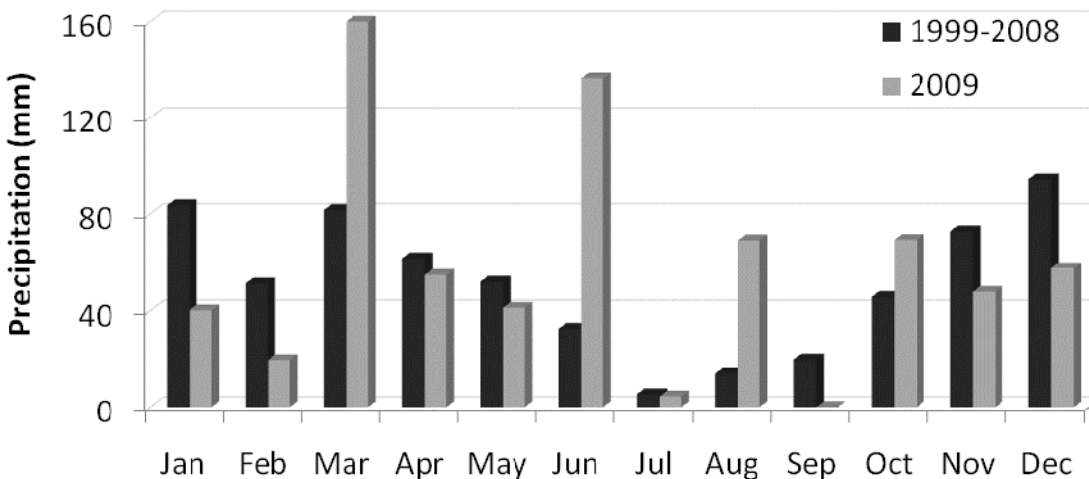


Figure B.4. Nine-year average seasonal precipitation compared with precipitation during the 2008-2009 season of study. During an average year, most of the annual precipitation falls during the autumn and winter months (Oct-Mar) and the summer (Jun-Sep) is dry. During the 2008-2009 period of study, winter precipitation was relatively low, spring rains were relatively high, and the dry summer was punctuated by a large rain event in August.

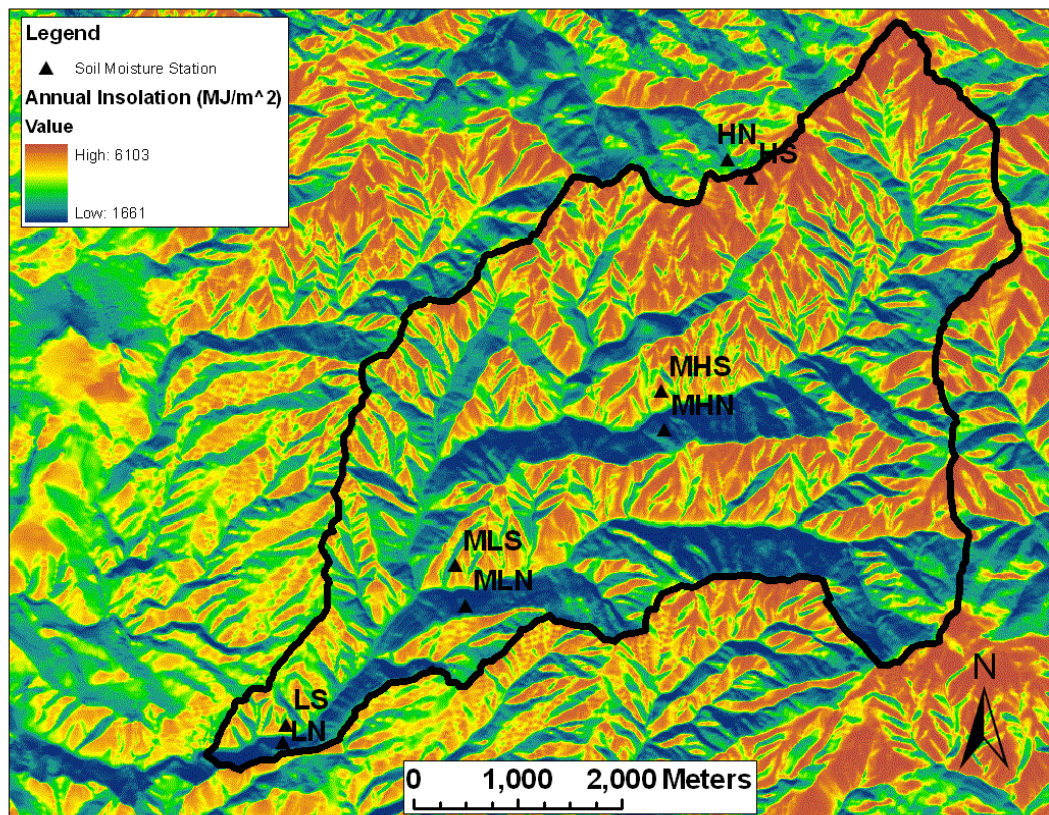


Figure B.5. Distribution of potential incident solar radiation (insolation) over the study area, modeled using the ArcGIS Solar Radiation tool. Values are total potential insolation modeled over the 2008 year, but they reflect the general distribution of potential insolation in any year. At a given elevation, a south-facing slope may receive nearly twice as much potential insolation as a complimentary north-facing slope.

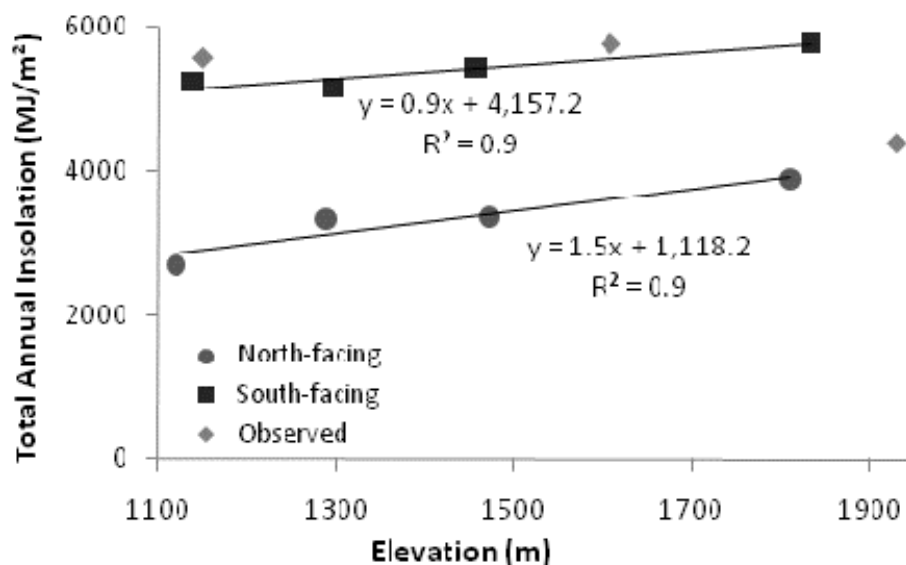


Figure B.6. Modeled values of total annual potential insolation at the study sites (squares and circles), with measured values from weather stations (diamonds) in the study area. The measured total annual potential insolation values confirm that the modeled values are realistic. Potential insolation increases slightly with increasing elevation, but the potential insolation difference across the aspect gradient is much larger than the difference across the elevation gradient.

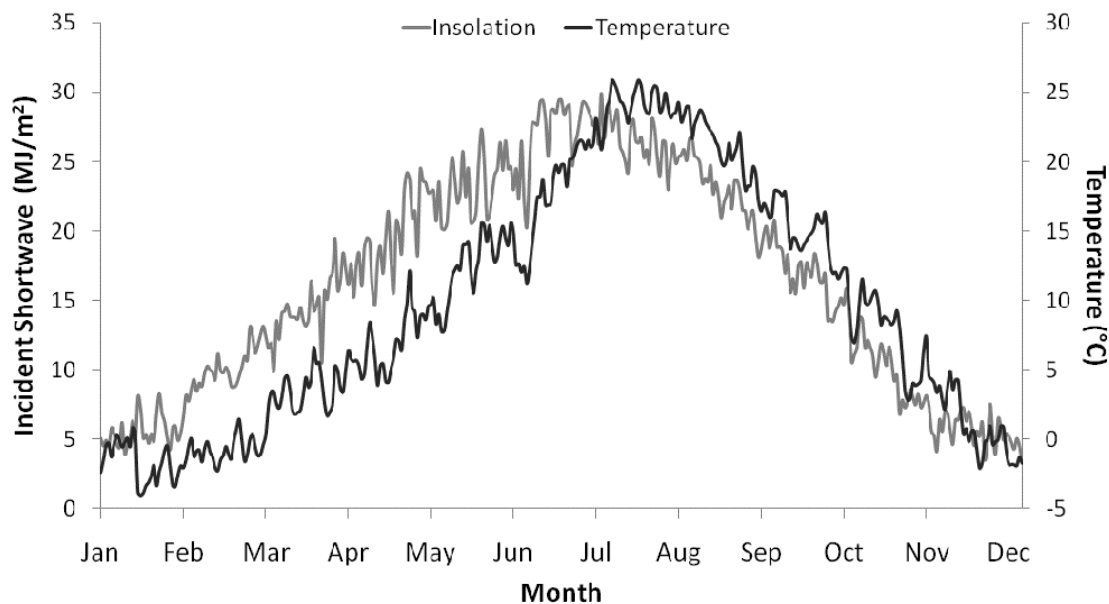


Figure B.7. Time series of mean daily temperature and total daily insolation measured from a weather station located at 1610 m elevation in the study area. Peak insolation occurs during the midsummer, around July. Air temperature lags slightly, reaching its peak around July to August.

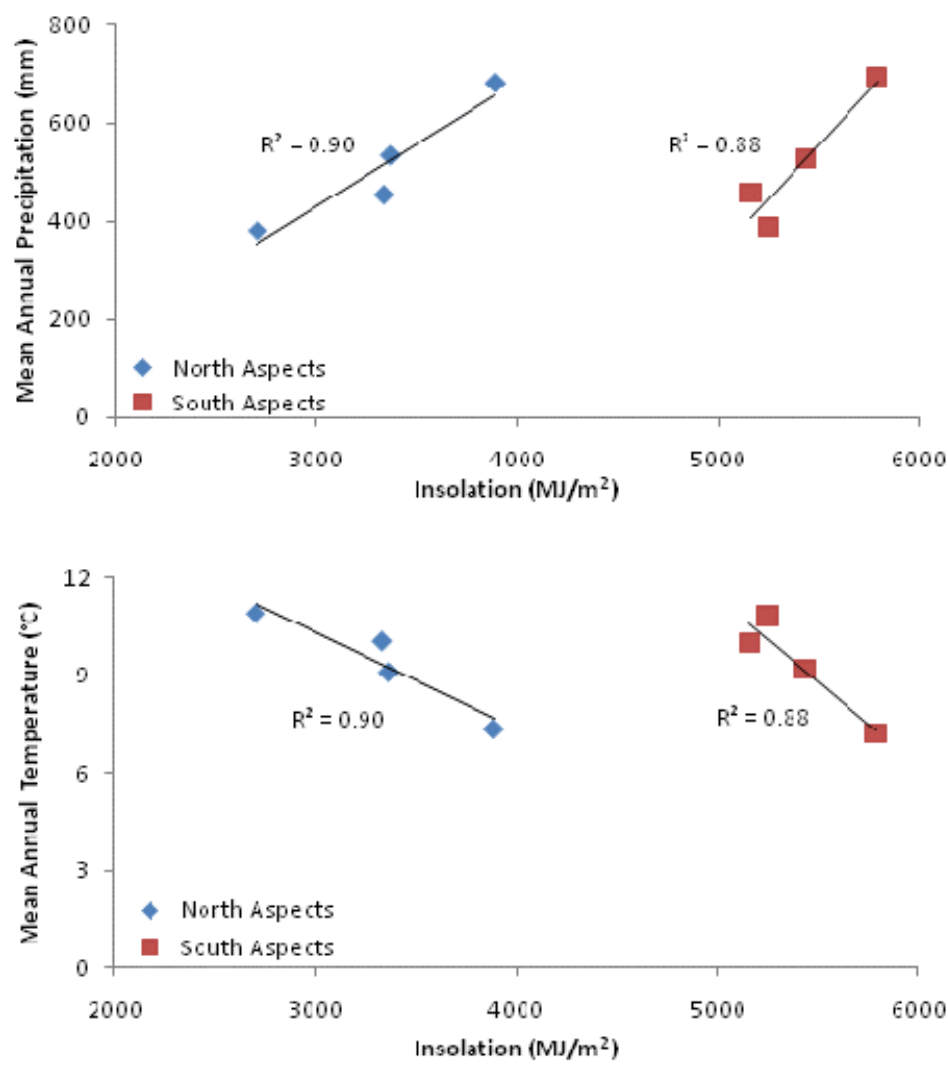


Figure B.8. Modeled (potential) insolation relates positively with mean annual precipitation and negatively with mean annual temperature in the study area. The amount of radiation received is distinctly different for north and south aspects (north aspects receive much less radiation than south aspects).

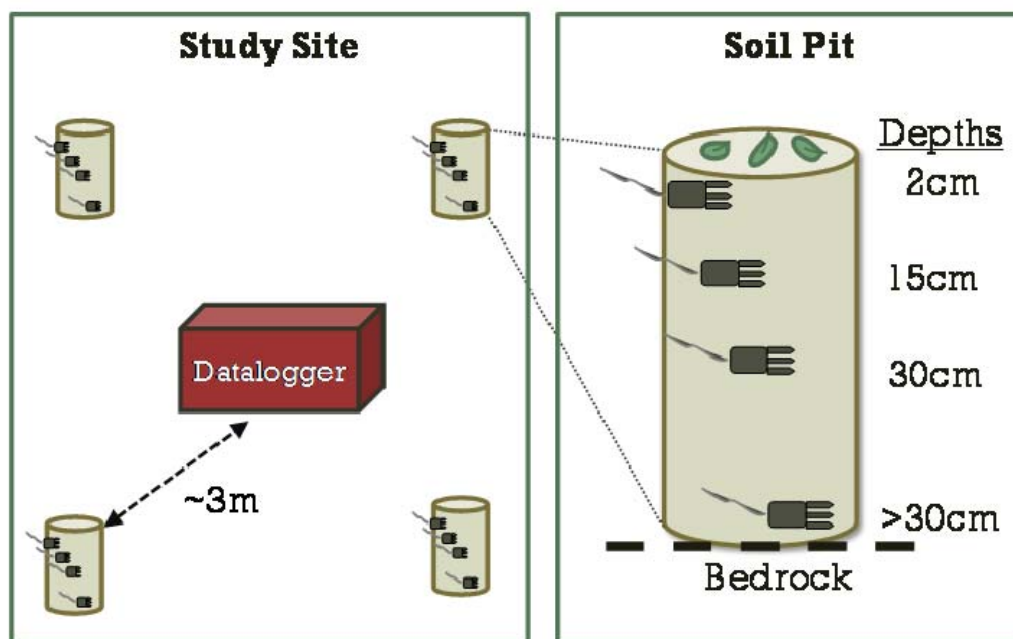


Figure B.9. Configuration of soil moisture stations and soil pits in this study. Each site is composed of four soil pits which are treated as replicates representing soil moisture and soil temperature at each site. In turn, each pit contains soil moisture and temperature sensors located at 2 cm, 15 cm, and 30 cm below ground surface. Most pits contain a fourth sensor located above the soil-bedrock interface, but at two sites (MLS and LS) soil was generally only about 30 cm deep.

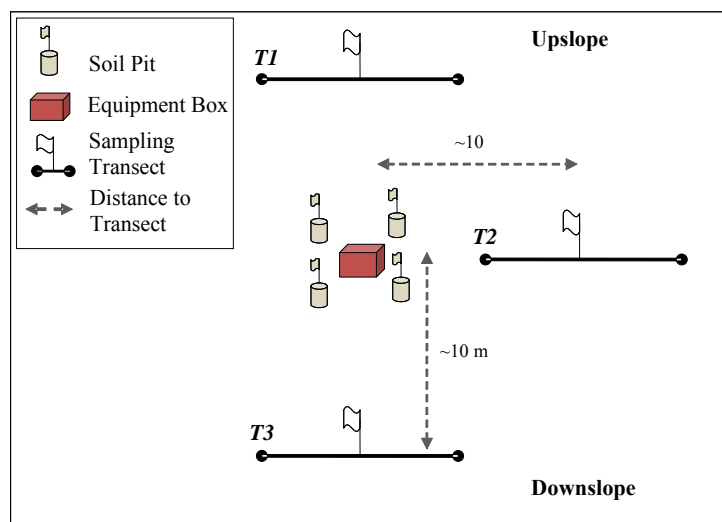


Figure B.10. General configuration of Plant Area Index (PAI) sampling transects at each soil moisture station. Three transects of 11 sampling points each were positioned around each station, allowing repeated measurement of 33 sample points per station during the 2009 growing season.

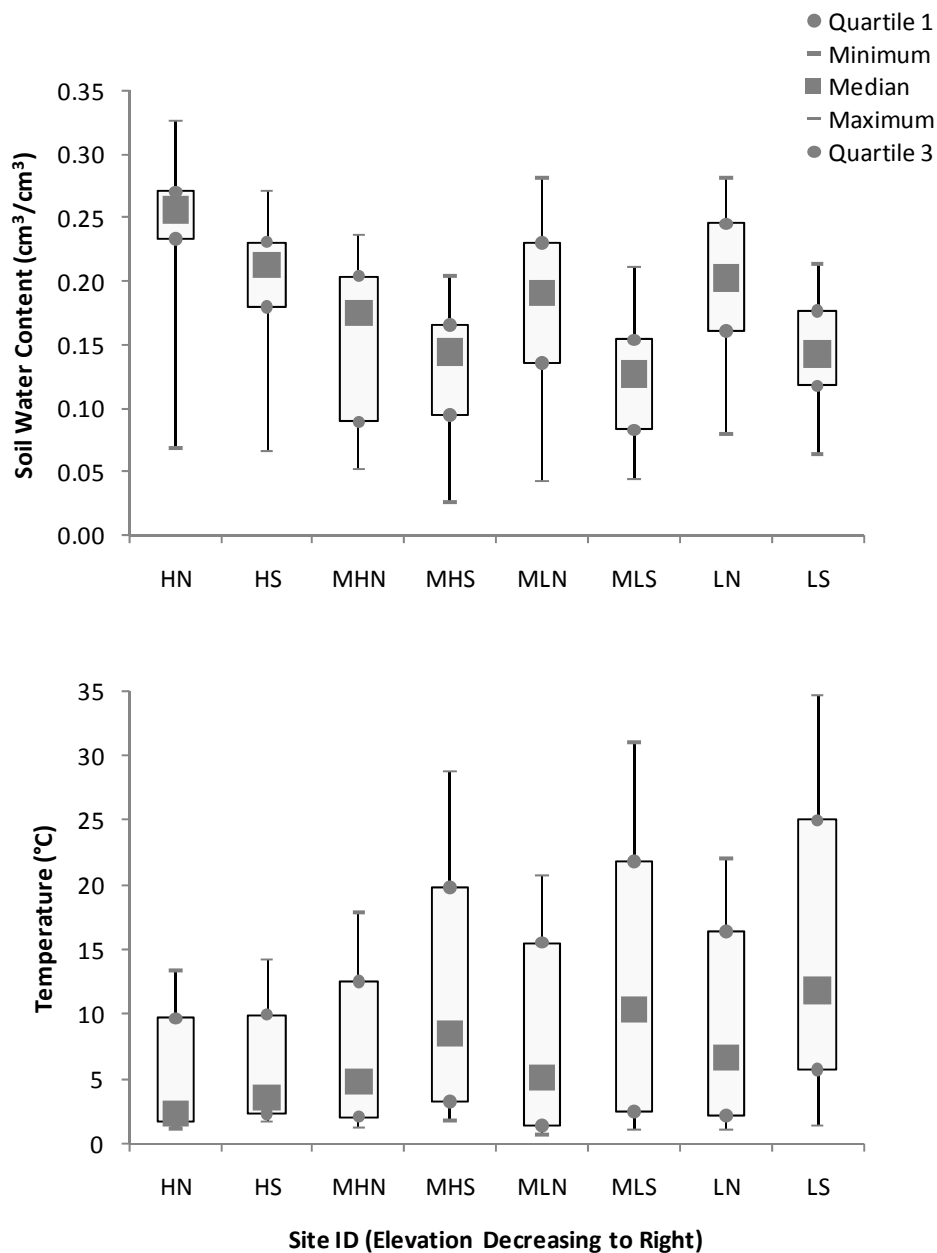


Figure B.11. Basic distributions of soil water content (top) and soil temperature (bottom) time series over the common measurement period, 11/20/2008 to 9/1/2009. Sample sizes are $n = 286$ days for each site. The height of the boxplots represents variation in time. The separation of box plots suggests that overall, growing season soil moisture and soil temperature differ with aspect and, to a lesser degree, with elevation. An exception is soil temperature at the highest elevation sites, which does not appear to differ significantly with aspect.

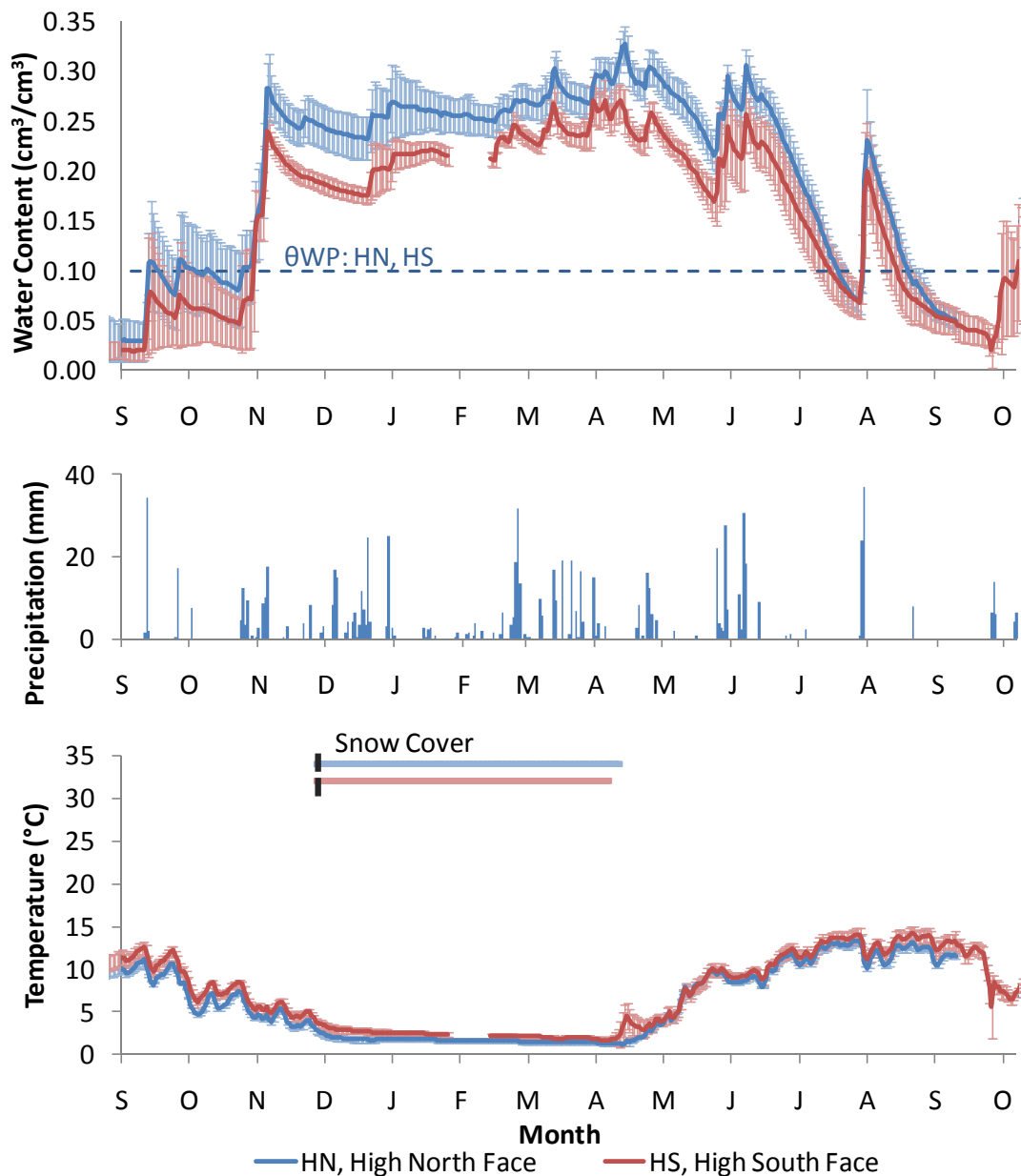


Figure B.12. Soil water content (top) and soil temperature (bottom) at the high elevation north facing (HN) and high elevation south-facing (HS) sites as profile- and site-averaged values. Error bars represent spatial variability as the standard deviation of profile-averaged values among the four pits at each site. Precipitation events (rain and snow) are plotted in the center graph. Dates of snow cover, inferred from dampened diurnal fluctuations in shallow soil temperature, are shown at top of the temperature plot. Dates of initial snow cover (marked by bold vertical dashes) are uncertain because the temperature trends may reflect snow cover or soil freezing, but dates of snow cover cessation are more certain. The north aspect has somewhat higher soil moisture, slightly lower soil temperature, and a slightly later snowmelt date than the south aspect.

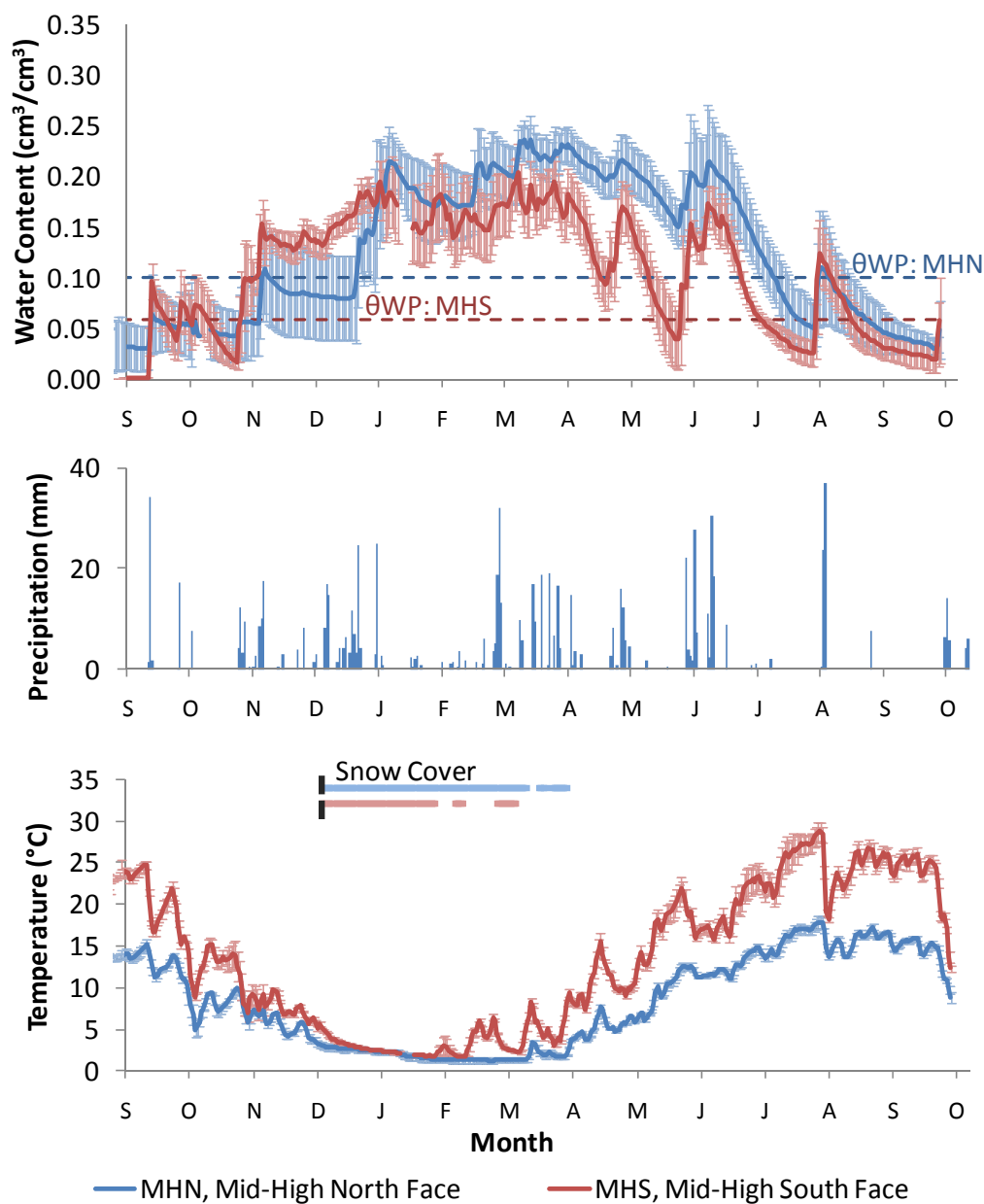


Figure B.13. Soil water content (top) and soil temperature (bottom) at the mid-high elevation north facing (MHN) and mid-high elevation south-facing (MHS) sites as profile- and site-averaged values. Error bars represent spatial variability as the standard deviation of profile-averaged values among the four pits at each site. Precipitation events (rain and snow) are plotted in the center graph. Dates of snow cover, inferred from dampened diurnal fluctuations in shallow soil temperature, are shown at top of the temperature plot. Dates of initial snow cover (marked by bold vertical dashes) are uncertain because the temperature trends may reflect snow cover or soil freezing, but dates of snow cover cessation are more certain. The north aspect generally has higher growing-season soil moisture, lower soil temperature, and a later snowmelt date than the south aspect.

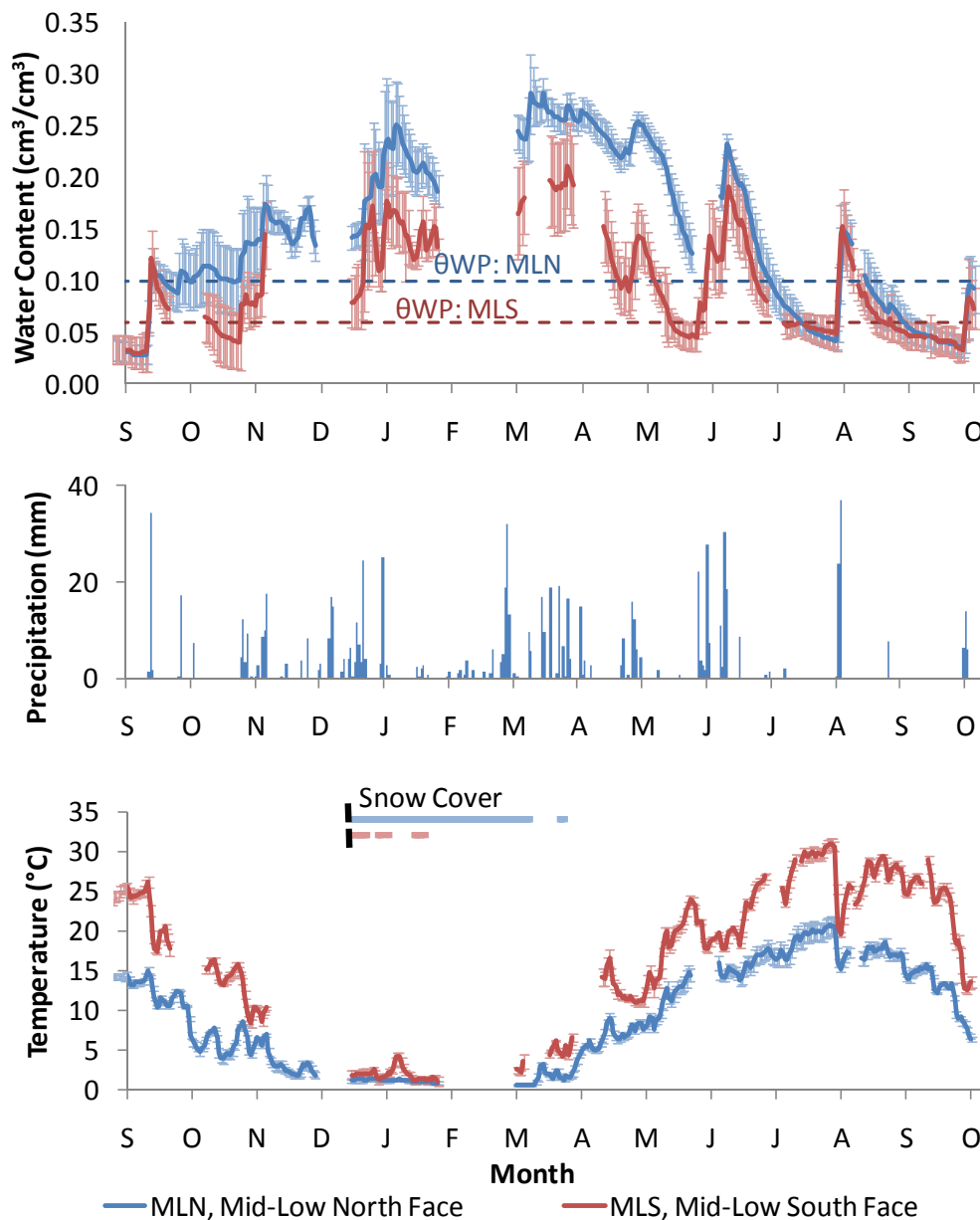


Figure B.14. Soil water content (top) and soil temperature (bottom) at the mid-low elevation north facing (MLN) and mid-low elevation south-facing (MLS) sites as profile- and site-averaged values. Error bars represent spatial variability as the standard deviation of profile-averaged values among the four pits at each site. Precipitation events (rain and snow) are plotted in the center graph. Dates of snow cover, inferred from dampened diurnal fluctuations in shallow soil temperature, are shown at top of the temperature plot. Dates of initial snow cover (marked by bold vertical dashes) are uncertain because the temperature trends may reflect snow cover or soil freezing, but dates of snow cover cessation are more certain. The north aspect generally has higher growing-season soil moisture, lower soil temperature, and a later snowmelt date than the south aspect.

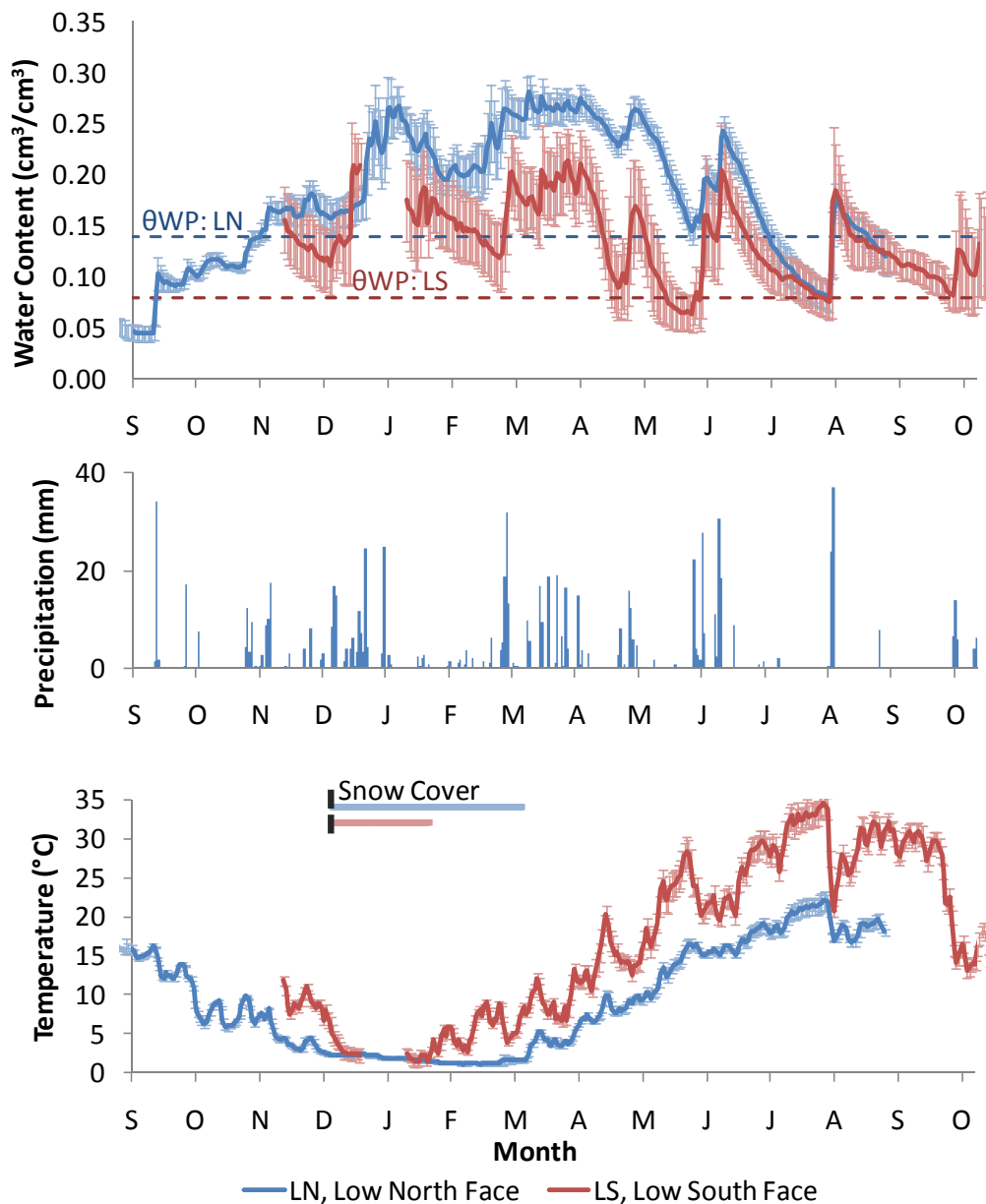


Figure B.15. Soil moisture (top) and soil temperature (bottom) at the low elevation north facing (LN) and low elevation south-facing (LS) sites as profile- and site-averaged values. Error bars represent spatial variability as the standard deviation of profile-averaged values among the four pits at each site. Precipitation events (rain and snow) are plotted in the center graph. Dates of snow cover, inferred from dampened diurnal fluctuations in shallow soil temperature, are shown at top of the temperature plot. Dates of initial snow cover (marked by bold vertical dashes) are uncertain because the temperature trends may reflect snow cover or soil freezing, but dates of snow cover cessation are more certain. The north aspect generally has higher growing-season soil moisture, lower soil temperature, and a later snowmelt date than the south aspect.

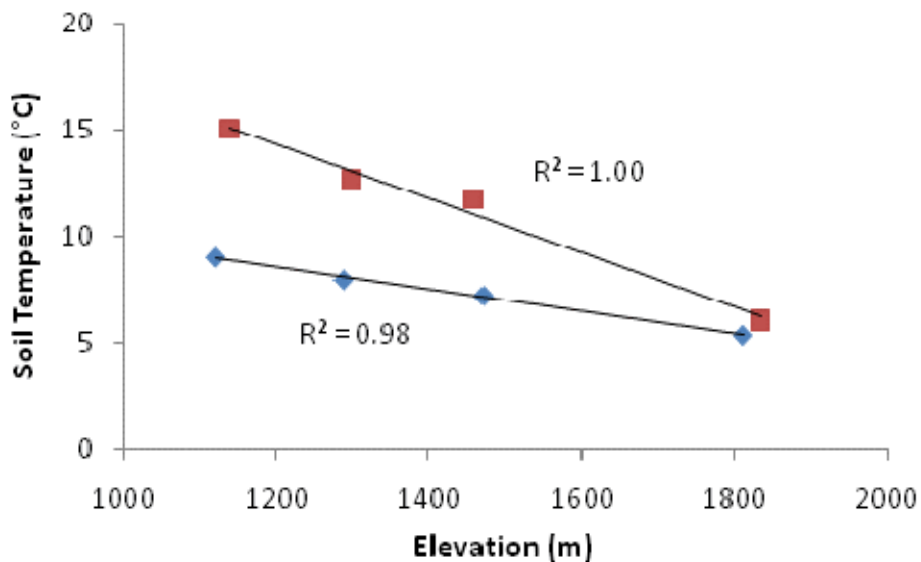


Figure B.16. Relationship between elevation and soil temperature at all sites, with means calculated from the common period of measurement, 11/20/2008 to 9/1/2009. Soil temperature shows a strong relationship with elevation at both aspects.

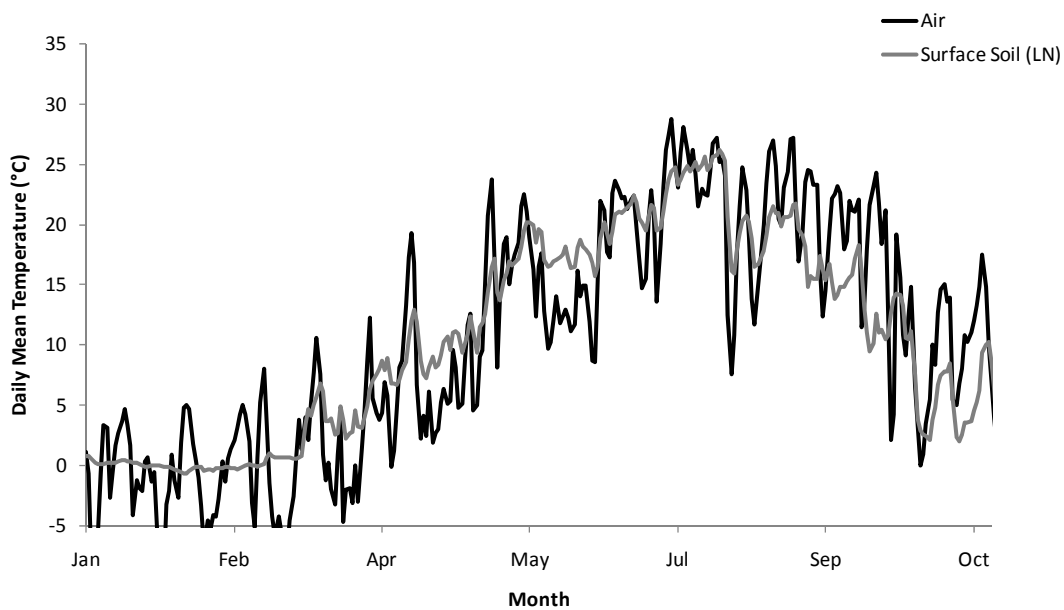


Figure B.17. Soil temperature measured at 2 cm bgs closely tracks trends in spring, summer, and fall air temperatures over 2009 where a study site and a meteorological station are collocated.

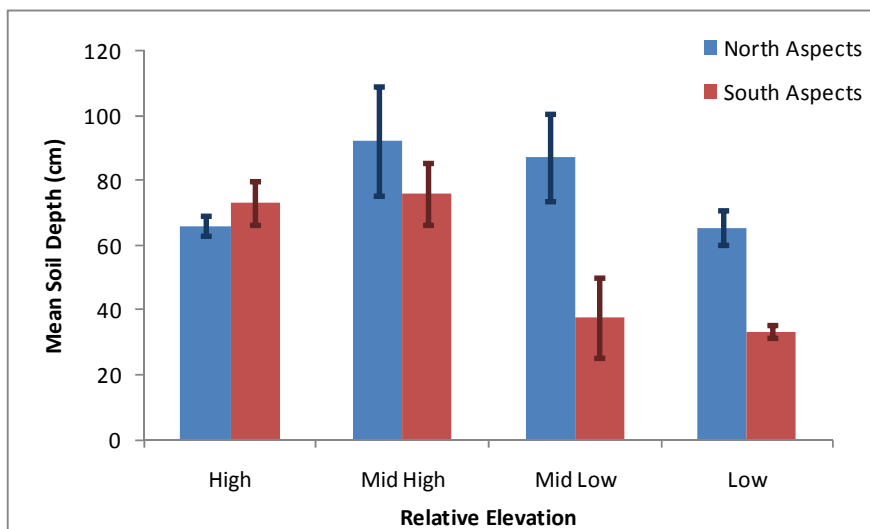


Figure B.18. Differences in soil depth with aspect and elevation. Error bars show standard deviation of soil depths among the four pits at each site. At all but the highest elevation sites, soils are deeper on north aspects than on south aspects, and soil depth increases with elevation.

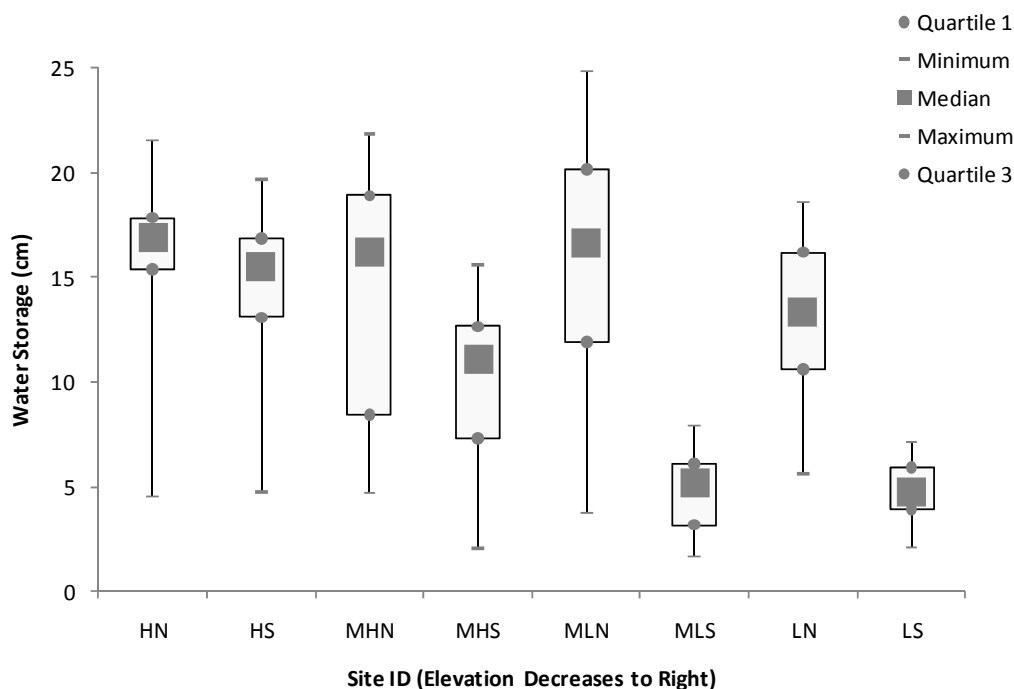


Figure B.19. Distributions of soil water stored in the profile over the common measurement period, 11/20/2008 to 9/1/2009. Sample size is $n = 286$ days at each site. The soil water storage calculation accounts for generally greater soil depths on north aspects and higher elevations.

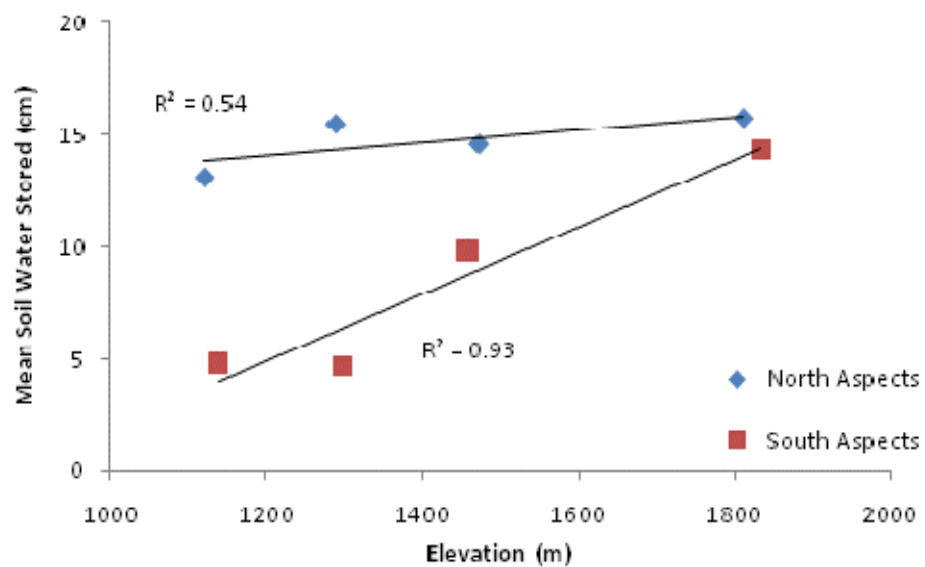


Figure B.20. Relationship between elevation and mean soil water storage at all sites, with means calculated from the common period of measurement, 11/20/2008 to 9/1/2009. By accounting for generally increasing soil depth at increasing elevations, soil water storage values show a stronger relationship with elevation on south aspects than did soil water content.

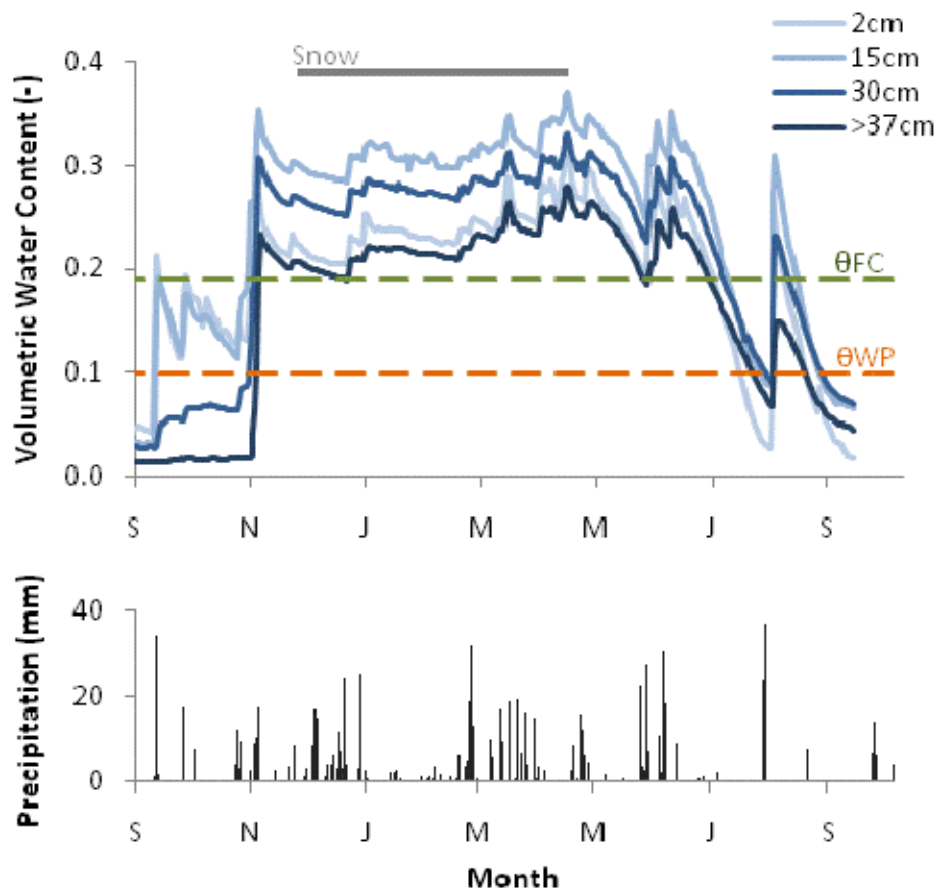


Figure B.21. Soil water content at different depths in the soil profile at site HN, the highest elevation north aspect. The green line indicates field capacity and orange line indicates approximate wilting point for the soil.

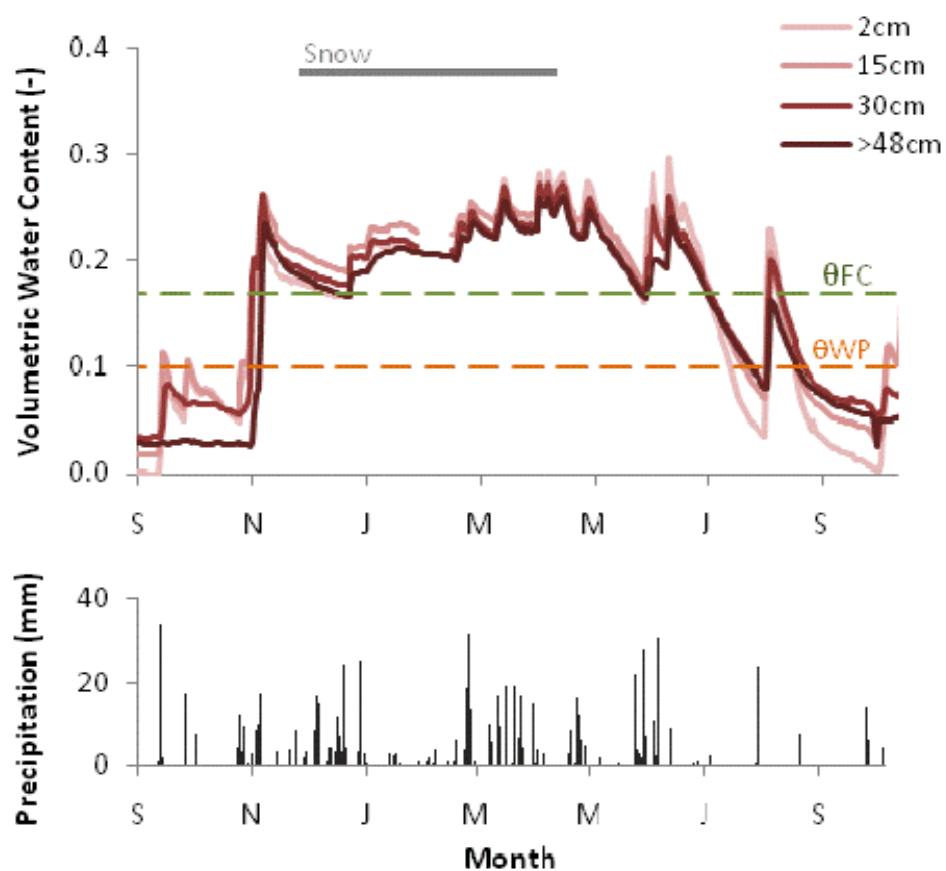


Figure B.22. Soil water content at different depths in the soil profile at site HS, the highest elevation south aspect. Green line indicates field capacity and orange line indicates approximate wilting point for the soil.

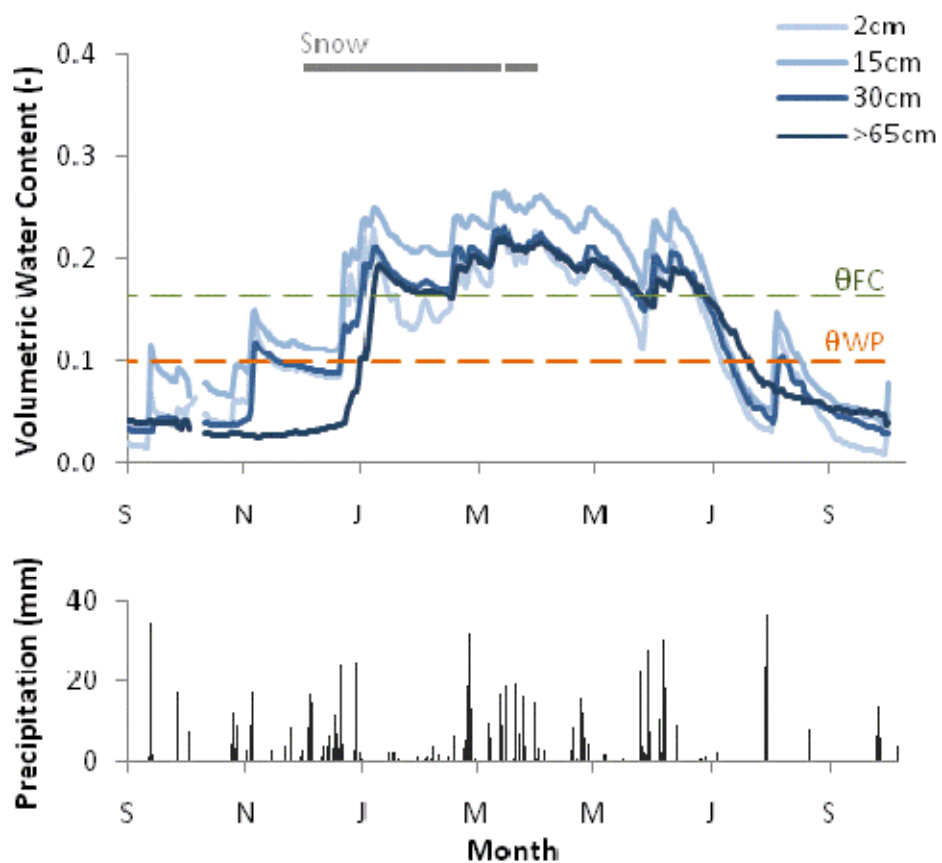


Figure B.23. Soil water content at different depths in the soil profile at site MHN, the mid-high elevation north aspect. Green line indicates field capacity and orange line indicates approximate wilting point for the soil.

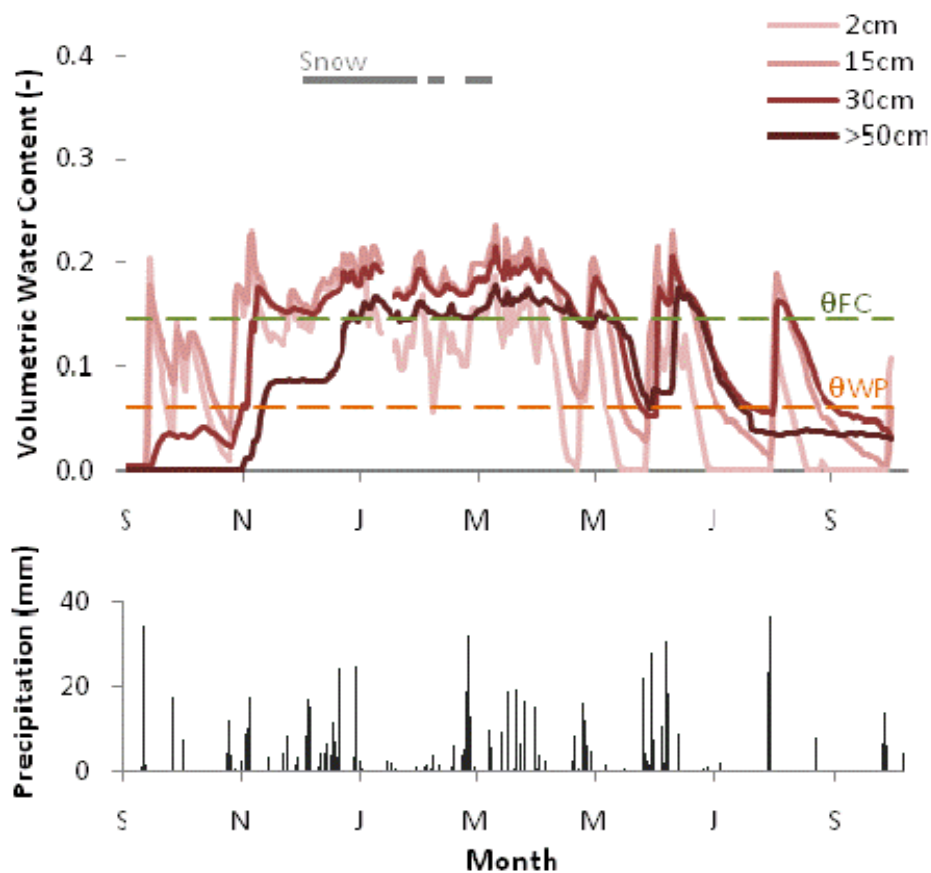


Figure B.24. Soil water content at different depths in the soil profile at site MHS, the mid-high elevation south aspect. Green line indicates field capacity and orange line indicates approximate wilting point for the soil. Data gaps were linearly interpolated to approximate number of days the bottom boundary exceeded field capacity.

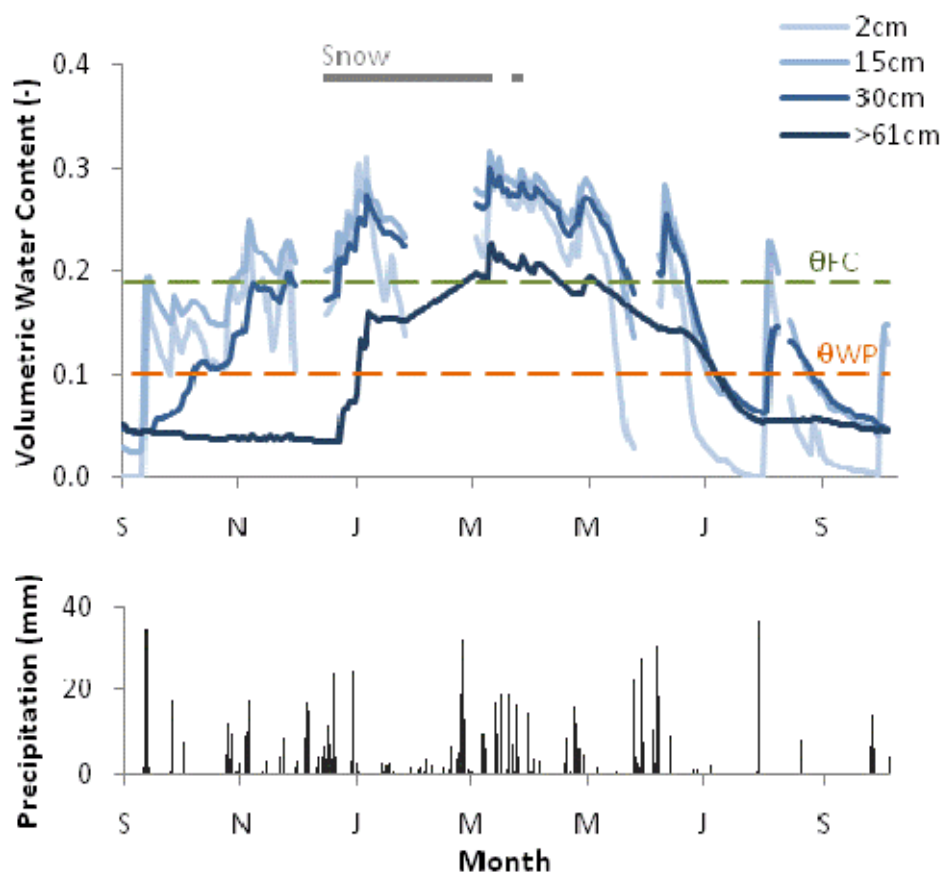


Figure B.25. Soil water content at different depths in the soil profile at site MLN, the mid-low elevation north aspect. Green line indicates field capacity and orange line indicates approximate wilting point for the soil. Data gaps were linearly interpolated to approximate number of days the bottom boundary exceeded field capacity.

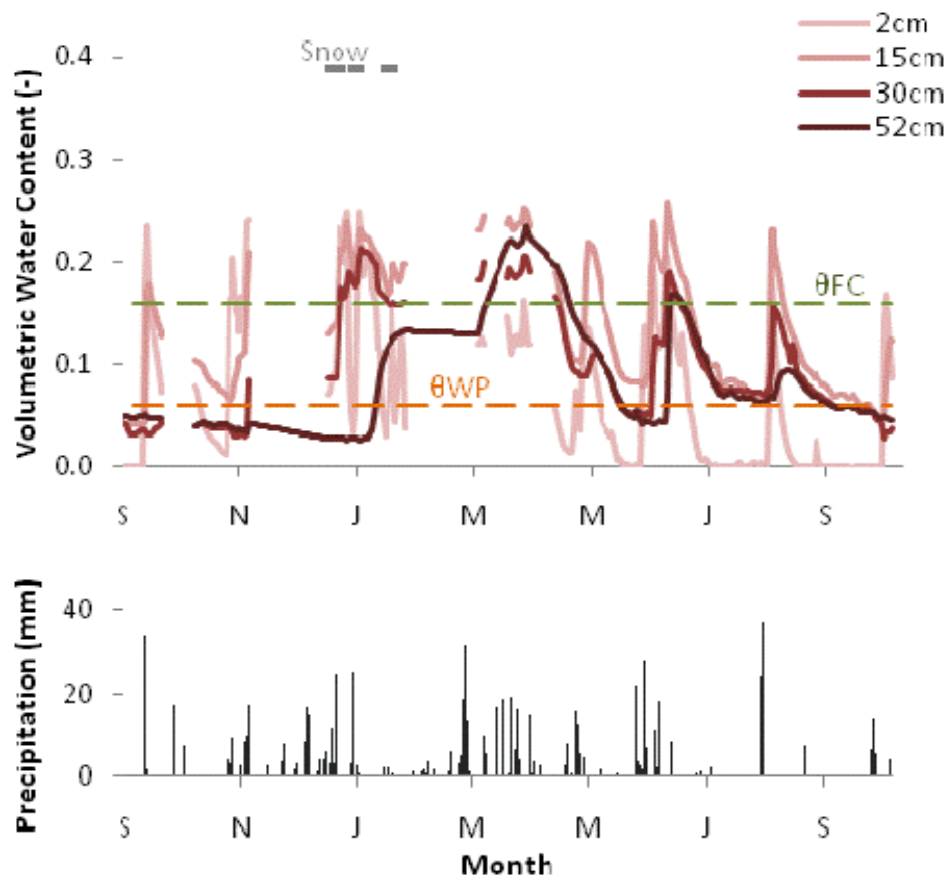


Figure B.26. Soil water content at different depths in the soil profile at site MLS, the mid-low elevation south aspect. Green line indicates field capacity and orange line indicates approximate wilting point for the soil. Data gaps were linearly interpolated to approximate number of days the bottom boundary exceeded field capacity.

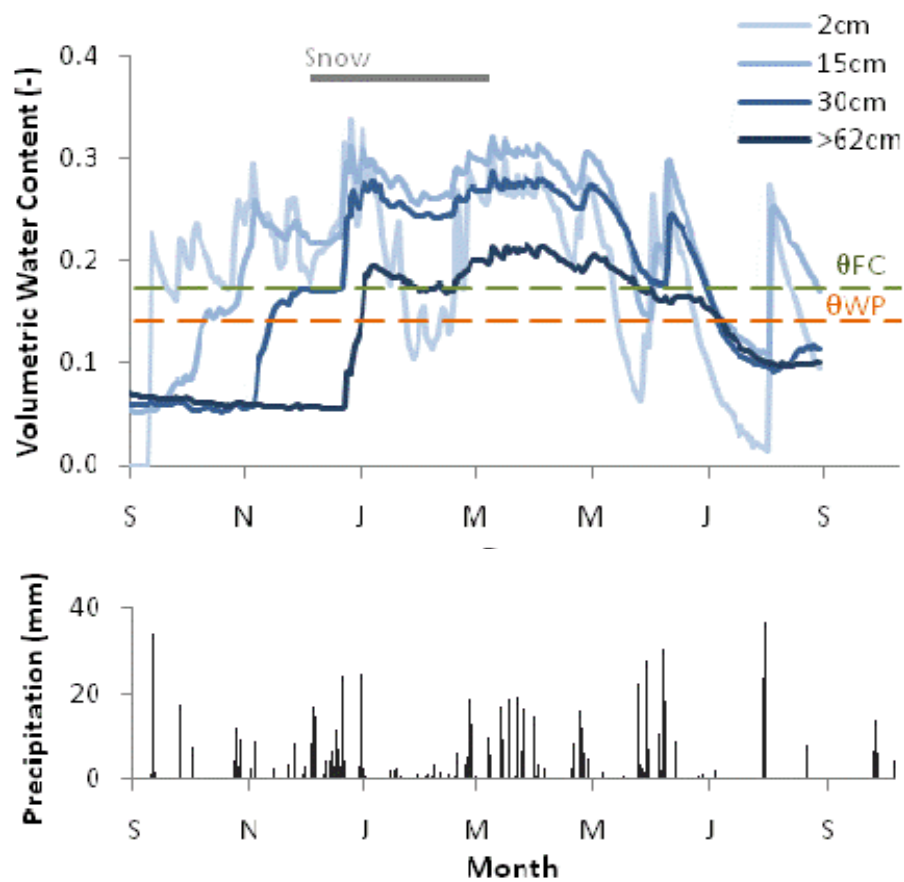


Figure B.27. Soil water content at different depths in the soil profile at site LN, the low elevation north aspect. Green line indicates field capacity and orange line indicates approximate wilting point for the soil.

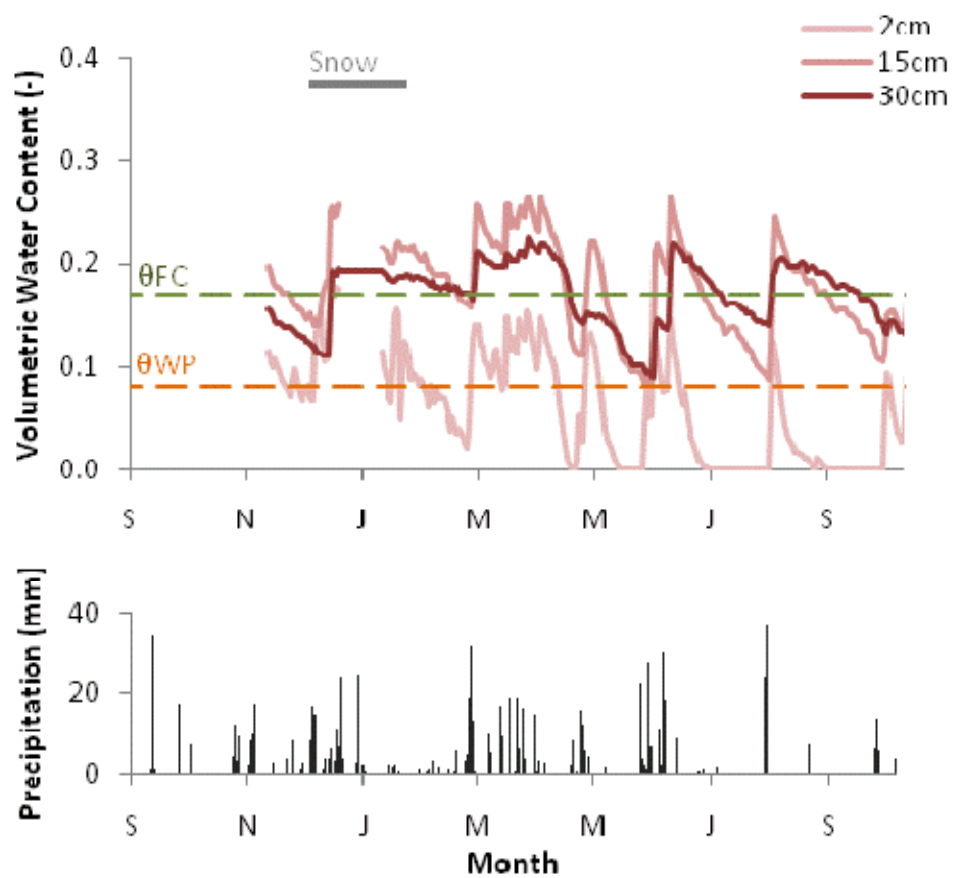


Figure B.28. Soil water content at different depths in the soil profile at site LS, the low elevation south aspect. Green line indicates field capacity and orange line indicates approximate wilting point for the soil. Data gaps were linearly interpolated to approximate number of days the bottom boundary exceeded field capacity.

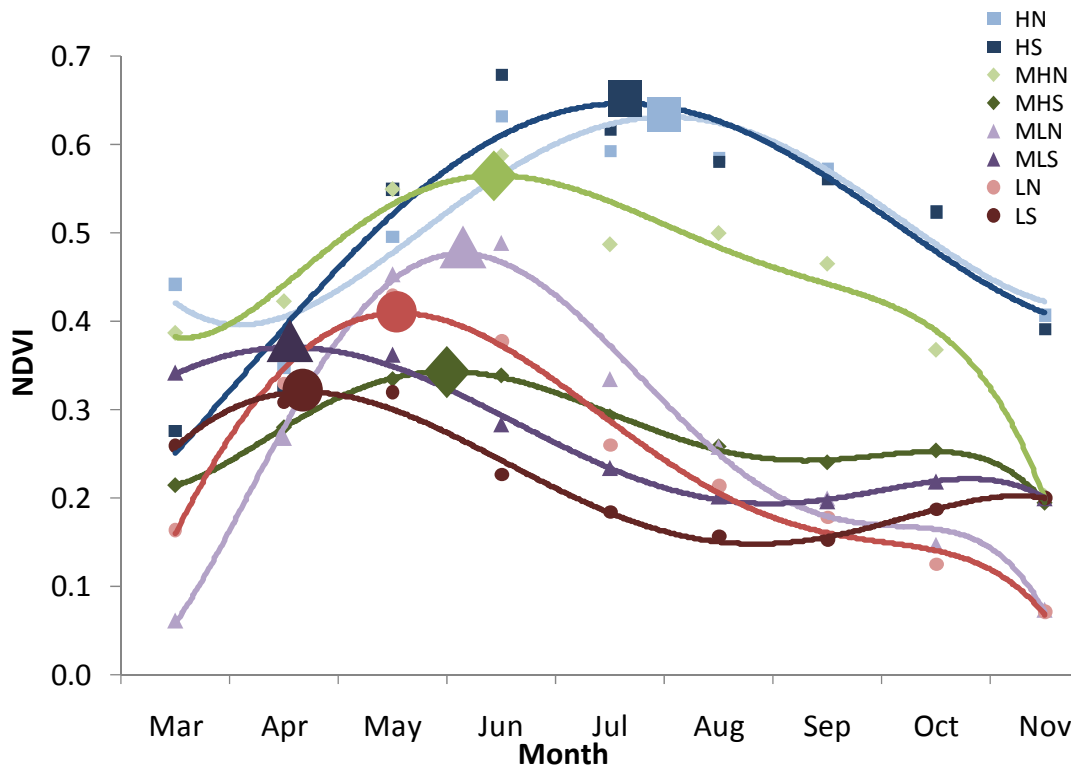


Figure B.29. Vegetation canopy cover during the growing season approximated using the Normalized Difference Vegetation Index (NDVI) derived from remote sensing images collected by Landsat-5 TM. Values shown are monthly averages over the growing seasons of the four-year period from 2006 to 2009. The series for each site has been fit with a fifth-order polynomial to clarify patterns and infer relative timing of peak NDVI. Colored shapes mark the inferred peak NDVI for each site. Forested sites have the highest NDVI; below them, north-facing sites have greater NDVI than south-facing sites at the lowest, mid-low, and mid-high elevations; on a given aspect, NDVI generally increases with elevation (MHS is an exception), and the date of peak NDVI generally occurs later on north aspects and on higher elevation sites (MLS is an exception).

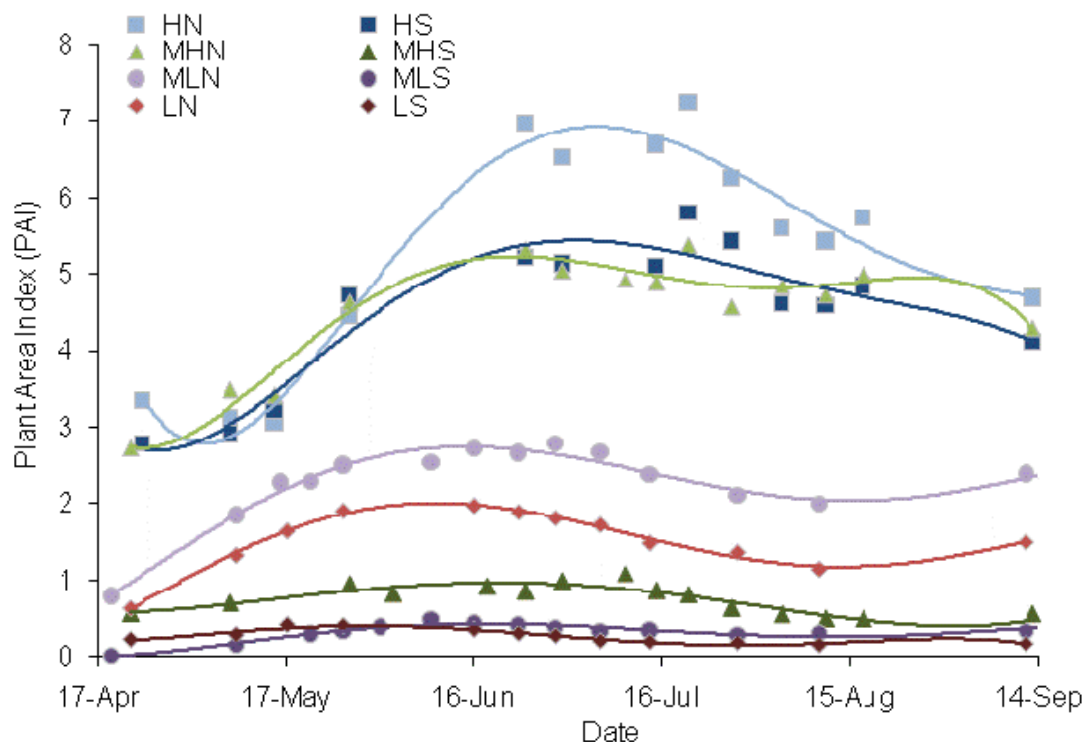


Figure B.30. Vegetation cover as Plant Area Index (PAI) measured during part of the 2009 growing season using a handheld AccuPAR LP-80 ceptometer. Measurements were taken on the ground to validate the NDVI values derived from remote sensing. As with NDVI, forested sites show the most dense canopy cover. Below them, north-facing sites have greater PAI than south-facing sites, and higher elevation sites have greater PAI on a given aspect. The date of peak PAI appears to occur later on north aspects and higher elevation sites relative to south aspects and lower elevation sites, but peak dates were not determined from the PAI dataset because early and late season measurements were prohibited by persistent cloudiness during the 2009 growing season.

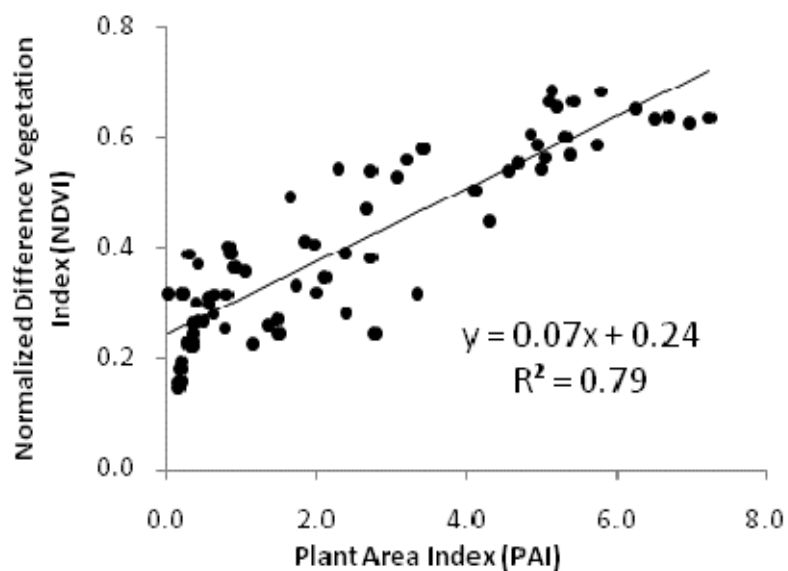


Figure B.31. Correlation between Plant Area Index (measured at 1 m resolution on the ground) and NDVI (measured at 30 m resolution from Landsat 5-TM satellite) for the 2009 growing season. The two methods of estimating vegetation cover are strongly correlated, offering validation for using the NDVI as a measure of vegetation canopy cover in the study area.

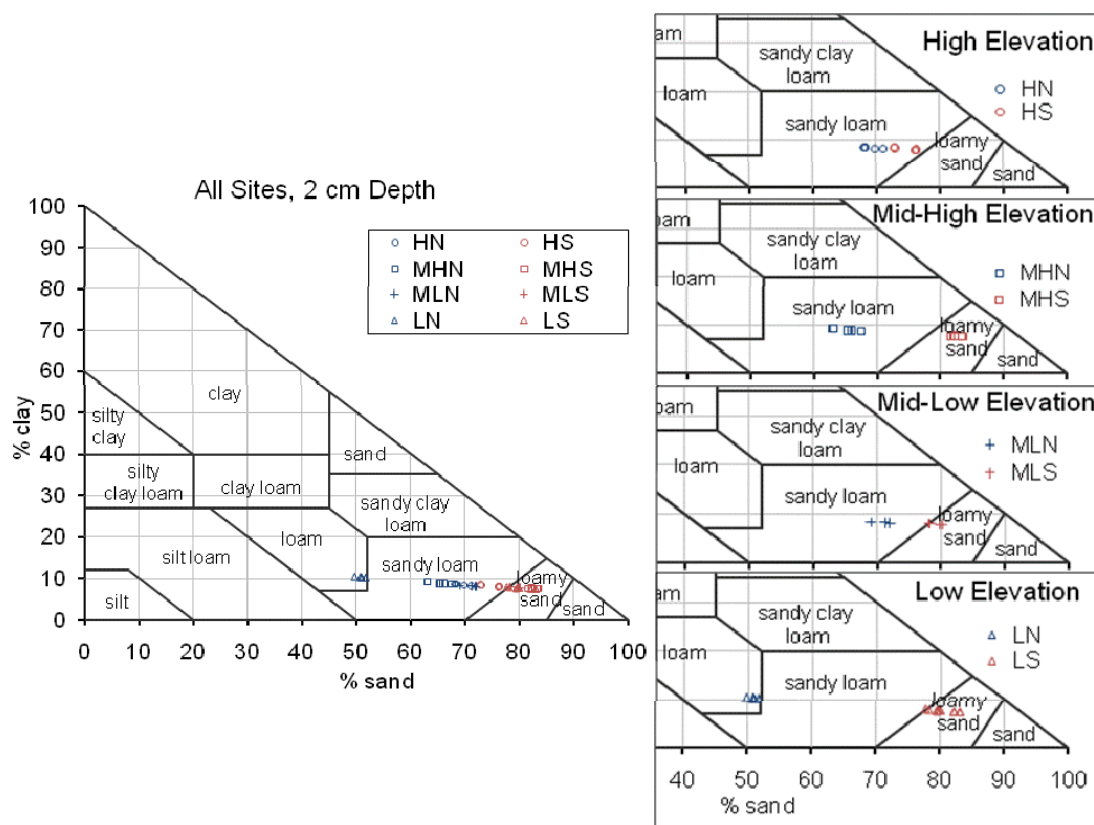


Figure B.32. Results of soil textural analyses for samples taken from 2 cm below ground surface. Soils on north aspects generally plot in a finer textural class than those on south aspects. Silt is the chief determinant of the fine fraction (ranging from 9.0% to 39.8% silt by mass), whereas clay content varies little (from 7.4% to 10.5% clay by mass). The low elevation north facing site LN is distinctly high in silt relative to all other samples. HN n = 6; HS n = 5; MHN n = 6; MHS n = 8; MLN n = 6; MLS n = 7; LN n = 6; LS n = 13. Thank you to A. Gerakis and B. Baer for the plotting program.

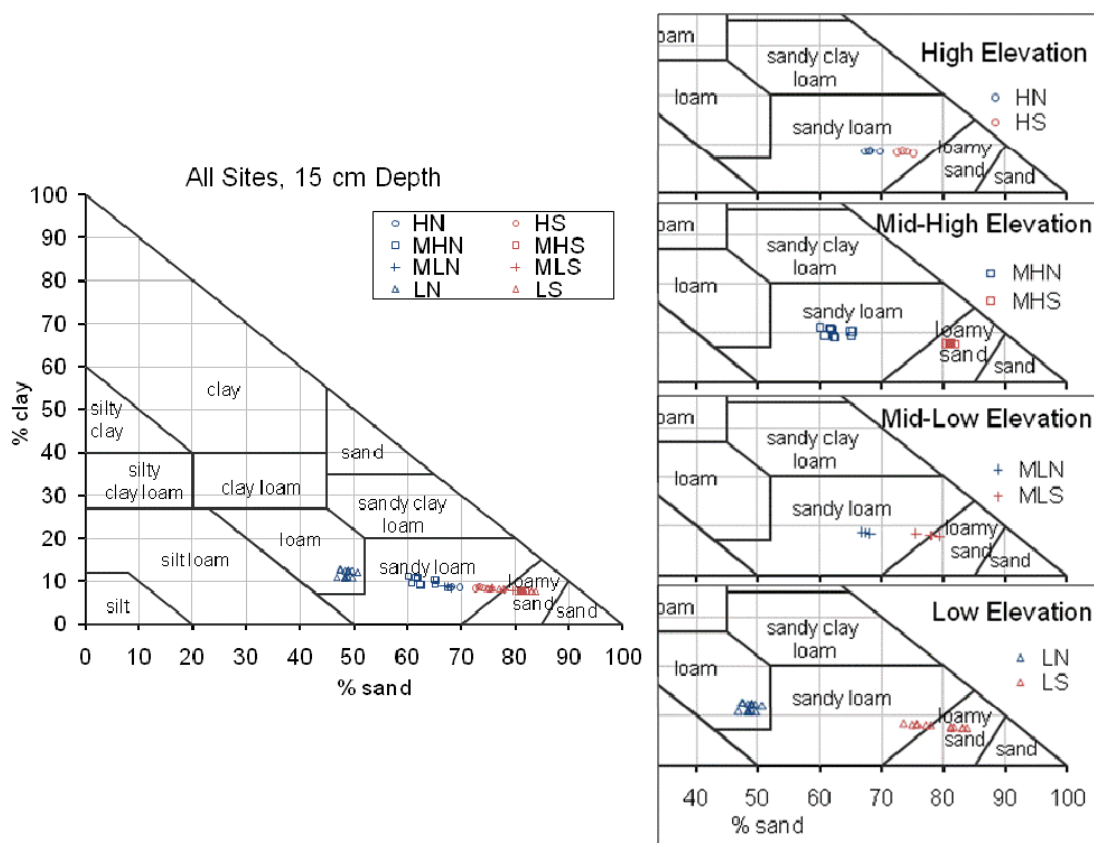


Figure B.33. Results of soil textural analyses for samples taken from 15 cm below ground surface. Soils on north aspects generally plot in a finer textural class than those on south aspects. Silt is the chief determinant of the fine fraction (ranging from 8.7% to 42.3% silt by mass), whereas clay content varies little (from 7.5% to 12.7% clay by mass). The low elevation north facing site LN is distinctly high in silt relative to all other samples. HN n = 4; HS n = 4; MHN n = 16; MHS n = 14; MLN n = 3; MLS n = 4; LN n = 16; LS n = 13. Thank you to A. Gerakis and B. Baer for the plotting program.

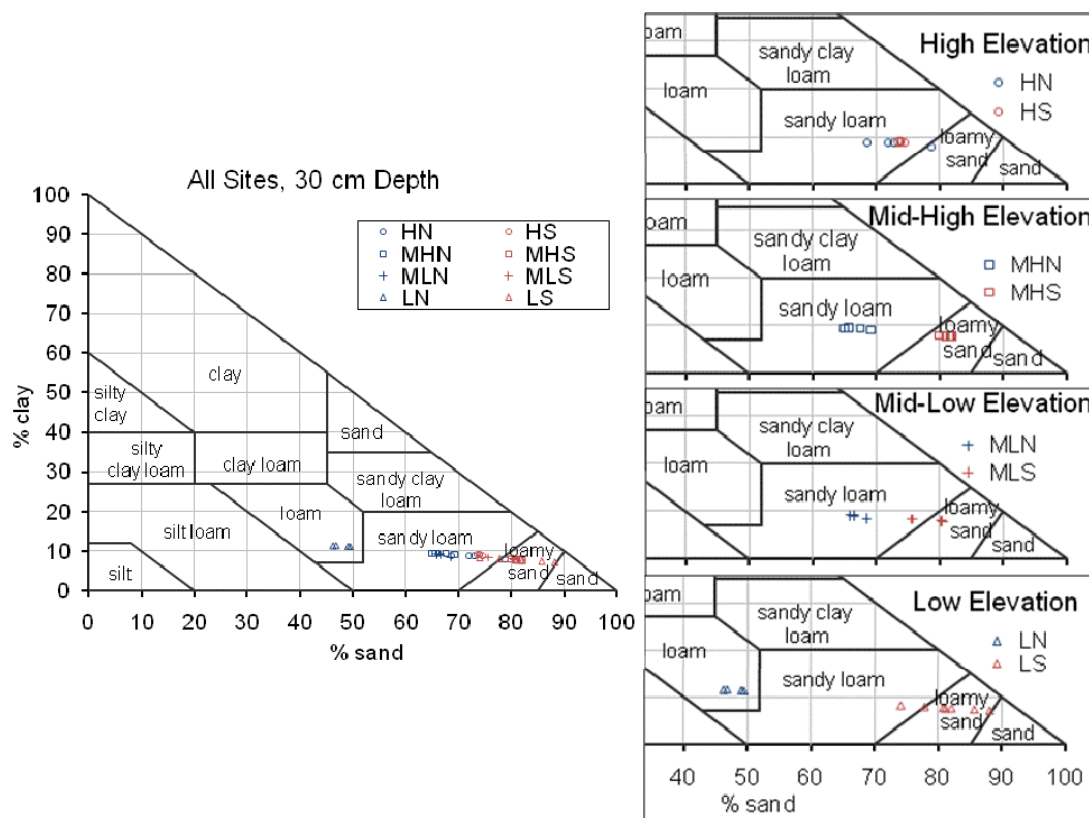


Figure B.34. Results of soil textural analyses for samples taken from 30 cm below ground surface. Soils on north aspects generally plot in a finer textural class than those on south aspects. Silt is the chief determinant of the fine fraction (ranging from 4.6% to 42.2% silt by mass), whereas clay content varies little (from 7.2% to 11.5% clay by mass). The low elevation north facing site LN is distinctly high in silt relative to all other samples. HN n = 4; HS n = 4; MHN n = 4; MHS n = 9; MLN n = 4; MLS n = 4; LN n = 4; LS n = 7. Thank you to A. Gerakis and B. Baer for the plotting program.

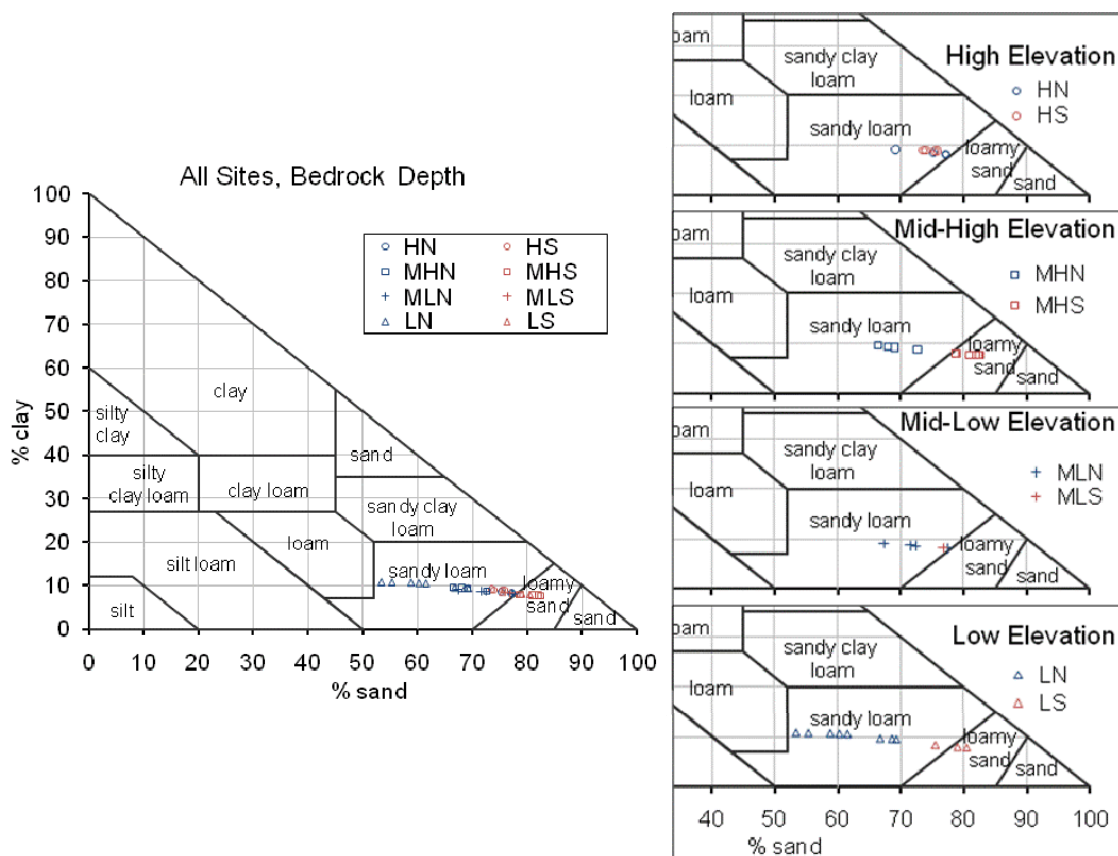


Figure B.35. Results of soil textural analyses for samples taken at the soil-bedrock interface, which occurred at varying depths. Soils on north aspects generally plot in a finer textural class than those on south aspects. Silt is the chief determinant of the fine fraction (ranging from 9.8% to 35.9% silt by mass), whereas clay content varies little (from 7.6% to 10.7% clay by mass). The low elevation north facing site LN is distinctly high in silt relative to all other samples. HN n = 4; HS n = 4; MHN n = 4; MHS n = 7; MLN n = 4; MLS n = 1; LN n = 8; LS n = 3. Thank you to A. Gerakis and B. Baer for the plotting program.

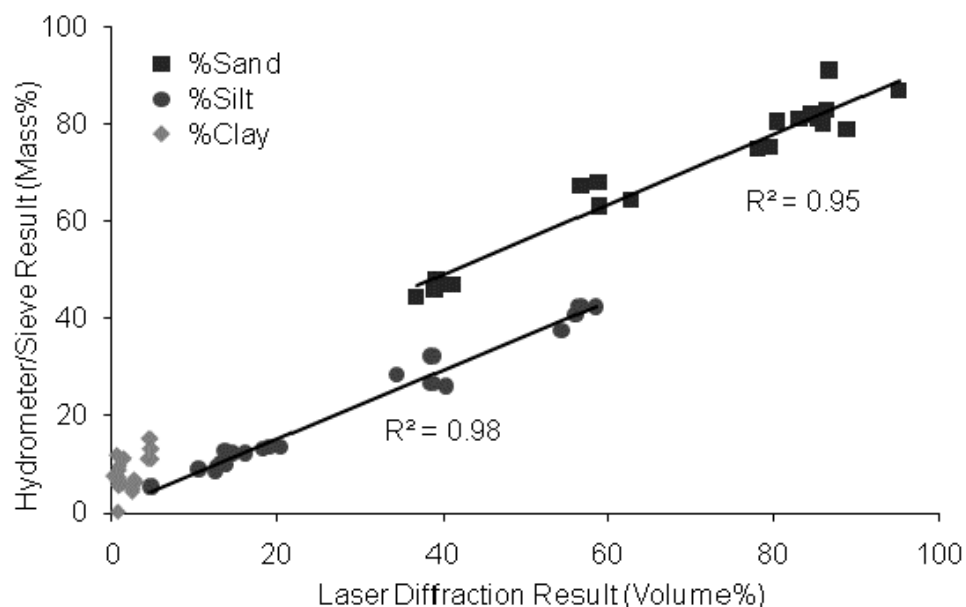


Figure B.36. Correlation between particle size fractions (excluding gravel) obtained using laser diffraction versus hydrometer/sieve methods. Linear relationships between the sand and silt fractions determined using both laser diffraction and mechanical analysis (hydrometer/sieve) were used to predict mechanical analysis results from laser diffraction results for soil samples. Because laser diffraction is a relatively new method in soil textural analysis, a converting results to the more traditional mechanical method allows us to relate our soil classifications with those in other studies.

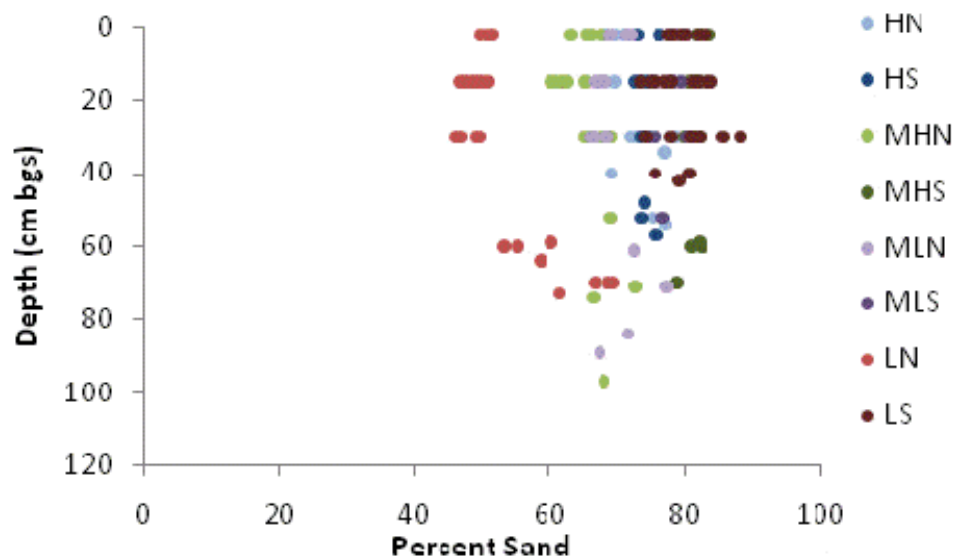


Figure B.37. Soil sand content does not generally appear to change systematically with depth; an exception is site LN, which contains less sand in the upper 30 cm bgs.

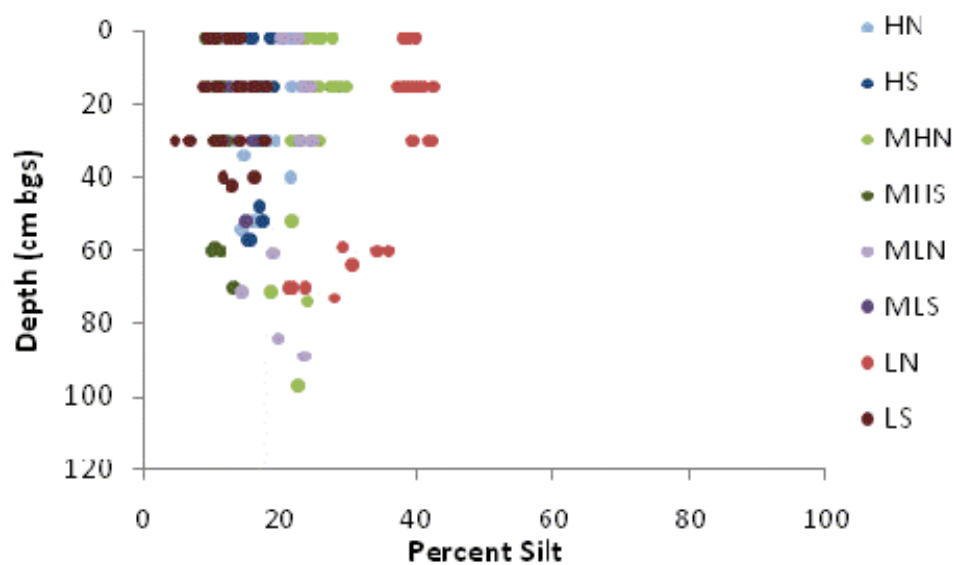


Figure B.38. Soil silt content does not generally appear to change systematically with depth; an exception is site LN, which contains more silt in the upper 30 cm bgs.

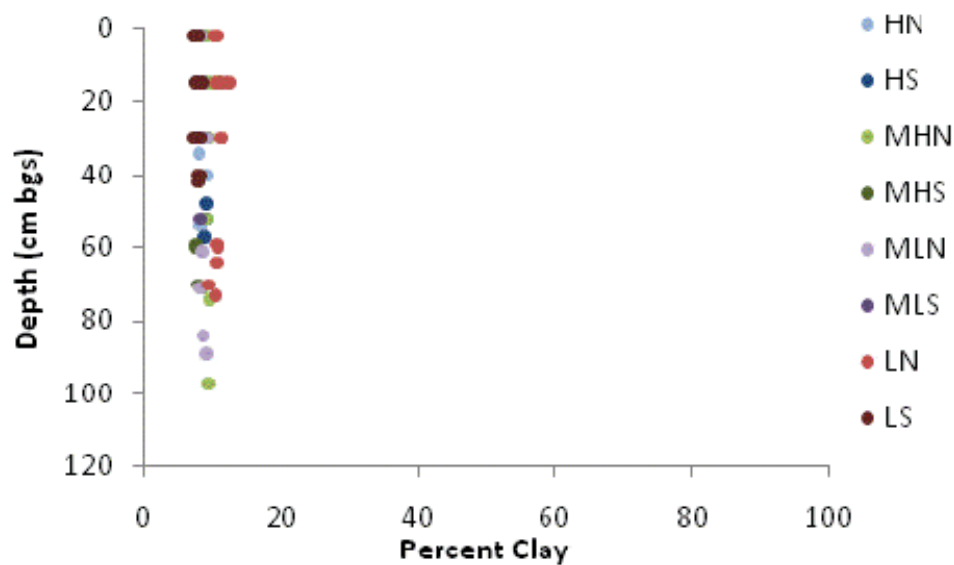


Figure B.39. Soil clay content does not generally appear to change systematically with depth at the study sites, and is low in all soil samples.

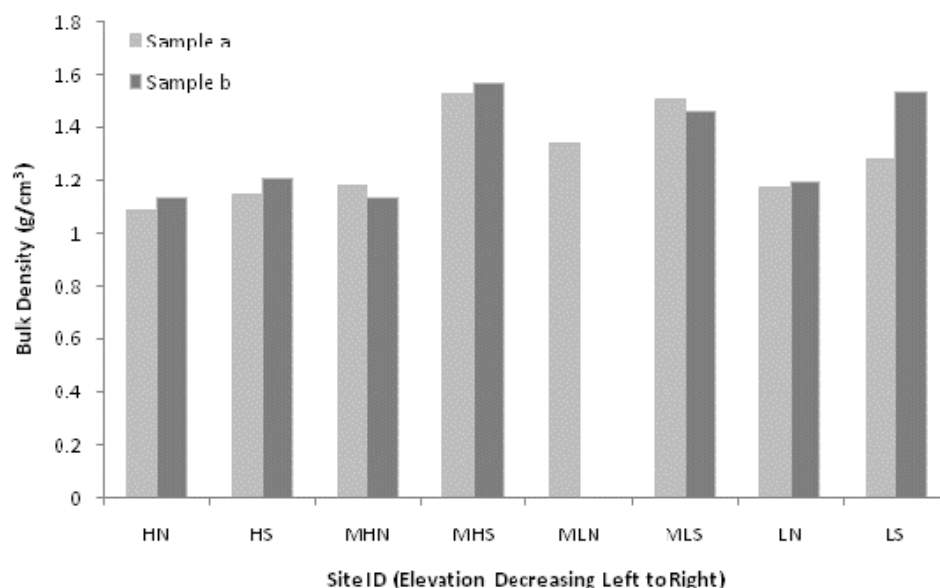


Figure B.40. Spatial trends in the bulk density of soil averaged over 5 to 30 cm below ground surface. Soil was sampled as two replicates from each site except MLN; bars show bulk density results from each sample to display uncertainty in results. Bulk density is generally greater where soil carbon content is lower - on south aspects relative to north aspects, and in lower elevations relative to higher elevations.

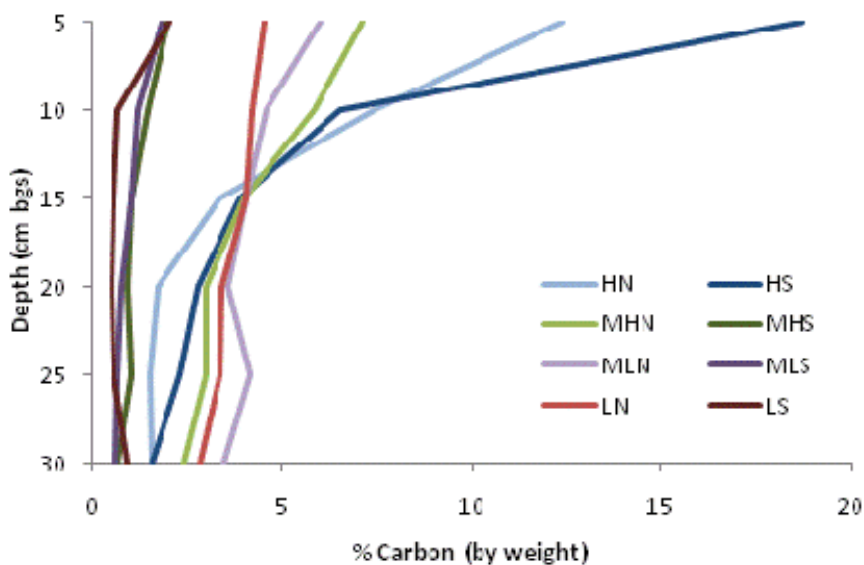


Figure B.41. Total soil carbon content as percent by weight over the profile at each site. Results are averaged from two field replicates at each site and random laboratory replicates; replicate values lay within 8% of the mean value for each depth.

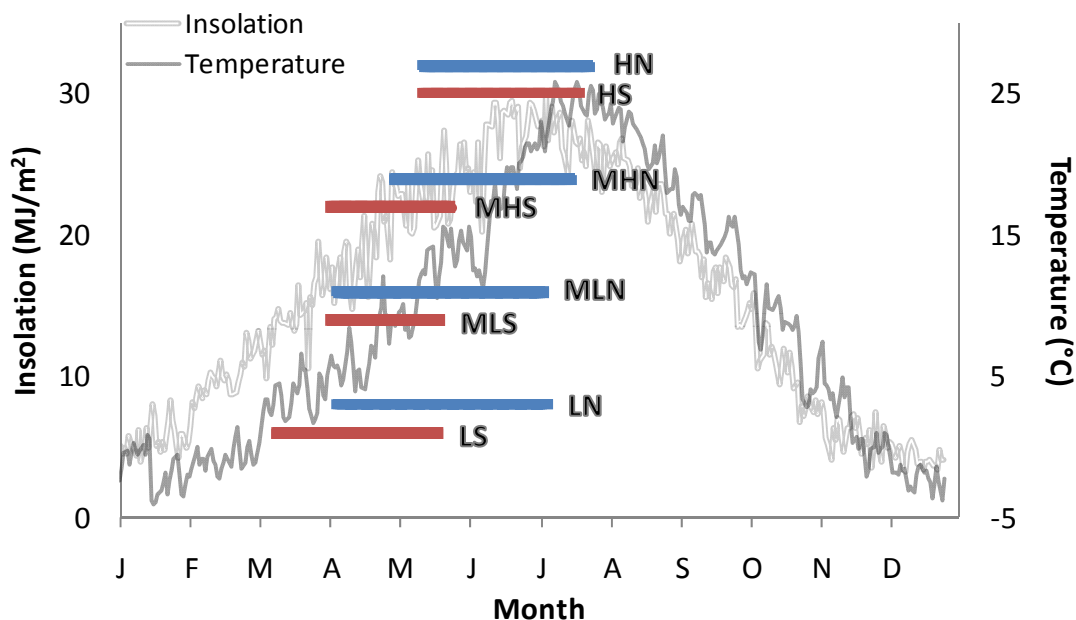


Figure B.42. Lengths of the potential growing season for each study site with mean annual trends in air temperature and insolation. Potential growing season was defined as the time period beginning when the shallow soil (2cm bgs) surpassed 5°C for the season and ending when the soil profile dried below the approximate wilting point. We see denser peak plant cover and greater soil carbon content at locations which retain plant-available soil water for a longer period of the warm, sunny summer.

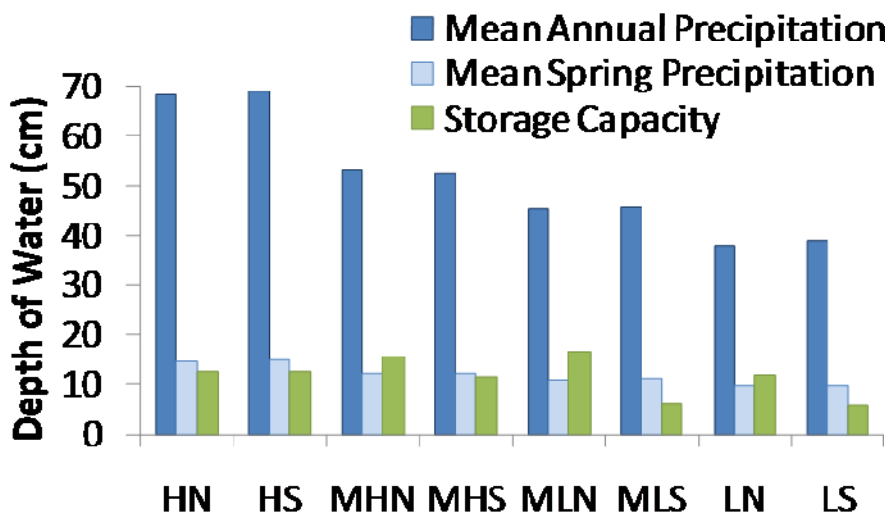


Figure B.43. Comparison of mean annual precipitation, mean spring (April-May-June) precipitation, and soil water storage capacity (field capacity * soil depth) at each study site. The storage capacity of soils is small relative to annual precipitation. Average amounts of spring precipitation are sufficient to recharge the soil water reservoir, and the timing of spring precipitation allows it to be utilized in ecosystem functions.

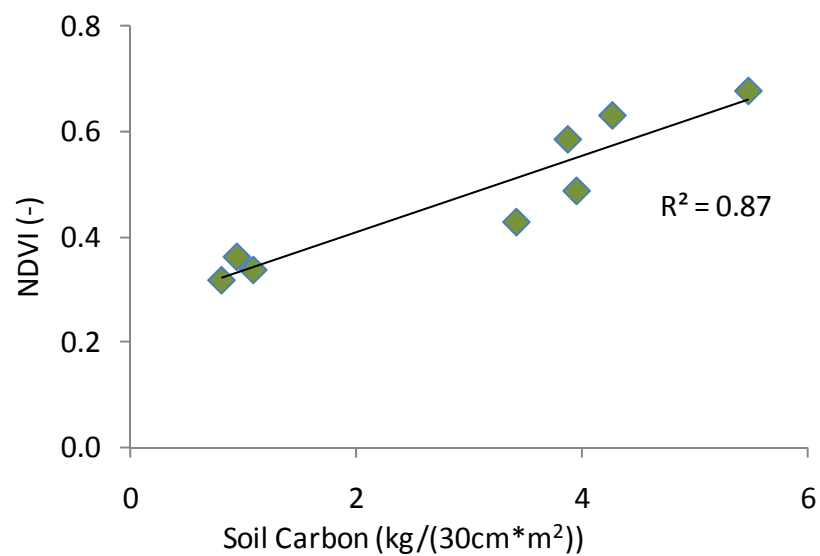


Figure B.44. Correlations between annual maximum, or “peak” vegetation cover (as Normalized Difference Vegetation Index, NDVI) and soil carbon content at study sites. The strength of the correlation between the variables is evidence that above and below ground carbon stocks respond to similar controlling factors.

APPENDIX C

Protocol for Plant Area Index Sampling and Data Processing

AccuPAR LP-80 Ceptometer Sampling Protocol

9/15/2009

First visit: At each site, lay out 3 transects, each 10m long, using field tape. Flag endpoints and every 1m point. To locate the transects, place a flag 10 paces (one step with each foot) directly upslope, directly downslope, and either directly east or directly west of the center of the polygon defined by soil pits. The flag marks the 5 m center point of the 10 m transect, as shown below.

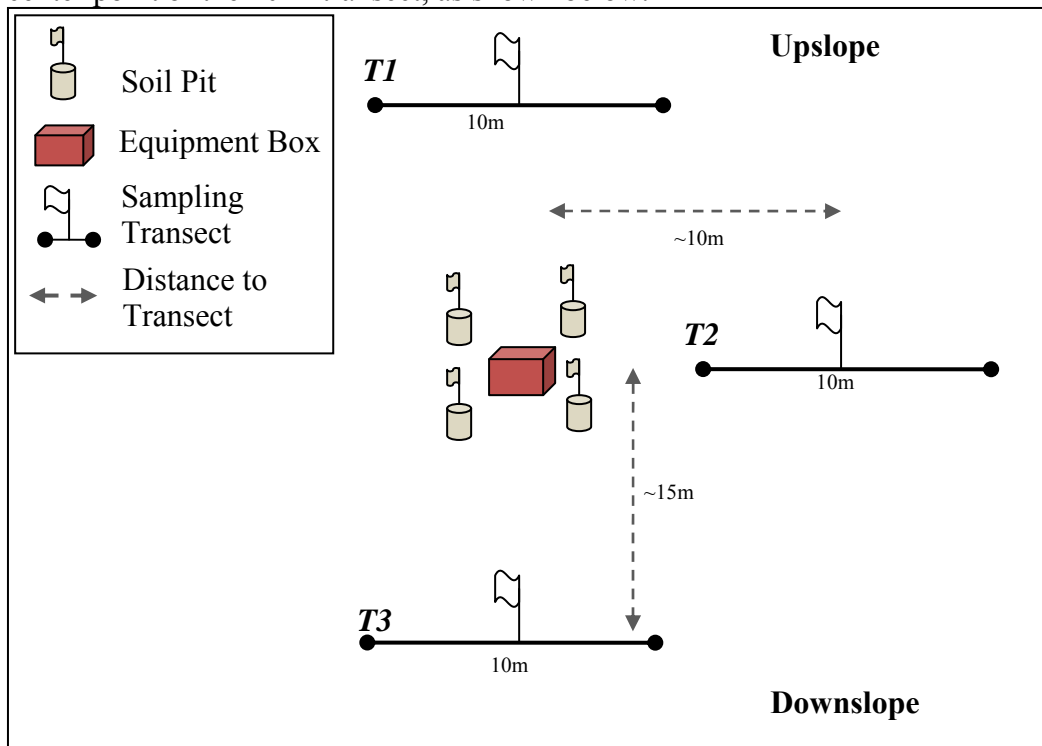


Figure C1. Configuration of Plant Area Index transects around soil moisture stations.

- 1) From these flagged points, construct each 10 m transect line according to Figure C2. At each 1m point on the transect, place a flag. The region directly upslope (shown as the dashed square in Figure C2) will be sampled weekly for leaf area index, so should not be trampled at all.

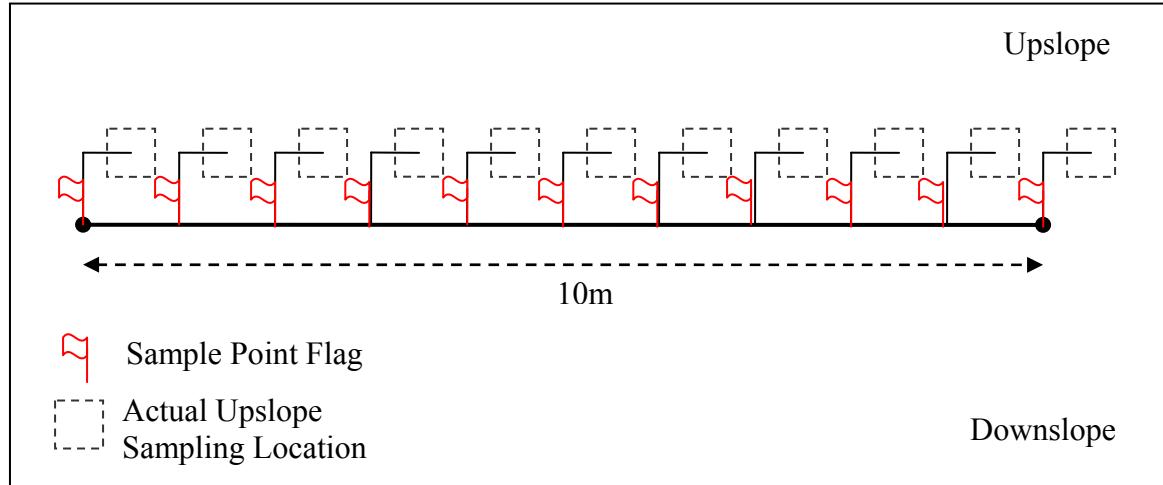


Figure C2. Layout for each transect.

Sampling Protocol

- 1) Take ceptometer readings around noon (10am to 2pm is ideal, though 9-3 is acceptable), on a uniformly cloudy or uniformly clear day, so that the sun angle and above-canopy radiation remain consistent. **Record the site name, date, and weather conditions, including estimate of cloud cover and wind, in your notebook. Please carefully note where the soil pits are located at each site (they are four points near the action packer, flagged) and avoid stepping on the area around the soil pits. Also note the location of the flagged transects, and do not walk on the area about 3m upslope of transects so as not to disturb the soils and vegetation we are measuring.**
- 2) You should have the following items with you each time you sample:
 - a) Field notebook and pencil
 - b) Current timepiece
 - c) Safety glasses
 - d) Isopropyl alcohol and lens cloth
 - e) LP-80 instrument
 - f) Extra flags
 - g) Girded-up loins
 - h) 4 Extra AAA batteries
- 3) **Power on the LP-80.**
- 4) **Setup:** Using the Menu button, go to the Setup Menu and set the first two sections as follows, leaving the other sections untouched:
 - a) **Date/time-** set to current; **daylight savings** (box will be checked from March 8, 2009 until November 1, 2009). It is very important that these be correct to calculate zenith angle! Hit Esc to return to Setup Menu.
 - b) **Location- Seattle** (Enter); then input correct latitude and longitude for Dry Creek Watershed: **44 lat, -116 long, GMT offset -6hrs** (during summer daylight savings time): **THEN HIT ESC TO SAVE!!!** You won't be able

to go back and check this entry because it will reset when you re-enter the screen, but if you hit ESC it will save the coordinates. Have faith.

5) **BEGINNING A TRANSECT:**

- a) Use the Menu button to Select File: New, and press Enter for OK. You can use File:View to see the filename (which is the time the file was opened) of the currently open file to which your data will be saved.
- b) Record the filename (time) and the transect (T1, T2, T3) you are sampling in your notebook for each transect you sample (the filenames are just the time, so if you record the time I can connect each file to the appropriate transect). If any mistakes are made as you sample the transect, please note them specifically within that time/transect note so that I can locate the errors when I process the data.
- c) Clean LP-80 rod with fiber-free lens cloth and isopropyl alcohol.
- d) Use the Menu button to go to PAR to begin sampling.
- e) I encourage you to record your measurements by hand in your notebook. The AccuPAR will save the data, but hand-recording the data will ensure that you can track any mistakes on paper for correction later, and that the data make it back to the office.

6) **Sampling All Transects**

- a) Sample the transects in sequence beginning with the upslope transect (T1), downslope through T2 and then T3.
- b) Always begin sampling at the easternmost flag (sample moving east to west).
- c) As you sample the transect, be sure to face the sun so that you will not cast a shadow on the sensor.
- d) The protocol for taking measurements at each 1m flag is to stop with one foot on the flag, face the sun, then gently (taking care not to disturb the ground surface and vegetation!) take one sidestep directly upslope (just big enough for you to balance somewhat comfortably) and position the length of the LP-80 sensor rod perpendicular to the slope (parallel with the transect), holding the sensor uphill from your body as far as possible while still allowing you to see the bubble level. It is important to hold the instrument far from your body so that you do not shade the instrument, and so that light is not reflected off you onto the instrument. Do not sit on the ground, but rather balance gently on your upslope foot to minimize disturbance of soil and vegetation.
- e) Clean the sensor frequently with the lens cloth and isopropyl alcohol, as debris on the sensor will obstruct the measurements.

7) **Sampling Grass/Shrub Areas (LN, LS, MLN, MLS, MHS)**

- a) Follow the same directions for “#5, BEGINNING A TRANSECT.”

- b) At the first flag, first take a series of 3 good readings above the canopy by holding the instrument level and pushing the up arrow button 3 times.
 - c) Then, carefully slide the entire instrument below the vegetation canopy, as close to the ground as possible while still allowing you to level the instrument using the bubble level. Try to slide the rod in underneath the vegetation, rather than bringing the rod straight down and flattening the vegetation. The rod should be oriented pointing toward the sun, parallel with the transect (perpendicular to the fall line of the slope). Do not place your hand anywhere on the sensor rod because you will interfere with light and will add oils to the sensor; keep your hands on the control box. Take 3 good readings from the leveled instrument by pressing the down arrow 3 times. The displayed readings are averages above and below.
 - d) Record the readings for average above- and below-canopy PAR (displayed values) in your notebook.
 - e) Hit enter to save the set of readings to file, then proceed carefully to the next flag along the transect.
- 8) **Sampling Forested Sites** (HN, HS, MHN): Getting above-canopy readings will be different for these sites.
- a) Follow the same directions for “#5, BEGINNING A TRANSECT.”
 - b) First take a series of 3 above-canopy reading (by hitting the UP ARROW button) in a clearing in direct sunlight. Then, take 3 below-canopy readings (DOWN ARROW button, in series of 3 button-pushes per flag) along the transect. Record the values for above and below and hit enter. Then take below-canopy readings (DOWN ARROW button, in series of 3 button-pushes per flag) for 5 more flags. Follow with another above-canopy reading in a clearing and a below canopy reading (record and hit enter), then take the rest of the below-canopy readings at the remaining flags, then close the set with a final above-canopy reading in a clearing and record and enter the data. Thus, you will be making an above-canopy reading at the beginning, middle, and the end of each transect.

AccuPAR LP-80 Ceptometer Data Entry Procedure

9/15/2009

I. Downloading Data

- 1) Connect the LP-80 to the serial port on your computer or laptop using the provided cable, and plug in the USB drive (provided).
- 2) Insert the AccuLink CD into your DVD or CD drive and open it. Follow the steps to install the software on your computer.
- 3) Open AccuLink and turn on the LP-80. Go to the Setup menu and scroll down to highlight "Download All Data;" hit ESC. Then go to "File" and select "Send." In the AccuLink dialogue box on the computer, set the Baud Rate to 9600. Click "Connect" in the AccuLink dialogue box. You should see all the files on the LP-80 listed. Click the top file, hold the Shift Key, and click the last file. This should select all the files in the list. Click "Save" and browse to the location you want to save them in (the provided USB drive). When you hit okay, the files should start saving into the location. After you click okay on the box that says your file was saved successfully, go to the specified location and open the file to see if it has every file you have in your notes. Sometimes the files fail to save, and you have to try it 2 or 3 times to make sure the complete file gets transferred. After you have confirmed that the data is downloaded from the LP-80, click Delete All in the AccuLink box to clear the LP-80 memory.

II. Entering Data into Spreadsheets

- 1) Get out your field notebook and open to the first record you have for the datafile you are entering. Open the .csv file you just downloaded from the LP-80. OPEN IT WITH EXCEL 2003, NOT EXCEL 2007.
- 2) OPEN EXCEL 2003, NOT EXCEL 2007. From Excel 2003 click the "Open File" button and navigate to E:\Research\LAI\AccuPAR_Data\GroomedDataFiles and open the file for the site corresponding to the first record.
- 3) Navigate to E:\Research\LAI\AccuPAR_Data\GroomedDataFiles\Templates and open either the Grassland or Forested AccuPAR template file, depending on whether the site was grassland (LN, LS, MLN, MLS, or MHS) or forest (MHN, HN, HS).
- 4) In the template file, right click on the spreadsheet tab and select "move or copy sheet." Copy the sheet into the book corresponding to the site, "move to the end", and be sure to click "create a copy."
- 5) In the site book, right-click the tab for the empty template (it should say "Date") and rename it the collection date of the data you are inputting. At the top right of the spreadsheet, type in the site name and date the data was collected in the cells below the headings for these entries (Site Name and Date).

- 6) In the raw data .csv file, confirm the date and time of the first transect at the site correspond with your field notes.
- a. For Grassland Sites:
 - i. In the raw data .csv file corresponding to the first set of transect readings, copy the file name (date and time of file) and paste it into the site book spreadsheet for the corresponding date in the box directly right of T1.
 - ii. Record your notebook notes on the climate conditions (sunny, cloudy, etc) in the Notes box (cell E2).
 - iii. Back in the raw data .csv file, hold the CTRL key and select all 11 SUM rows for the T1 record. Copy and paste them into the empty box below T1 in the site book spreadsheet for the corresponding date.
 - iv. Check values in columns C and D in the pasted data to be sure that they match with your field notes (C is average above- and D is average below- canopy readings for each flag).
 - v. Repeat i and ii for T2 and T3 for that date.
 - vi. Navigate to E:\Research\LAI\AccuPAR_Data\GroomedDataFiles and open LAI_Extract_AllSites.xls.
 - vii. Copy row 2 (site name, date, average LAI, standard deviation, and notes) in the site book and paste it onto the bottom of the data record for the corresponding site in LAI_Extract_AllSites.xls. Check to make sure the data point is now plotted on the pertinent graph at right.
 - b. For Forested Sites:
 - i. In the raw data .csv file corresponding to the first set of transect readings, copy the file name (date and time of file) and paste it into the site book spreadsheet for the corresponding date in the box directly right of T1.
 - ii. In cell E5 of the site book, enter the day of year, in Ordinal date format (converter at <http://www.fs.fed.us/raws/book/julian.shtml>), on which the data was collected. Hit return and the day will copy itself down.
 - iii. In cell D5 of the site book, enter the Standard time in hours at which the first transect, T1, was measured. When we are in Mountain Daylight Time (Summer, about March 8-Nov 1 in 2009), subtract one hour from the time the measurement was taken (if the filename is Sep-13-09 11:13, your Standard time in hours will be 10.22, because $11-1=10$ and $13/60=0.22$).
 - iv. Back in the raw .csv file, locate the first SUM row in the date/time file you are working with. Holding the Ctrl button, highlight the cells in columns C, D, and F of that row. Copy them and paste them to the right somewhere in column M.

- v. Next, holding the Ctrl button highlight the cells in column D of the next four SUM rows (four is flexible, depending on how the data was collected. You want to highlight the SUM-row cells with 0's to the left of them). Copy them, and paste them in column N beneath the previous row of data you pasted.
- vi. Holding the Ctrl button, highlight the cells in columns C,D, and F of the next SUM row (the next SUM row with numbers in all of those cells). Copy and paste into M beneath the last row of data pasted in N.
- vii. Holding the Ctrl button highlight the cells in column D of the next four (give or take) SUM rows (again, those with 0's to the left of them). Copy them, and paste them in column N beneath the previous row of data you pasted.
- viii. Holding the Ctrl button, highlight the cells in columns C,D, and F of the last SUM row (with numbers in all of those cells). Copy and paste into M beneath the last row of data pasted in N.
- ix. Your spreadsheet should look like the image below.

	A	B	C	D	E	F	G	H	I	J	K	L	M	N	O	P	Q	R	S
1174	BLW	630	83.8	74.19	35.59	27.89	26.89	94.4	391.7	172.5	0								
1175	BLW	630	82.9	74.19	34.7	26.89	26.89	98.3	380.79	170.6	0								
1176	SUM	630	755.59	112.8	0.14	2.05	1	0.87	68										
1177	Sum-13-09 11.13																		
1178	ABV	678	713.5	545.2	737	572.59	777.2	867.2	910.29	888.79	0								
1179	ABV	678	729.2	557.9	752.7	596.29	794.79	883.9	927.9	903.4	0								
1180	ABV	678	727.2	555.9	751.59	595.2	792.7	882.79	926.79	904.29	0								
1181	BLW	681	3.9	2.9	2.9	1.9	2.9	3.9	4.9	5.0	0								
1182	BLW	681	3.9	2.9	2.9	1.9	2.9	3.9	4.9	4.9	0								
1183	BLW	681	3.9	2.9	2.9	1.9	2.9	3.9	4.9	4.9	0								
1184	SUM	681	761.4	3.5	0	6.15	1	0.66	59										
1185	BLW	682	3.9	3.9	5.9	3.9	5.9	7.8	8.8	11.8	0								
1186	BLW	682	3.9	3.9	5.9	3.9	5.9	7.8	8.8	11.8	0								
1187	BLW	682	3.9	3.9	5.9	3.9	5.9	7.8	8.8	11.8	0								
1188	SUM	682	0	6.5	0	0	1	0	0										
1189	BLW	684	8.8	6.9	12.8	13.8	20.7	23.6	25.6	25.6	0								
1190	BLW	684	8.8	6.9	12.8	13.8	20.7	23.6	25.6	25.6	0								
1191	BLW	684	8.8	6.9	12.8	13.8	20.7	23.6	25.6	25.6	0								
1192	SUM	684	0	17.2	0	0	1	0	0										
1193	BLW	684	18.7	14.8	21.7	17.7	24.7	29.6	34.5	36.5	0								
1194	BLW	684	18.7	15.8	21.7	17.7	24.7	29.6	34.5	36.5	0								
1195	BLW	684	18.7	15.8	21.7	17.7	24.7	29.6	34.5	36.5	0								
1196	SUM	685	0	24.79	0	0	1	0	0										
1197	BLW	685	25.7	18.79	23.7	17.79	22.7	25.7	26.7	25.7	0								
1198	BLW	685	25.7	18.79	23.7	17.79	22.7	25.7	27.7	25.7	0								
1199	BLW	685	25.7	19.7	23.7	17.79	22.7	25.7	27.7	25.7	0								
1200	SUM	685	0	23.5	0	0	1	0	0										
1201	ABV	689	710.09	546.09	737.79	571.79	773.29	862.2	903.7	854.29	0								
1202	ABV	689	705.7	542.79	734.29	570.5	772.79	863.59	904.09	849.79	0								
1203	ABV	689	702.59	540.7	733.2	568.4	768.7	857.5	899	844.7	0								
1204	BLW	691	17.79	12.8	16.79	12.8	16.79	19.7	19.7	19.7	0								
1205	BLW	691	17.79	12.8	16.79	12.8	16.79	19.7	19.7	19.7	0								
1206	BLW	691	17.79	12.8	16.79	12.8	16.79	19.7	19.7	19.7	0								
1207	SUM	691	742.4	17	0.02	4.4	1	0.58	57										
1208	BLW	692	18.79	15.8	22.7	17.79	23.7	24.7	22.7	22.7	0								
1209	BLW	692	18.79	15.8	22.7	17.79	23.7	24.7	22.7	22.7	0								
1210	BLW	692	18.79	15.8	22.7	17.79	23.7	24.7	22.7	22.7	0								
1211	SUM	692	0	21.1	0	0	1	0	0										
1212	BLW	692	17.79	15.8	22.7	18.79	23.7	27.7	27.7	29.7	0								
1213	BLW	692	18.79	15.8	23.7	18.79	24.7	27.7	28.7	29.7	0								
1214	BLW	692	18.79	15.8	22.7	18.79	24.7	27.7	27.7	29.7	0								
1215	SUM	693	0	23.2	0	0	1	0	0										
1216	BLW	693	23.7	18.79	25.7	18.79	24.7	27.7	27.7	25.7	0								
1217	BLW	693	23.7	18.79	25.7	18.79	24.7	27.7	27.7	25.7	0								
1218	BLW	693	23.7	18.79	25.7	18.79	24.7	27.7	27.7	25.7	0								
1219	SUM	693	n	34.1	n	n	n	n	n										

- x. Select the square of data you have pasted in columns M-O as shown above, copy it, and paste it in cell L11 (or the cell in column L aligned with the top line of data for the transect you are working with). Check it now to make sure the values agree with those

- recorded in your field notes. If they don't, find your error and figure out which set of values to enter into the sheet.
- xii. Copy L11 (or the first above-canopy reading) and paste into A11.
 - xiii. Copy L16 (or the second above-canopy reading) and paste into A16.
 - xiv. Copy L21 (or the third above-canopy reading) and paste into A21.
 - xv. The equations between A11, A16, and A21 assume that the values decrease moving down the column. When the values increase, you need to select the first equation (either A12 or A17 depending on whether the numbers increase from A11 to A16, or from A16 to A21), change the first (-) sign to a plus sign, and drag the box to copy the equation down to the next 3 cells below.
 - xvi. Select and delete L and M 11-21, shifting the LP-80 LAI values (column N) left so they line up with the predicted LAI column. Check them to see if they are close to the values predicted in the LAI column. If the measured values are much more than about 1 LAI unit different than the predicted values, double check the spreadsheet for errors (more error is expected if the above-canopy reading did not correspond with the 6th flag, as the spreadsheet assumes). Your sheet should look like the below:

1	A	B	C	D	E	F	G	H	I	J	K	L	M	N	O	P	Q
2	Site Name	Date	Average LAI	Standard Deviat	Notes												
3	MH	05/13/09	#N/D/I	#N/D/I													
4	L, Latitude (rad), Solar Declinat, Standard time (h), J, Day Off, LC, Latitude, ET, Equatic (for ET), to, Time of SC, PAR, Solar Constant (µmol/m ² /s)																
5	T1	0.763	0.073	10.220	256.000	-0.733	0.065	9.285	12.668	2550.000							
6	T2	0.763	0.073		256.000	-0.733	0.065	9.285	12.668	2550.000							
7	T3	0.763	0.073		256.000	-0.733	0.065	9.285	12.668	2550.000							
8	r = ABV/(SC*cos(ZenithAngle))																
9	T1	Sep-13-09 11:13															
10	AboveCanopy	BelowCanopy	Tau (ratio of P)	SolarZenithAngle	% Fraction	h(BeamFr A	x	K	LAI	LAI From LP.00							
11	761.4	3.5	0.005	0.892	0.475	0.439	0.861	1.000	0.796	6.593	6.15						
12	767.800	6.5	0.009	0.892	0.473	0.433	0.861	1.000	0.796	6.823							
13	763.800	17.2	0.023	0.892	0.471	0.427	0.861	1.000	0.796	4.623							
14	750.000	24.79	0.033	0.892	0.468	0.421	0.861	1.000	0.796	4.166							
15	746.200	23.5	0.031	0.892	0.466	0.416	0.861	1.000	0.796	4.221							
16	742.4	17	0.023	0.892	0.463	0.410	0.861	1.000	0.796	4.607	4.4						
17	758.300	21.1	0.028	0.892	0.473	0.434	0.861	1.000	0.796	4.384							
18	774.200	23.2	0.030	0.892	0.463	0.459	0.861	1.000	0.796	4.309							
19	750.100	24.1	0.031	0.892	0.463	0.461	0.861	1.000	0.796	4.302							
20	806.000	7.69	0.010	0.892	0.503	0.504	0.861	1.000	0.796	5.755							
21	821.9	6.9	0.008	0.892	0.613	0.626	0.861	1.000	0.796	6.936	6.73						
22											Average	4.974					
23	Filename																
24	AboveCanopy	BelowCanopy	Tau (ratio of P)	SolarZenithAngle	% Fraction	h(BeamFr A	x	K	LAI								
25	0.000	#N/D/I	2.291	0.000	1.395	0.861	1.000	-0.759	#N/D/I								
26	0.000	#N/D/I	2.291	0.000	1.395	0.861	1.000	-0.759	#N/D/I								
27	0.000	#N/D/I	2.291	0.000	1.395	0.861	1.000	-0.759	#N/D/I								
28	0.000	#N/D/I	2.291	0.000	1.395	0.861	1.000	-0.759	#N/D/I								
29	0.000	#N/D/I	2.291	0.000	1.395	0.861	1.000	-0.759	#N/D/I								
30	0.000	#N/D/I	2.291	0.000	1.395	0.861	1.000	-0.759	#N/D/I								
31	0.000	#N/D/I	2.291	0.000	1.395	0.861	1.000	-0.759	#N/D/I								
32	0.000	#N/D/I	2.291	0.000	1.395	0.861	1.000	-0.759	#N/D/I								
33	0.000	#N/D/I	2.291	0.000	1.395	0.861	1.000	-0.759	#N/D/I								
34	0.000	#N/D/I	2.291	0.000	1.395	0.861	1.000	-0.759	#N/D/I								
35	0.000	#N/D/I	2.291	0.000	1.395	0.861	1.000	-0.759	#N/D/I								
36											Average	#N/D/I					
37	Filename																
38	AboveCanopy	BelowCanopy	Tau (ratio of P)	SolarZenithAngle	% Fraction	h(BeamFr A	x	K	LAI								
39	0.000	#N/D/I	2.291	0.000	1.395	0.861	1.000	-0.759	#N/D/I								
40	0.000	#N/D/I	2.291	0.000	1.395	0.861	1.000	-0.759	#N/D/I								
41	0.000	#N/D/I	2.291	0.000	1.395	0.861	1.000	-0.759	#N/D/I								
42	0.000	#N/D/I	2.291	0.000	1.395	0.861	1.000	-0.759	#N/D/I								
43	0.000	#N/D/I	2.291	0.000	1.395	0.861	1.000	-0.759	#N/D/I								
44	0.000	#N/D/I	2.291	0.000	1.395	0.861	1.000	-0.759	#N/D/I								
45	0.000	#N/D/I	2.291	0.000	1.395	0.861	1.000	-0.759	#N/D/I								

- xvii. Always check the column with the orange heading, “*r,FractionPotentialPARReachingProbe (All Values > 0.82 Set=0.82. Values< 0.2,Set=0.2.)”. As it instructs, if the values are > 0.82 or < 0.2, you need to manually adjust them. Usually this only happens if it was an intermittently cloudy day, or if you measure outside the 9am-3pm time frame. Failure to check this can lead to big errors.
- xviii. Repeat the above i through xvii (except ii) for T2 and T3, remembering to manually enter the corresponding Standard time in hours into cells D6 and D7, respectively, for each transect file.
- xix. Check your values against your field notes for accuracy.
- xx. Navigate to E:\Research\LAI\AccuPAR_Data\GroomedDataFiles and open LAI_Extract_AllSites.xls.
- xxi. Copy row 2 (site name, date, average LAI, standard deviation, and notes) in the site book and paste it onto the bottom of the data record for the corresponding site in LAI_Extract_AllSites.xls. Check to make sure the data point is now plotted on the pertinent graph at right.

APPENDIX D

Protocol for NDVI Data Assembly and Processing

Performing NDVI Analyses in DCEW using Landsat 5 Remotely Sensed Data

- 1) Finding and downloading Landsat Data:
 - a) Go to: <http://edcsns17.cr.usgs.gov/EarthExplorer/>
 - b) Enter Search terms:
Address/Place Name: Boise ID (Hit “Search” after this, so that the lat/long show up in the boxes below)
 - c) In “From” and “To” specify dates desired, and check “Search these months only”
 - d) At left bar, navigate to **Landsat Archive**, then down to **Landsat 4-5 TM**
Additional Search Criteria: choose **Cloud cover < 10%**.
 - i) These criteria return images for Path 41 row 30, and Path 42 row 30, from Landsat 5. Look for clouds obscuring Dry Creek (in far upper right corner). Most data has been downloaded to G:\Boisefront\ToniSmith folder, as well as to the M: drive (see Jason Watt for access to backup copies). See the document entitled AvailableLandsat5DataforDryCreek.doc for a list of files found for the different growing seasons using the above criteria.
- 2) Unzipping Files: Landsat files arrive as compressed .tar.gz files. I used Power Archiver to unzip the .gz files into .tar files, leaving me with a folder for each image containing individual files for each band as well as a readme file and a metadata file. I then saved the folders to the D: drive on my computer for faster processing.
- 3) In ENVI 4.6.1, I use File: Open External File: Landsat: GeoTIFF to open the files for B20, B30 and B40 (bands 2, 3 and 4, or green, red and NIR, respectively). Load the 3 bands as a false color 4,3,2 (RGB) image and check for clouds obscuring the image. If the key locations are cloud free, then proceed with processing the image. The raw DN values are not corrected for atmospheric affects, sensor issues, etc. to top-of-atmosphere reflectance, so in order to compare band to band within an image we need to convert DN to reflectance.
 - a) Convert raw DN values to reflectance for each of Band 2, Band 3 and Band 4 for each image date, using ENVI Band Math. The sample equation below combines two equations provided in Chander and Markham, 2003, discussed later under “Explanation of Equation”.... Open and load the file for a given band, Go to Basic Tools: Band Math, and enter the appropriate expression for the specific band, taking care to calculate d and θ_s for the date and band you are working on. Open

the associated Landsat file ending in _MTL.txt using Wordpad to obtain solar elevation for calculating θ_s .

Example Band Math Expression for DN to reflectance conversion in Band 2:

$$(((367.84/255)*float(B2))-2.84)*3.14159*(d^2)/(1826*\cos\theta_s)$$

Example Band Math Expression for DN to reflectance conversion in Band 3:

$$(((265.17/255)*float(B3))-1.17)*3.14159*(d^2)/(1554*\cos\theta_s)$$

Example Band Math Expression for DN to reflectance conversion in Band 4:

$$(((222.51/255)*float(B4))-1.51)*3.14159*(d^2)/(1036*\cos\theta_s)$$

Where:

- d = Earth-Sun distance in astronomical units (interpolated from Chander and Markham 2003, Table III)
- θ_s = solar zenith angle in degrees (= 90° - solar elevation; solar elevation available in Landsat file ending in _MTL.txt associated with date of the Landsat folder you're working with)

After entering the equation into band math *with the appropriate parameter values*, click “Add to List” and OK, and then identify variable B4 (or the variable in your expression) as the appropriate Band file in the Available Bands list. Spatially subset the data by image by finding Dry Creek Watershed and drawing a generous square around the watershed (this makes processing faster). Save to a folder marked as “DN to Reflectance Conversions” with image date in file title. Repeat for each of Band 2, 3, and 4.

- *Explanation of equation in example Band Math Expression, from Chander and Markham 2003:*

$$P_p = (\pi * L_\lambda * d^2) / (ESUN_\lambda * \cos\theta_s)$$

$$\text{In which } L_\lambda = [((L_{\max_\lambda} - L_{\min_\lambda}) / Q_{\text{calmax}}) * Q_{\text{cal}}] + L_{\min_\lambda}$$

Where:

- L_λ = spectral radiance at sensor's aperture in $W/(m^2 * sr * \mu m)$
- L_{\max_λ} = spectral radiance scaled to Q_{calmax} in $W/(m^2 * sr * \mu m)$ (from metadata file associated with Landsat file or Chander and Markham 2003, Table I, Band-specific)
- L_{\min_λ} = spectral radiance scaled to Q_{calmin} in $W/(m^2 * sr * \mu m)$ (from metadata file associated with Landsat file or Chander and Markham 2003, Table I; Band-specific)
- Q_{cal} = calibrated pixel value in Digital Numbers (DNs) (the raw value of pixels in the Landsat image)
- Q_{calmax} = maximum calibrated pixel value (DN) corresponding to L_{\max_λ} (DN = 255)
- Q_{calmin} = minimum calibrated pixel value (DN) corresponding to L_{\min_λ} (DN = 0)
- P_p = unitless planetary top-of-atmosphere reflectance
- L_λ = spectral radiance at sensor's aperture (radiance image calculated in (a) above)
- d = Earth-Sun distance in astronomical units (in Chander and Markham 2003, Table III)
- $ESUN_\lambda$ = mean solar exoatmospheric irradiances in $W/(m^2 * \mu m)$ (from Chander and Markham 2003, Table II)
- θ_s = solar zenith angle in degrees (= 90° - solar elevation; solar elevation available in Landsat file ending in _MTL.txt associated with date of the Landsat folder you're working with)

If you choose not to combine the equations (takes longer but less room for error), here are samples for each stepwise conversion (DN to radiance, then radiance to reflectance):

An example calculation in the Band Math window for a Band 4 image from 4/13/2008, convert DN to radiance, is:

$$(((221+1.51)/255)*float(B4))-1.51$$

Example Band Math calculation converting radiance to reflectance for a June 23, 2008 image of Band 4 is:

$$(3.141592654*\text{float}(B4)*1.032764063)/(1036*0.8879491327)$$

- 4) Perform Layer Stacking for the three bands processed above to combine them into one file. Go to Map: Layer Stacking; under Selected Files for Layer Stacking, Import the Reflectance image for B2 B3 or B4 created above, subset the image By File using the file NDVI_ISUClass_20080623 in the NDVI folder; click “Exclusive: range encompasses file overlap;” select the other Reflectance bands from that date as the file for layer stacking, and name the output file appropriately (place in a folder of StackedRed,NIRFiles).
- 5) Next, perform NDVI processing on the stacked images produced in (b) above using the following equation in Band Math:

$$\text{NDVI} = (\text{NIR}-\text{red})/(\text{NIR}+\text{red}); \text{ for Landsat 5, NDVI} = (B4-B3)/(B4+B3)$$

Where B4 and B3 are converted reflectance values for the NIR and red wavebands.

- *Band Math expression for NDVI: (float(B4)-float(B3))/(float(B4)+float(B3))*

- Identify the variables in the expression by selecting the respective reflectance images from the stacked image. Spatially Subset the data, By File, selecting the file NDVI_ISUClass_20080623 in the NDVI folder; rename it NDVI_(imagedate), then save to the NDVI folder.
- 6) Save each NDVI file as a Geotif/tif format with a modified name (I add “geotif” to the end of the file name as in “NDVI_date_geotiff”) and then you can open them in ArcGIS.
 - 7) Open all of the geotiffs for a given season (year) into a new ArcMap .mxd file titled “NDVI_year_DatesAsLayers.mxd.”

a) For each layer,

- i) Click the layer to highlight it, then go to ArcToolbox, Data Management Tools, Projections and Transformations, Raster, Project Raster.
 - (1) In the Project Raster dialogue box, select the image as your input raster.
 - (2) The next box, Input Coordinate System, should automatically say WGS_1984_UTM_Zone_11N because the geotiff contains this information. Otherwise, you can select that system.
 - (3) Give your Output Raster Dataset a name and location (I click the folder box and navigate to the location, then type in a name).
 - (4) Choose your Output Coordinate System by clicking the finger/paper browse button to the right of the box, go to XY Coordinate System tab,

click Select, Projected Coordinate Systems, UTM, NAD 1983, and NAD 1983 UTM Zone 11N.prj.

- (5) For Geographic Transformation, select NAD_1983_To_WGS_1984_5.
 - (6) For Resampling Technique, I use Cubic, and I keep Output Cell Size as 30.
 - (7) Hit OK. You just made the projection of the Landsat data match the projection of all our Dry Creek data. Be sure to do this for **every single layer**.
 - ii) If the added geotifs don't show up well, or show up as black squares, you need to stretch the values. Right-click each layer and go to Properties, navigate to the Symbology tab. Low in the dialogue box you'll see a section titled "Stretch, Type:" in the type box select Histogram Equalize and OK, then click "yes" to the dialogue box asking if you want to compute histograms . This will stretch the values so that a) you can see the NDVI image instead of a big black box, and b) the values will closely match the distribution, max mean and min, of the values the image had in ENVI (the numbers will differ very slightly, by less than about 0.01, due to the cubic convolution resampling technique chosen in reprojection above). You can check it in ENVI by loading the NDVI image, right clicking on it, and selecting "Quick Stats" which reports the statistical distribution of the image values. Be sure to do this for **every single layer**.
- 8) Now that you have the season's worth of NDVI data loaded as layers into the map file, and you have them all stretched so the data values are correct, and they are reprojected into NAD 83 so they'll match our other Dry Creek data, you can get out the values at all the important locations you have UTM coordinates for (have them saved in a database IV, .dbf file, with all columns formatted as numbers. You can Save As this file format from an excel file).
- a) Load your locations (point data), either as the existing .shp or .lyr files, or as your .dbf file (to to Tools-Add XY data to get the tabulated locations mapped onto the image, and Save As a layer file if you want).
 - b) Go to ArcToolbox: Spatial Analyst Tools: Extraction: Sample. You may need to enable the Spatial Analyst toolbox by going to "Tools: Extensions..." and clicking the box for Spatial Analyst, then "Close." In "Input Rasters" select all of

the raster layers that you've loaded into the map file. For Input location raster or point features, select the file of your point locations. Use the folder button to select a location and name for your Output Table. I select "Nearest" for Resampling Technique. Then hit OK.

- c) Once the output file shows up in the map file (under Source tab, not usually Display) you can open its attribute table and go to Options: Export, select All Records and specify the location you want to save it to.

APPENDIX E

Methodology for Particle Size Analysis by Sieving and Laser Diffraction

PARTICLE SIZE ANALYSIS PROCEDURE BY SIEVING and LASER DIFFRACTION

(adapted from ASTM Standard D 422-63 and Gee and Or 2002)

Supplies

- Balance accurate to 0.01 g
- Deionized water (DI)
- Ziploc sample bags
- Sharpie pen
- Wax paper
- Thermometer
- 4% sodium hexametaphosphate (SHP) dispersing agent, 40g/L (mix VERY well in distilled by stirring vigorously in a beaker)
- Clock or timing device
- Standard Sieves (9.5mm, #4, #10, and #200)
- Sieve Shaker Apparatus
- Milkshake mixer and mixing cups
- Mortar and pestle
- 250 and 500 mL Beaker
- Metal Spatula
- Metal spoon
- Paper plates

Dry Sieving:

1. If the sample is moist, air-dry the field sample in its opened ziploc sample bag for 24 hrs in a 20°C room. Weigh the total sample and record the Total Sample Mass, Sample ID, Date Collected, and any notes on the Sieve Datasheet (headings table below). Paper plates and wax paper can be used as a weighing surface for the balance, just remember to zero the balance to the weighing surface.
2. Use the mortar and pestle to gently break up obvious aggregates of particles, tackling the samples in small portions of (roughly 2 tablespoons worth) soil at a time. Prepare a stack of 9.5mm, #4, #10, and #200 sieves, and pour the total sample onto the top sieve. Sieve the sample dry through a 9.5mm, #4, #10, and #200 sieves, shaking in sieve shaker for 10 minutes. Weigh the mass of sample retained on each sieve; if needed, use the mortar and pestle again to gently break up obvious aggregates of particles for the portion held on each sieve (especially the larger sieves, where aggregates are typically more obvious), then pour it back onto the sieve and shake/tap it a few times to allow fine particles to pass through before weighing. Record the mass retained on each sieve.
3. Label and individually bag portions a) > 2mm (retained on #10, #4, and 9.5mm sieves), b) < 2mm but > 0.075mm (retained on #200), and c) < 0.075mm (passing #200, retained in bottom pan). Mark bag of material < 0.075mm (passing #200) as “for LD analysis” (for laser diffraction analysis).
4. Enter resulting data carefully into the spreadsheet provided.

Wet Sieving:

1. Prepare enough 4% solution of sodium hexametaphosphate and distilled water to cover each sample you plan to run the next day in 125 mL of solution. I recommend placing the desired amount of SHP in a large beaker, then adding the appropriate amount of deionized water and stirring vigorously, letting the solution soak while you complete other work to help the crystals dissolve completely.
2. Obtain the bagged portion labeled “< 2mm but > 0.075mm” (the bag may just marked as “< 2mm”). On Wet Sieve Datasheet, record Sample ID, date collected, and today’s date as “Date of Wet Sieve Test.” Zero the balance with a paper plate as the weighing surface, then weigh the contents of the bag on the paper plate and record as “Dry Mass of < 2mm Fraction Before Wet Sieve.” Place each sample in a labeled 250mL beaker and record Beaker ID on datasheet. Cover each sample with 125mL of 4% SHP solution (or more, if needed, to cover the soil sample) and stir until the soil is thoroughly wetted. Cover each beaker and allow it to soak for at least 16 hrs.
3. Wash as many baking pans as you plan to need and allow them to dry. Make sure they are all labeled uniquely and clearly.
4. After soaking, use a spatula to stir the soil sample up again. Using the spatula and a squirt bottle of DI, transfer the entire soil sample into a metal mixing cup and add enough DI to fill cup to 1/3 full. Stir in milkshake mixer for 1 minute, then use spatula and DI squirt bottle to transfer entire contents of mixing cup into the #200 large bucket sieve poised over the sink. Fine material can go down the drain.
5. Wash the sieve contents with tap water until the wash water is clear. Weigh a baking pan and record the Pan ID and mass on the datasheet, then carefully transfer all the material retained on the #200 sieve to the marked baking pan (using a squirt bottle and more water if needed), and dry overnight in an oven at about 110 degrees Celsius.
6. Next day, remove samples from oven and allow to cool until mass stabilizes. Then weigh and record mass of pan and sample as “Dry Mass of < 2mm, > 0.075mm Fraction and Pan After Wet Sieve (g).” The spreadsheet will calculate the mass of dry soil in the pan.
7. Scrape the sample out of the pan as best you can and bag it, labeling the bag with the original sample ID, date collected, as well as the words “< 2mm, > 0.075mm, wet-sieved.”
8. Enter data carefully into the spreadsheet provided.

Laser Diffraction:

1. Prepare enough 4% solution of sodium hexametaphosphate and distilled water to cover each sample you plan to run the next day in 10 mL of solution. I recommend placing the desired amount of SHP in a large beaker, then adding the appropriate amount of deionized water and stirring vigorously, letting the solution soak while you work to help the crystals dissolve completely.

2. Obtain the bagged fraction $< 0.075\text{mm}$ labeled “for LD analysis” (for laser diffraction analysis). Zero the balance with a small piece of wax paper as a weighing surface, then spoon and weigh out a subsample of 0.1 to 0.2g soil $< 0.075\text{mm}$ for laser diffraction. Place each subsample in a labeled test tube and record tube ID, sample ID, and sample mass on attached Laser Diffraction Datasheet.
3. Cover each sample with 10 ml of 4% (40g/L) sodium hexametaphosphate solution- please remember to stir this solution thoroughly and dissolve the SHP completely in deionized water! Cap the tube and invert 10 times to mix thoroughly, then let soak for ≥ 16 hours (but < 24 hours).
4. Run the sample through the Mastersizer according to the Mastersizer SOP document using the Toni’sSoils SOP.

APPENDIX F

Protocol for Preparation of Soil Samples for Analysis of Carbon Content

Preparation of Air-Dried Soil Samples for Soil Carbon Analysis

(from M. Kunkel, personal communication, March 2008)

1. Weigh and record weights for soil bags and pans; weigh five groups of 10 bags or pans, dividing the total weight of each group by 10; the result is the average weight, with error, of the sample bags or pans, determined from 50 individuals.
2. Weigh original soil sample and bag and record weight.
3. Place in freezer to await processing or start processing steps.
4. Air dry over night with bag open. Very moist samples may require longer drying (until weight becomes constant).
5. Label two new bags with code.
6. Sieve sample with 2 mm and 1 mm sieves. Using the metal pestle, lightly stir sample on the 1 mm grate to break up any clumps and make sure all material < 1 mm goes through.
7. Put remaining sample (> 1 mm) back into original bag and label bag “coarse.” Weigh and record coarse weight.
8. Weigh the < 1 mm portion in the pan. Record weight.
9. Pour < 1 mm sample onto a piece of wax or freezer paper and roll sample back and forth to homogenize.
10. Take 1 Tbsp sub-sample and place on paper plate. Re-homogenize sample and take another 1 Tbsp sub-sample and place on plate; repeat this a third time.
11. Place remaining sample in a new Ziploc bag labeled with code and “< 1 mm”. Weigh and record weight.
12. Pour sub-sample on paper plate back on to the wax or freezer paper and homogenize.
13. Take ¼ tsp sub-sample and place in 250 µm sieve.

14. Place the soil remaining on wax paper in a new bag labeled with code and “Subsample 1”. Weigh and record.
15. Process the soil on the 250 μm sieve. Shake sieve and tap on counter to remove all material $< 250 \mu\text{m}$.
16. Pour sub-sample that did not go through the sieve onto the paper plate.
17. Place sub-sample on plate into the agate mortar and pestle and grind sample by hand for about 30-60 seconds.
18. Put sub-sample into 250 μm sieve and shake and tap sieve.
19. Sub-sample that did not go through the sieve can either be ground by hand again, or placed in the capsule and ground in the WIG-L-BUG.
20. When the entire sub-sample goes through the 250 μm sieve, swirl sub-sample until homogenized.
21. Label tin.
22. Transfer ground soil to the tin.
23. Place soil tin in oven at 105°C for 1 hour.
24. Remove soil tin from oven, let cool for 1 minute.
25. Weigh and record weight.
26. Transfer soil in tin into small, labeled, glass vial (make a funnel out of weighing paper, or put on paper plate and fold, or bend the tin cup) and place in a Rubbermaid container with about 2 cm of Drierite (or return to freezer to await analyses).
27. Analyze sample for organic and inorganic carbon using Flash EA Elemental Analyzer according to standard operating procedures developed by M. Kunkel.

APPENDIX G

**Soil Texture Results by Laser Diffraction and Hydrometer/Sieve Conversion
Methods**

Table G1. Soil Texture Results by Laser Diffraction and Hydrometer/Sieve Conversion Methods. Samples whose depth is labeled “BR” were taken from the decomposed granite horizon treated as bedrock. Gravel content was derived from the whole sample.

Site ID	Pit	Depth (cm)	Laser Diffraction Results				Hydrometer/Sieve Conversion Results				Original Gravel Content
			% Sand	% Silt	% Clay	USDA Texture Class	% Sand	% Silt	% Clay	USDA Texture Class	% Gravel
HN	1	2	67	31	2	sandy loam (SL)	68	23	8	sandy loam (SL)	22
HN	1	15	67	31	2	sandy loam (SL)	68	23	8	sandy loam (SL)	21
HN	1	30	82	17	1	loamy sand (LS)	79	14	8	loamy sand (LS)	38
HN	1	34	80	19	1	loamy sand (LS)	77	15	8	sandy loam (SL)	34
HN	2	2	69	29	2	sandy loam (SL)	70	22	8	sandy loam (SL)	22
HN	2	2	69	29	2	sandy loam (SL)	70	22	8	sandy loam (SL)	22
HN	2	15	66	32	2	sandy loam (SL)	67	24	8	sandy loam (SL)	18
HN	2	30	72	26	2	loamy sand (LS)	72	20	9	sandy loam (SL)	21
HN	2	40	68	29	3	sandy loam (SL)	69	22	9	sandy loam (SL)	27
HN	3	2	71	27	1	sandy loam (SL)	71	21	8	sandy loam (SL)	22
HN	3	15	67	32	2	sandy loam (SL)	68	24	8	sandy loam (SL)	41
HN	3	30	68	30	2	sandy loam (SL)	69	23	9	sandy loam (SL)	21
HN	3	54	80	19	2	loamy sand (LS)	77	15	8	sandy loam (SL)	23
HN	4	2	67	31	2	sandy loam (SL)	68	23	8	sandy loam (SL)	16
HN	4	2	67	31	2	sandy loam (SL)	68	23	8	sandy loam (SL)	16

Site ID	Pit	Depth (cm)	% Sand	% Silt	% Clay	USDA Texture Class	% Sand	% Silt	% Clay	USDA Texture Class	% Gravel
HN	4	15	69	29	2	sandy loam (SL)	70	22	8	sandy loam (SL)	19
HN	4	30	74	24	2	loamy sand (LS)	73	18	9	sandy loam (SL)	19
HN	4	52	77	21	2	loamy sand (LS)	75	16	8	sandy loam (SL)	15
HS	1	2	78	20	1	loamy sand (LS)	76	16	8	sandy loam (SL)	31
HS	1	15	73	25	2	loamy sand (LS)	73	19	8	sandy loam (SL)	28
HS	1	30	75	23	3	loamy sand (LS)	74	18	9	sandy loam (SL)	21
HS	1	48	75	22	3	loamy sand (LS)	74	17	9	sandy loam (SL)	24
HS	2	2	74	25	2	loamy sand (LS)	73	19	8	sandy loam (SL)	19
HS	2	2	74	24	2	loamy sand (LS)	73	19	8	sandy loam (SL)	19
HS	2	15	75	23	2	loamy sand (LS)	74	18	8	sandy loam (SL)	20
HS	2	30	75	22	3	loamy sand (LS)	74	17	9	sandy loam (SL)	20
HS	2	52	75	23	3	loamy sand (LS)	74	18	9	sandy loam (SL)	22
HS	3	2	78	21	1	loamy sand (LS)	76	16	8	sandy loam (SL)	20
HS	3	15	77	22	1	loamy sand (LS)	75	17	8	sandy loam (SL)	27
HS	3	30	76	22	2	loamy sand (LS)	75	17	9	sandy loam (SL)	23
HS	3	57	77	20	2	loamy sand (LS)	76	16	9	sandy loam (SL)	25
HS	4	2	78	20	1	loamy sand (LS)	76	16	8	sandy loam (SL)	43
HS	4	15	74	24	2	loamy sand (LS)	73	18	8	sandy loam (SL)	22

Site ID	Pit	Depth (cm)	% Sand	% Silt	% Clay	USDA Texture Class	% Sand	% Silt	% Clay	USDA Texture Class	% Gravel
HS	4	30	75	22	3	loamy sand (LS)	74	17	9	sandy loam (SL)	27
HS	4	57	78	20	2	loamy sand (LS)	76	16	9	sandy loam (SL)	27
LN	1	2	42	53	4	silt loam (SiL)	51	39	11	loam (L)	24
LN	1	15	41	52	7	silt loam (SiL)	49	38	12	loam (L)	40
LN	1	15	42	51	6	silt loam (SiL)	50	37	12	loam (L)	40
LN	1	15	41	54	5	silt loam (SiL)	50	40	11	loam (L)	40
LN	1	30	40	54	5	silt loam (SiL)	49	40	11	loam (L)	41
LN	1	60	46	49	5	sandy loam (SL)	53	36	11	sandy loam (SL)	34
LN	1	BR	68	29	3	sandy loam (SL)	69	22	9	sandy loam (SL)	47
LN	2	2	43	53	4	silt loam (SiL)	51	39	10	loam (L)	24
LN	2	2	43	53	4	silt loam (SiL)	51	39	10	loam (L)	24
LN	2	15	40	55	5	silt loam (SiL)	49	40	11	loam (L)	28
LN	2	15	39	56	5	silt loam (SiL)	48	41	11	loam (L)	28
LN	2	15	39	56	5	silt loam (SiL)	48	41	11	loam (L)	28
LN	2	15	39	56	5	silt loam (SiL)	48	41	11	loam (L)	28
LN	2	15	39	56	5	silt loam (SiL)	48	41	11	loam (L)	28
LN	2	15	39	54	7	silt loam (SiL)	48	39	12	loam (L)	28
LN	2	15	40	54	7	silt loam (SiL)	49	39	12	loam (L)	28
LN	2	30	41	54	5	silt loam (SiL)	49	39	11	loam (L)	37
LN	2	60	49	47	5	sandy loam (SL)	55	34	11	sandy loam (SL)	30
LN	2	BR	65	32	3	sandy loam (SL)	67	24	9	sandy loam (SL)	50
LN	3	2	41	55	4	silt loam (SiL)	49	40	11	loam (L)	28
LN	3	15	38	55	7	silt loam (SiL)	47	40	13	loam (L)	32

Site ID	Pit	Depth (cm)	% Sand	% Silt	% Clay	USDA Texture Class	% Sand	% Silt	% Clay	USDA Texture Class	% Gravel
LN	3	15	40	53	7	silt loam (SiL)	49	39	13	loam (L)	32
LN	3	15	38	55	7	silt loam (SiL)	47	40	13	loam (L)	32
LN	3	15	37	58	5	silt loam (SiL)	47	42	11	loam (L)	32
LN	3	30	36	58	6	silt loam (SiL)	46	42	12	loam (L)	35
LN	3	59	56	40	4	sandy loam (SL)	60	29	10	sandy loam (SL)	65
LN	3	70 (BR)	69	28	3	sandy loam (SL)	69	22	9	sandy loam (SL)	64
LN	4	2	44	52	4	silt loam (SiL)	52	38	10	loam (L)	36
LN	4	2	44	52	4	silt loam (SiL)	51	38	10	loam (L)	36
LN	4	15	39	57	4	silt loam (SiL)	48	41	11	loam (L)	35
LN	4	15	40	53	7	silt loam (SiL)	49	39	12	loam (L)	35
LN	4	30	37	57	6	silt loam (SiL)	47	42	12	loam (L)	28
LN	4	64	54	42	5	sandy loam (SL)	59	31	11	sandy loam (SL)	38
LN	4	73 (BR)	58	38	4	sandy loam (SL)	61	28	10	sandy loam (SL)	47
LS	1a	2	88	12	0	sand (S)	83	10	7	loamy sand (LS)	26
LS	1a	2	88	12	0	sand (S)	83	10	7	loamy sand (LS)	26
LS	1a	15	88	11	1	sand (S)	83	10	7	loamy sand (LS)	44
LS	1a	15	88	11	1	sand (S)	83	10	7	loamy sand (LS)	44
LS	1a	30	85	14	1	loamy sand (LS)	81	11	7	loamy sand (LS)	58
LS	1a	40	77	21	2	loamy sand (LS)	76	16	8	sandy loam (SL)	66
LS	1b	2	83	16	1	loamy sand (LS)	80	13	7	loamy sand (LS)	22
LS	1b	2	83	16	1	loamy sand (LS)	80	13	7	loamy sand (LS)	22

Site ID	Pit	Depth (cm)	% Sand	% Silt	% Clay	USDA Texture Class	% Sand	% Silt	% Clay	USDA Texture Class	% Gravel
LS	1b	2	83	16	1	loamy sand (LS)	80	13	7	loamy sand (LS)	22
LS	1b	2	83	16	1	loamy sand (LS)	80	13	7	loamy sand (LS)	22
LS	1b	2	83	16	1	loamy sand (LS)	80	13	7	loamy sand (LS)	22
LS	1b	15	85	14	1	loamy sand (LS)	81	11	7	loamy sand (LS)	29
LS	1b	15	85	14	1	loamy sand (LS)	81	11	7	loamy sand (LS)	29
LS	1b	15	85	14	1	loamy sand (LS)	81	11	7	loamy sand (LS)	29
LS	1b	15	86	13	1	sand (S)	82	11	7	loamy sand (LS)	29
LS	1b	30	95	5	0	sand (S)	88	5	7	sand (S)	52
LS	2	2	87	13	1	sand (S)	82	11	7	loamy sand (LS)	24
LS	2	2	87	13	1	sand (S)	82	11	7	loamy sand (LS)	24
LS	2	15	89	10	1	sand (S)	84	9	7	loamy sand (LS)	40
LS	2	30	87	13	1	sand (S)	82	11	7	loamy sand (LS)	62
LS	3a	2	81	18	1	loamy sand (LS)	78	14	8	loamy sand (LS)	23
LS	3a	15	74	24	2	loamy sand (LS)	73	18	8	sandy loam (SL)	58
LS	3a	30	75	23	2	loamy sand (LS)	74	18	8	sandy loam (SL)	70
LS	3a	40	84	15	1	loamy sand (LS)	81	12	7	loamy sand (LS)	60
LS	3b	2	80	18	1	loamy sand (LS)	78	14	8	loamy sand (LS)	16
LS	3b	15	77	21	2	loamy sand (LS)	76	16	8	sandy loam (SL)	37

Site ID	Pit	Depth (cm)	% Sand	% Silt	% Clay	USDA Texture Class	% Sand	% Silt	% Clay	USDA Texture Class	% Gravel
LS	3b	15	78	21	2	loamy sand (LS)	76	16	8	sandy loam (SL)	37
LS	3b	30	92	8	1	sand (S)	86	7	7	loamy sand (LS)	52
LS	4	2	84	16	1	loamy sand (LS)	80	13	7	loamy sand (LS)	19
LS	4	2	84	15	1	loamy sand (LS)	80	13	7	loamy sand (LS)	19
LS	4	15	76	22	2	loamy sand (LS)	75	17	8	sandy loam (SL)	41
LS	4	30	81	18	1	loamy sand (LS)	78	14	8	loamy sand (LS)	50
LS	4	42	82	17	1	loamy sand (LS)	79	13	8	loamy sand (LS)	62
LS	4b	15	81	18	1	loamy sand (LS)	78	14	8	loamy sand (LS)	30
LS	4b	15	80	19	1	loamy sand (LS)	77	15	8	sandy loam (SL)	30
LS	4b	30	85	14	1	loamy sand (LS)	81	12	7	loamy sand (LS)	36
MHN	1	2	64	34	2	sandy loam (SL)	66	25	9	sandy loam (SL)	32
MHN	1	15	63	33	4	sandy loam (SL)	65	25	10	sandy loam (SL)	35
MHN	1	15	63	33	4	sandy loam (SL)	65	25	10	sandy loam (SL)	35
MHN	1	15	63	35	3	sandy loam (SL)	65	26	9	sandy loam (SL)	35
MHN	1	30	68	29	3	sandy loam (SL)	69	22	9	sandy loam (SL)	35
MHN	1	71	73	25	2	loamy sand (LS)	73	19	8	sandy loam (SL)	34
MHN	2	2	63	35	2	sandy loam (SL)	65	26	9	sandy loam (SL)	37
MHN	2	2	63	35	2	sandy loam (SL)	65	26	9	sandy loam (SL)	37

Site ID	Pit	Depth (cm)	% Sand	% Silt	% Clay	USDA Texture Class	% Sand	% Silt	% Clay	USDA Texture Class	% Gravel
MHN	2	15	58	37	5	sandy loam (SL)	62	28	11	sandy loam (SL)	34
MHN	2	15	58	37	5	sandy loam (SL)	62	27	11	sandy loam (SL)	34
MHN	2	15	59	39	3	sandy loam (SL)	62	29	9	sandy loam (SL)	34
MHN	2	15	59	39	3	sandy loam (SL)	62	29	9	sandy loam (SL)	34
MHN	2	15	59	39	3	sandy loam (SL)	62	29	9	sandy loam (SL)	34
MHN	2	30	63	35	3	sandy loam (SL)	65	26	9	sandy loam (SL)	26
MHN	2	97	67	30	3	sandy loam (SL)	68	23	9	sandy loam (SL)	32
MHN	3	2	66	32	2	sandy loam (SL)	68	24	8	sandy loam (SL)	32
MHN	3	15	56	39	5	sandy loam (SL)	60	29	11	sandy loam (SL)	34
MHN	3	15	56	39	5	sandy loam (SL)	60	29	11	sandy loam (SL)	34
MHN	3	15	57	40	3	sandy loam (SL)	61	30	9	sandy loam (SL)	34
MHN	3	30	64	33	3	sandy loam (SL)	66	25	9	sandy loam (SL)	39
MHN	3	52	68	29	3	sandy loam (SL)	69	22	9	sandy loam (SL)	29
MHN	4	2	60	38	3	sandy loam (SL)	63	28	9	sandy loam (SL)	26
MHN	4	2	60	38	3	sandy loam (SL)	63	28	9	sandy loam (SL)	26
MHN	4	15	59	39	3	sandy loam (SL)	62	29	9	sandy loam (SL)	29
MHN	4	15	59	39	3	sandy loam (SL)	62	29	9	sandy loam (SL)	29
MHN	4	15	59	39	3	sandy loam (SL)	62	29	9	sandy loam (SL)	29

Site ID	Pit	Depth (cm)	% Sand	% Silt	% Clay	USDA Texture Class	% Sand	% Silt	% Clay	USDA Texture Class	% Gravel
MHN	4	15	58	37	5	sandy loam (SL)	61	28	11	sandy loam (SL)	29
MHN	4	15	58	37	5	sandy loam (SL)	62	27	11	sandy loam (SL)	29
MHN	4	30	66	31	3	sandy loam (SL)	68	23	9	sandy loam (SL)	29
MHN	4	74	65	32	3	sandy loam (SL)	66	24	9	sandy loam (SL)	40
MHS	1	2	88	11	1	sand (S)	84	9	7	loamy sand (LS)	26
MHS	1	2	89	11	1	sand (S)	84	9	7	loamy sand (LS)	26
MHS	1	15	85	14	1	loamy sand (LS)	81	11	7	loamy sand (LS)	14
MHS	1	15	85	14	1	sand (S)	81	11	7	loamy sand (LS)	14
MHS	1	15	84	15	1	loamy sand (LS)	81	12	7	loamy sand (LS)	14
MHS	1	15	84	15	1	loamy sand (LS)	81	12	7	loamy sand (LS)	14
MHS	1	15	84	15	1	loamy sand (LS)	81	12	7	loamy sand (LS)	14
MHS	1	30	84	16	1	loamy sand (LS)	80	13	7	loamy sand (LS)	21
MHS	1	30	83	16	1	loamy sand (LS)	80	13	7	loamy sand (LS)	21
MHS	1	30	84	15	1	loamy sand (LS)	80	13	7	loamy sand (LS)	21
MHS	1	70	82	17	1	loamy sand (LS)	79	14	8	loamy sand (LS)	25
MHS	1	70	82	17	1	loamy sand (LS)	79	14	8	loamy sand (LS)	25
MHS	2	2	87	12	1	sand (S)	82	10	7	loamy sand (LS)	18
MHS	2	15	87	13	1	sand (S)	82	11	7	loamy sand (LS)	21

Site ID	Pit	Depth (cm)	% Sand	% Silt	% Clay	USDA Texture Class	% Sand	% Silt	% Clay	USDA Texture Class	% Gravel
MHS	2	15	86	13	1	sand (S)	82	11	7	loamy sand (LS)	21
MHS	2	15	85	14	1	sand (S)	81	11	7	loamy sand (LS)	21
MHS	2	15	86	14	1	sand (S)	81	11	7	loamy sand (LS)	21
MHS	2	15	86	14	1	sand (S)	82	11	7	loamy sand (LS)	21
MHS	2	30	86	13	1	sand (S)	82	11	7	loamy sand (LS)	24
MHS	2	30	86	13	1	sand (S)	82	11	7	loamy sand (LS)	24
MHS	2	59	86	13	1	sand (S)	82	11	7	loamy sand (LS)	22
MHS	3	2	86	13	1	sand (S)	82	11	7	loamy sand (LS)	20
MHS	3	2	86	13	1	sand (S)	82	11	7	loamy sand (LS)	20
MHS	3	2	86	13	1	sand (S)	82	11	7	loamy sand (LS)	20
MHS	3	15	85	14	1	loamy sand (LS)	81	12	7	loamy sand (LS)	19
MHS	3	15	85	14	1	loamy sand (LS)	81	12	7	loamy sand (LS)	19
MHS	3	30	85	14	1	loamy sand (LS)	81	12	7	loamy sand (LS)	24
MHS	3	30	85	14	1	loamy sand (LS)	81	12	7	loamy sand (LS)	24
MHS	3	60	85	14	1	loamy sand (LS)	81	12	7	loamy sand (LS)	19
MHS	3	60	85	14	1	loamy sand (LS)	81	12	7	loamy sand (LS)	19
MHS	4	2	87	13	1	sand (S)	82	10	7	loamy sand (LS)	21
MHS	4	2	87	13	1	sand (S)	82	10	7	loamy sand (LS)	21

Site ID	Pit	Depth (cm)	% Sand	% Silt	% Clay	USDA Texture Class	% Sand	% Silt	% Clay	USDA Texture Class	% Gravel
MHS	4	15	86	13	1	sand (S)	82	11	7	loamy sand (LS)	21
MHS	4	15	87	13	1	sand (S)	82	11	7	loamy sand (LS)	21
MHS	4	30	87	13	1	sand (S)	82	11	7	loamy sand (LS)	22
MHS	4	30	86	13	1	sand (S)	82	11	7	loamy sand (LS)	22
MHS	4	60	87	12	1	sand (S)	83	10	7	loamy sand (LS)	29
MHS	4	60	87	12	1	sand (S)	83	10	7	loamy sand (LS)	29
MLN	1	30	64	33	3	sandy loam (SL)	66	25	9	sandy loam (SL)	21
MLN	1	84	72	26	2	sandy loam (SL)	72	20	8	sandy loam (SL)	68
MLN	2	2	72	26	1	loamy sand (LS)	72	20	8	sandy loam (SL)	23
MLN	2	2	72	26	1	loamy sand (LS)	72	20	8	sandy loam (SL)	23
MLN	2	15	67	31	2	sandy loam (SL)	68	24	8	sandy loam (SL)	26
MLN	2	30	67	31	2	sandy loam (SL)	68	23	8	sandy loam (SL)	26
MLN	2	89	66	32	3	sandy loam (SL)	67	24	9	sandy loam (SL)	26
MLN	3	2	68	30	1	sandy loam (SL)	69	23	8	sandy loam (SL)	20
MLN	3	2	68	30	1	sandy loam (SL)	69	23	8	sandy loam (SL)	20
MLN	3	15	65	33	2	sandy loam (SL)	67	25	9	sandy loam (SL)	27
MLN	3	30	65	33	2	sandy loam (SL)	66	25	9	sandy loam (SL)	27

Site ID	Pit	Depth(cm)	% Sand	% Silt	% Clay	USDA Texture Class	% Sand	% Silt	% Clay	USDA Texture Class	% Gravel
MLN	3	61	73	25	2	loamy sand (LS)	73	19	8	sandy loam (SL)	58
MLN	4	2	71	27	1	loamy sand (LS)	71	21	8	sandy loam (SL)	22
MLN	4	2	71	27	1	loamy sand (LS)	71	21	8	sandy loam (SL)	22
MLN	4	15	66	32	2	sandy loam (SL)	67	24	8	sandy loam (SL)	18
MLN	4	30	65	33	3	sandy loam (SL)	66	25	9	sandy loam (SL)	19
MLN	4	71	80	19	1	loamy sand (LS)	78	15	8	sandy loam (SL)	39
MLS	1	2	83	16	1	loamy sand (LS)	80	13	7	loamy sand (LS)	19
MLS	1	2	83	16	1	loamy sand (LS)	80	13	7	loamy sand (LS)	19
MLS	1	15	81	18	1	loamy sand (LS)	78	14	8	loamy sand (LS)	18
MLS	1	30	77	21	2	loamy sand (LS)	76	16	8	sandy loam (SL)	23
MLS	2	2	84	15	1	loamy sand (LS)	80	12	7	loamy sand (LS)	20
MLS	2	2	84	15	1	loamy sand (LS)	80	12	7	loamy sand (LS)	20
MLS	2	15	83	16	1	loamy sand (LS)	80	13	7	loamy sand (LS)	21
MLS	2	30	84	15	1	loamy sand (LS)	81	12	8	loamy sand (LS)	23
MLS	3	2	81	18	1	loamy sand (LS)	78	14	8	loamy sand (LS)	21
MLS	3	2	81	18	1	loamy sand (LS)	78	14	8	loamy sand (LS)	21
MLS	3	15	81	18	1	loamy sand (LS)	78	14	8	loamy sand (LS)	24

Site ID	Pit	Depth (cm)	% Sand	% Silt	% Clay	USDA Texture Class	% Sand	% Silt	% Clay	USDA Texture Class	% Gravel
MLS	3	30	78	21	2	loamy sand (LS)	76	16	8	sandy loam (SL)	24
MLS	3	52	79	19	1	loamy sand (LS)	77	15	8	sandy loam (SL)	22
MLS	4	2	81	18	1	loamy sand (LS)	78	14	8	loamy sand (LS)	17
MLS	4	15	77	21	2	loamy sand (LS)	76	16	8	sandy loam (SL)	21
MLS	4	30	84	15	1	loamy sand (LS)	80	12	8	loamy sand (LS)	43

APPENDIX H

Time Series of Soil Moisture and Soil Temperature at 10-minute Sampling Intervals

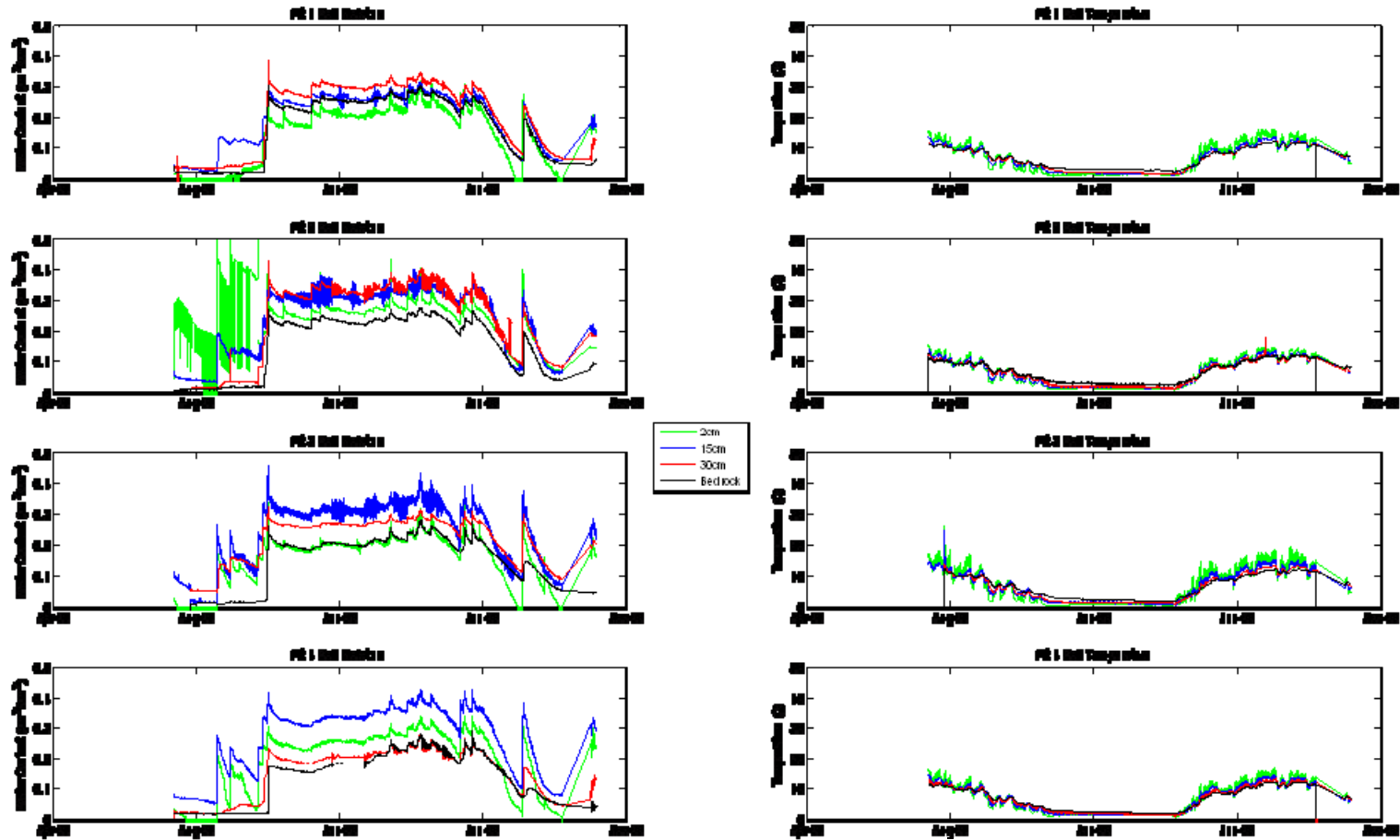


Figure H1. Volumetric water content and temperature of soil for site HN at original 10-minute sampling intervals.

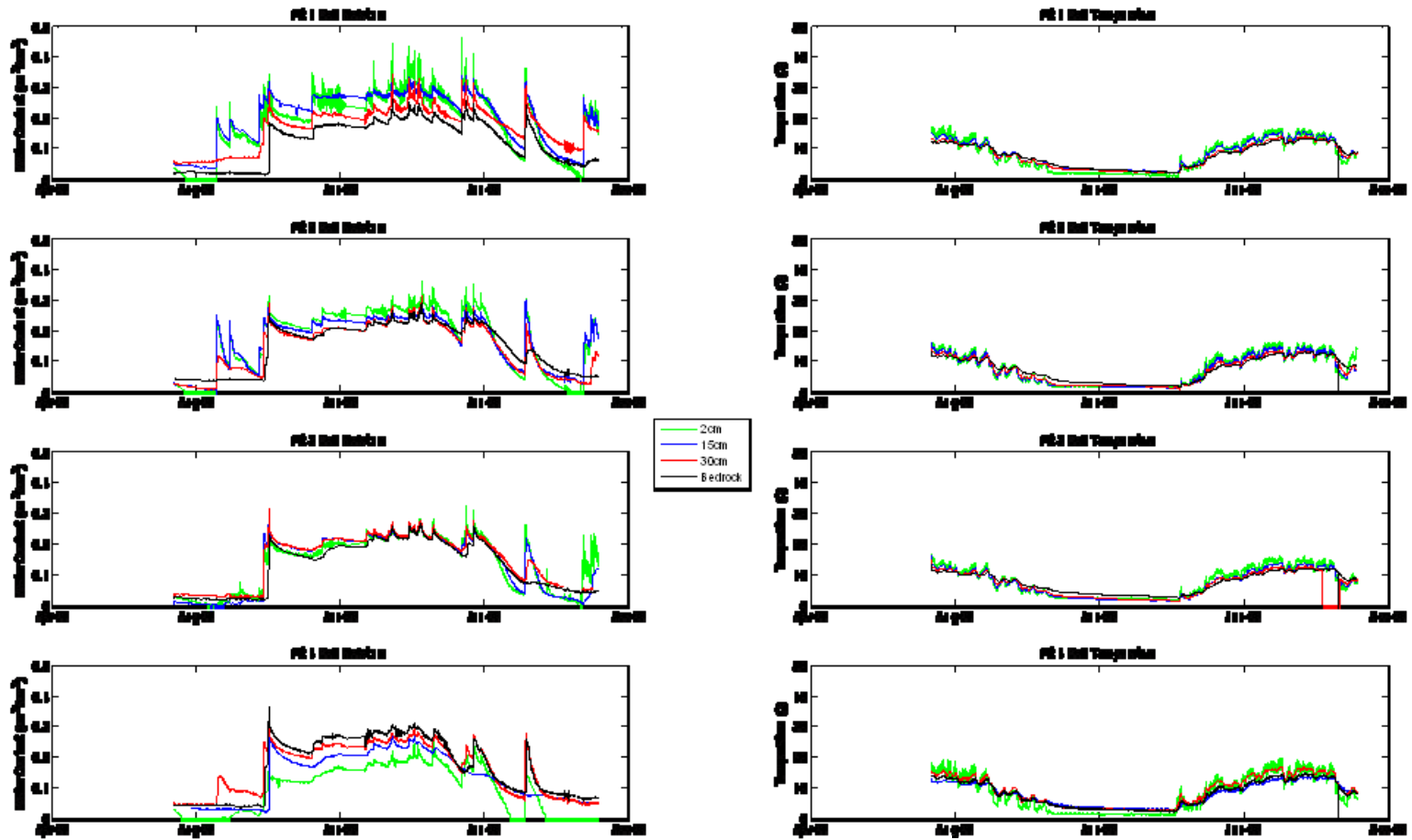


Figure H2. Volumetric water content and temperature of soil for site HS at original 10-minute sampling intervals.

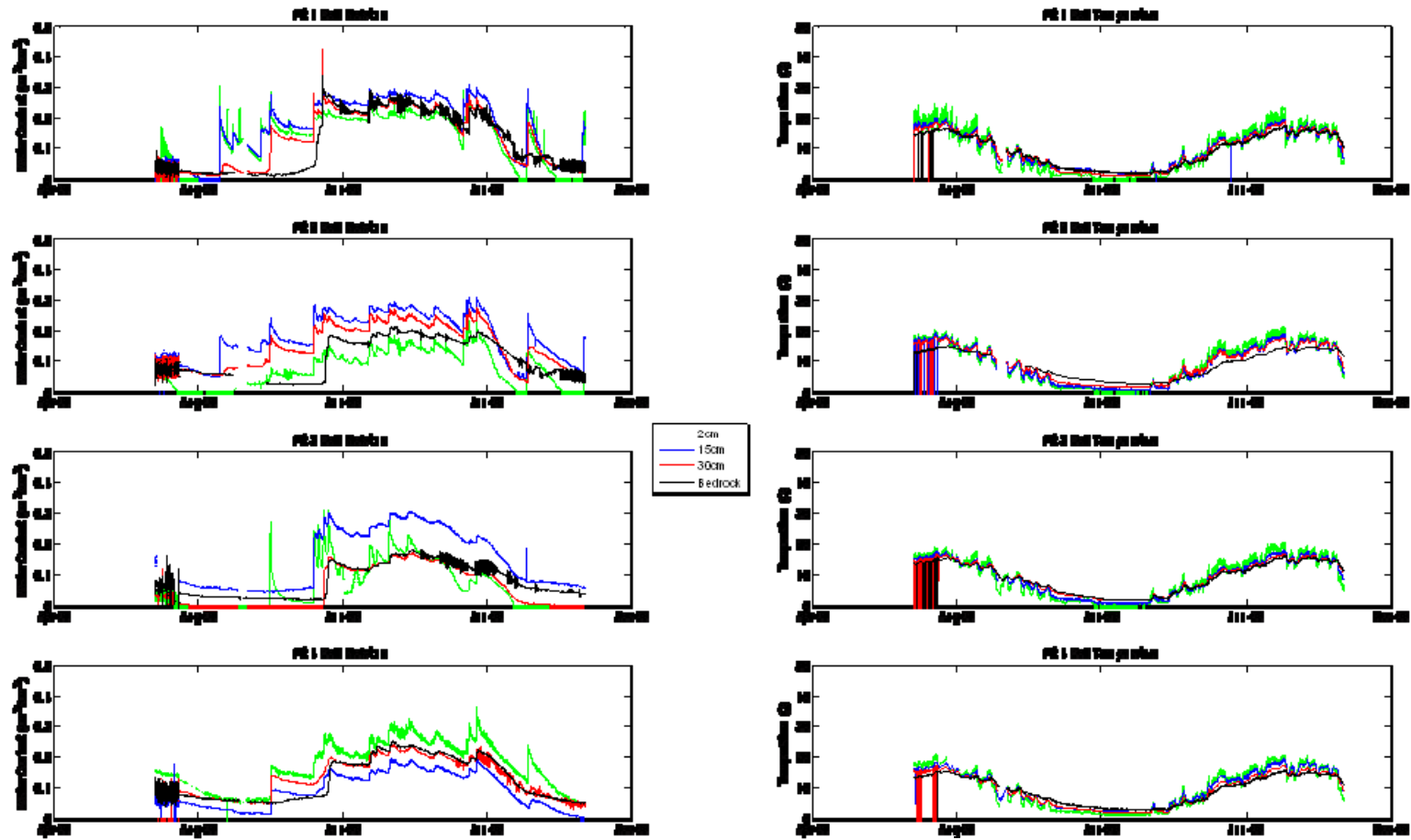


Figure H3. Volumetric water content and temperature of soil for site MHN at original 10-minute sampling intervals.

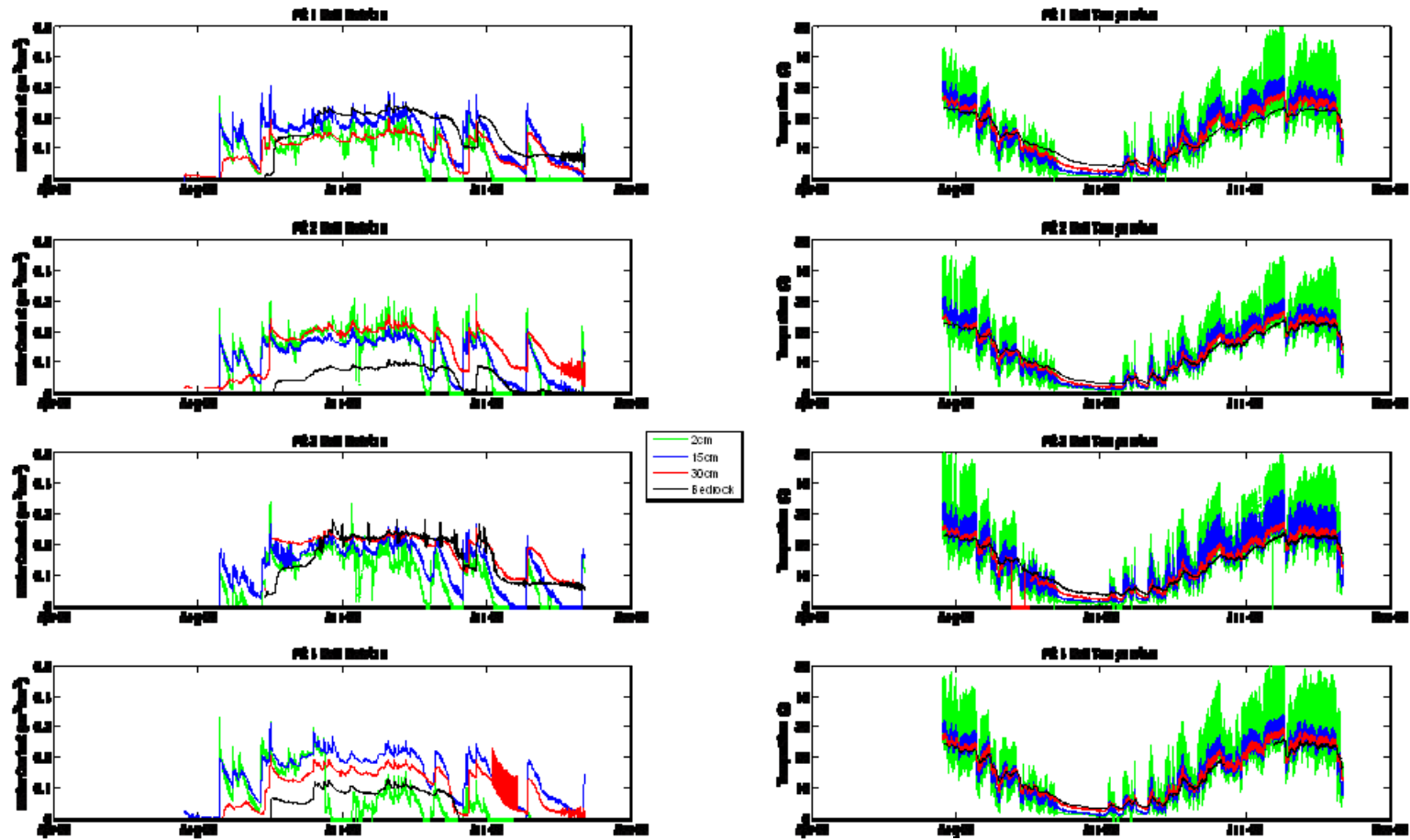


Figure H4. Volumetric water content and temperature of soil for site MHS at original 10-minute sampling intervals.

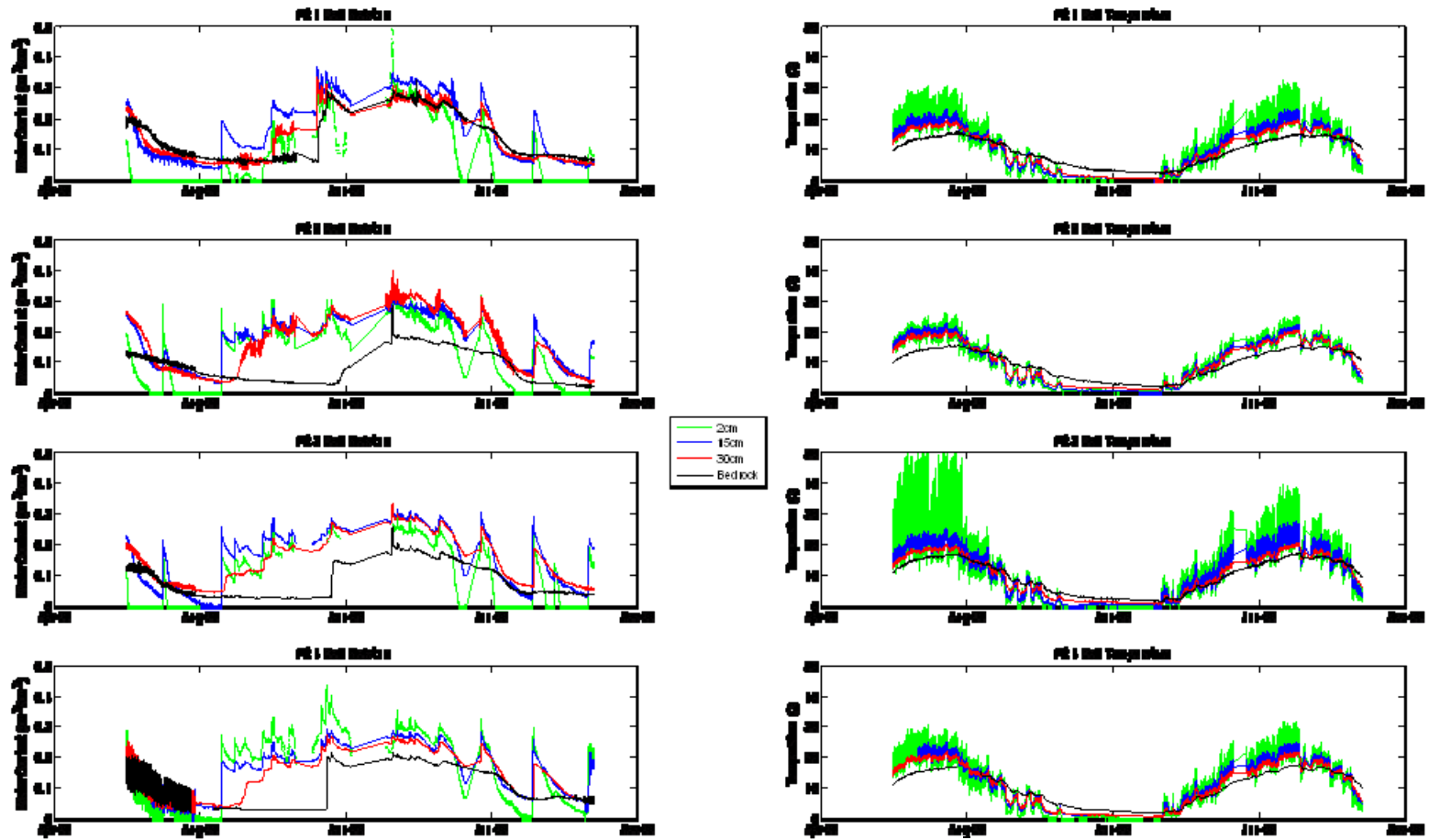


Figure H5. Volumetric water content and temperature of soil for site MLN at original 10-minute sampling intervals.

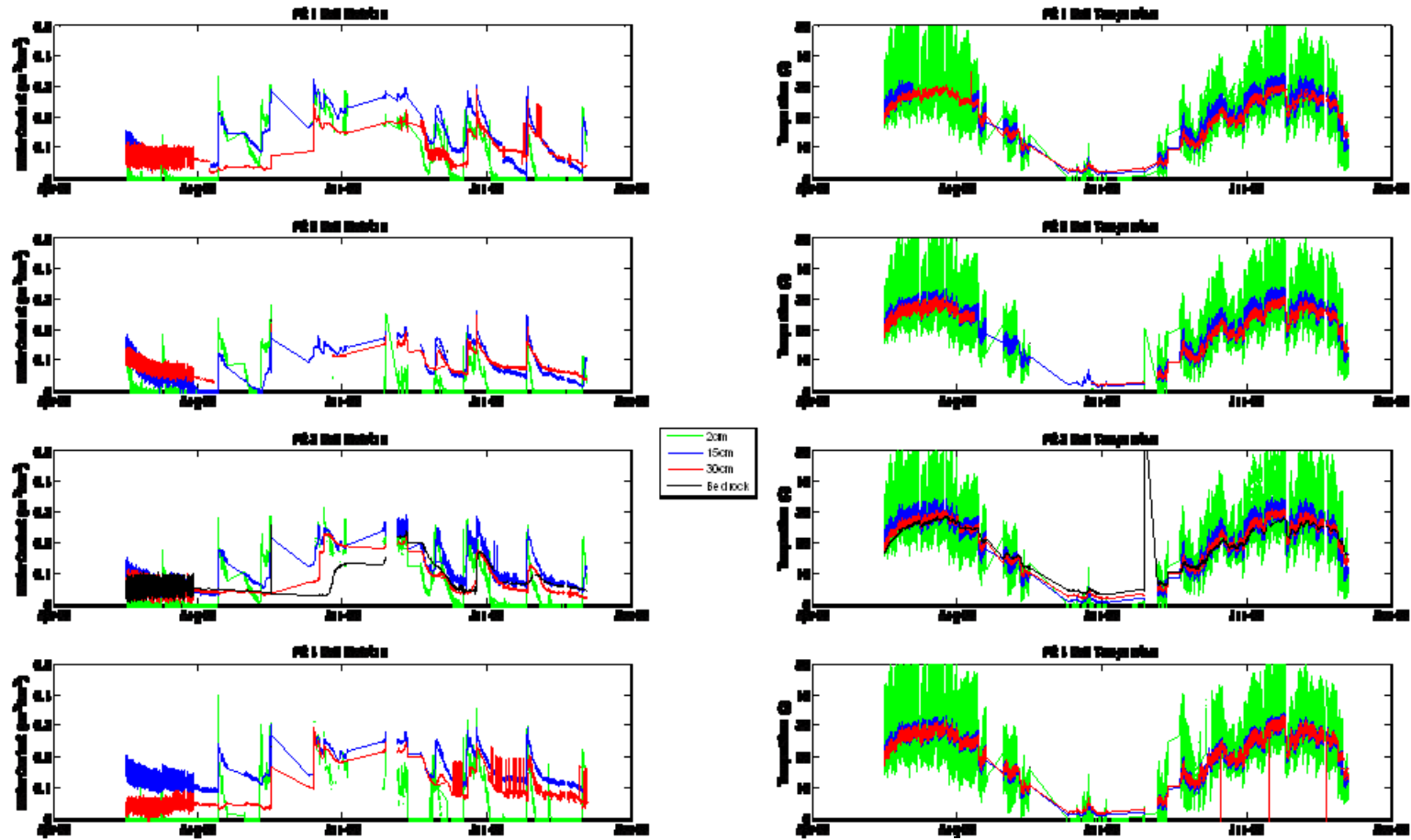


Figure H6. Volumetric water content and temperature of soil for site MLS at original 10-minute sampling intervals.

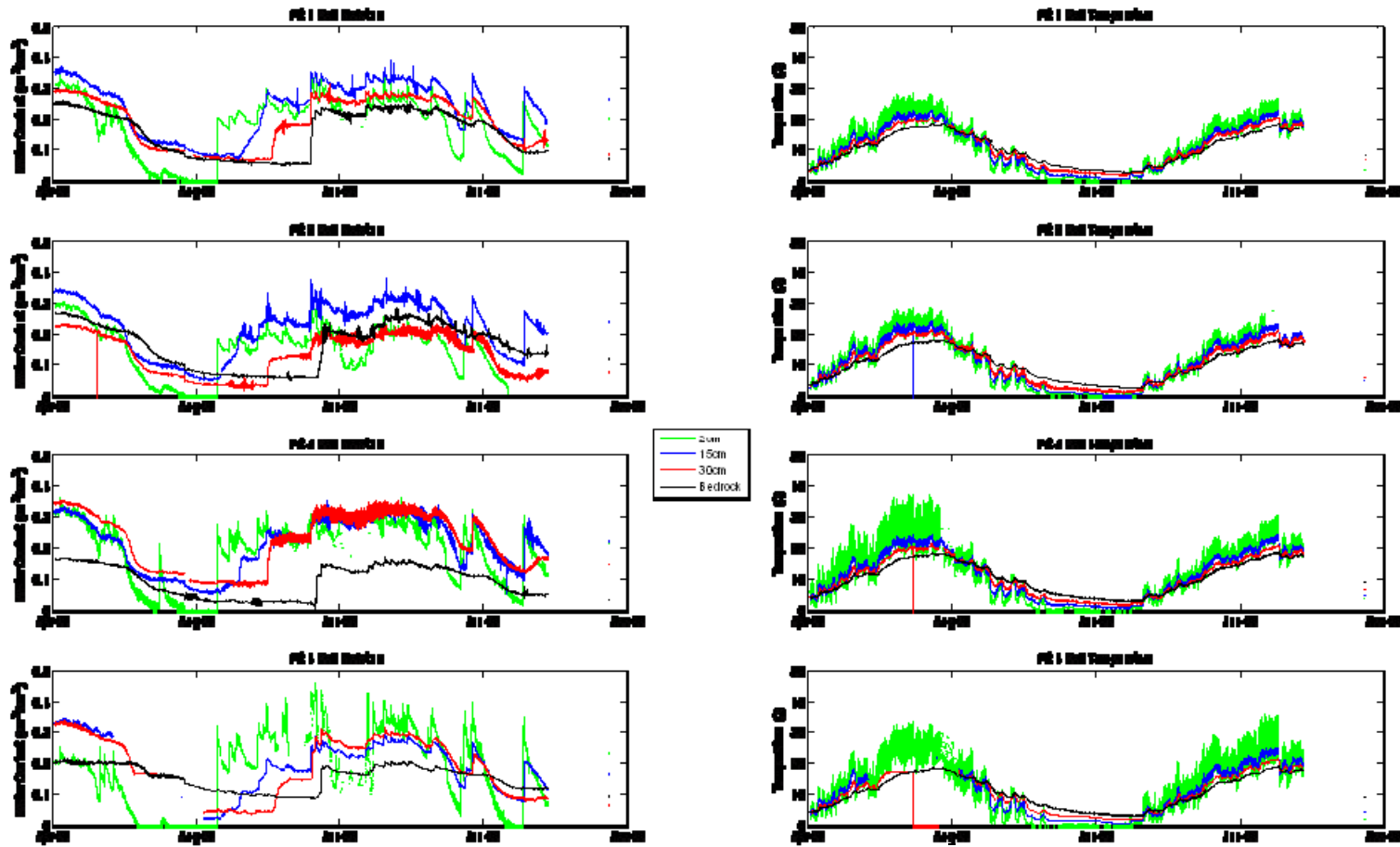


Figure H7. Volumetric water content and temperature of soil for site LN at original 10-minute sampling intervals.

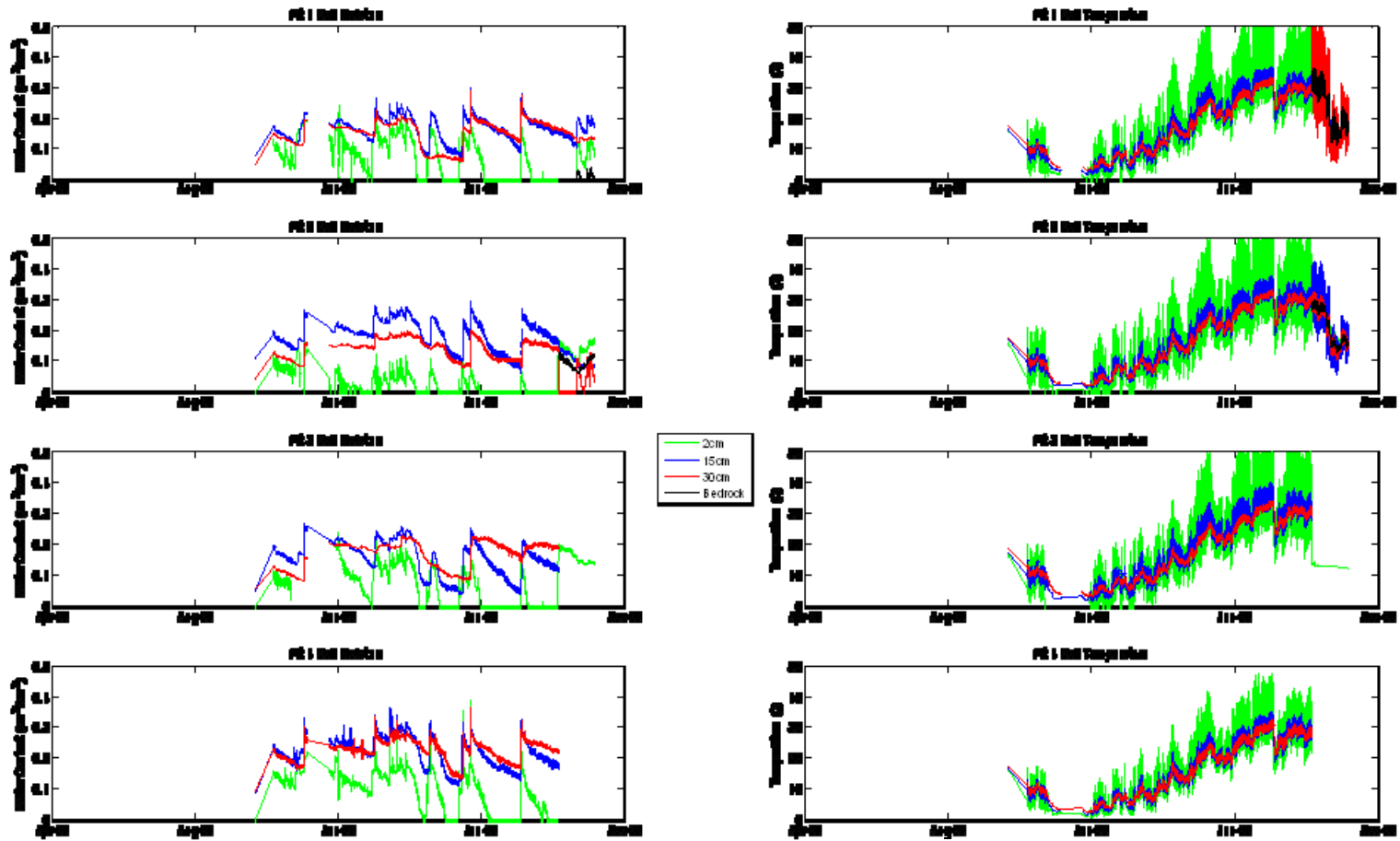


Figure H8. Volumetric water content and temperature of soil for site LS at original 10-minute sampling intervals.

APPENDIX I

Site-by-Site Description of Soil Moisture and Soil Temperature Observations

The following sections detail characteristic trends in soil water and soil temperature at the soil moisture study sites. Descriptions are ordered first by individual site, from the highest elevations to the lowest with north aspect site followed by south aspect site at each elevation. Next, north-south aspect pairs at each elevation are directly contrasted, with comparisons ordered from highest elevation to lowest elevation. Last, observed trends across the elevation gradient at each aspect is reported. Data are tabulated in Table A.7.

HN: High Elevation, North Aspect Site

Site HN represents the highest-elevation, north-facing slope in this study. It is located at an elevation of 1812 m a.s.l., on a slope of approximately 23° and an aspect due directly north. Figure A28 shows the time series of soil water content and soil temperature with timing of precipitation and snow cover at site HN (blue). Table A7 summarizes the dates and values given here. Snow covered the site continuously from 12/5/2008 to 4/20/2009. Mean soil water content at the site over the shared period (the period of record common to all sites, 11/29/2008 to 9/1/2009) was 0.24. The soil profile reached a maximum water content of 0.33 on 4/22/2009. The minimum observed water content was 0.03 on 9/18/2008; a site failure during late summer dry down prevented observation of a real minimum moisture value in 2009. The profile dropped below the

wilting point water content of 0.10 on 7/27/2009. Mean profile-averaged soil temperature over the shared period was 5.3°C, with a maximum of 13.4°C on 8/4/2009 and a minimum of 1.2°C on 4/21/2009. The mean depth of water stored in the soil profile was 15.7 cm, with a minimum storage of 1.9 cm on 9/7/2008 and a maximum of 21.5 cm on 4/22/2009.

Figure A29 shows the differences in soil water content at different depths in the soil profile, along with the field capacity and wilting point water contents at the site. The shallowest (2 cm bgs) and deepest (37-54 cm bgs) were generally the driest portions of the profile, while the 15 and 30 cm depths tended to be the wettest. Mean standard deviation over the profile was 0.04 for water content and 0.76°C for temperature. The bottom of the profile exceeded the field capacity water content of 0.190 for 225 days during the winter and spring. **The soil-bedrock interface wetted up in mid-November 2008, remained wet through winter, and responded to large rain events in spring and summer.**

HS: High Elevation, South Aspect Site

Site HS represents the highest elevation, south-facing slope in this study. It is located at an elevation of 1835 m a.s.l., on a slope of approximately 25° and an aspect due approximately 13° west of south. Figure A28 shows the time series of soil water content and soil temperature with timing of precipitation and snow cover at site HS (red). Table A7 summarizes the dates and values given here. Snow covered the site

continuously from 12/5/2008 to 4/15/2009. Mean soil water content at the site over the shared period was 0.20. The soil profile reached a maximum water content of 0.27 on 3/21/2009, 4/8/2009, 4/13/2009, and 4/20/2009. The minimum observed water content was 0.02 on 9/14/2008 and 10/3/2009. The profile dropped below the wilting point water content of 0.1 on 7/23/2009. Mean profile-averaged soil temperature over the shared period was 6.3°C, with a maximum of 14.2°C on 8/29/2009 and a minimum of 1.7°C on 4/14/2009. The mean depth of water stored in the soil profile was 14.3 cm, with storage minima of 1.4 cm on 9/14/2008 and 1.5 cm on 10/3/2009, and maximum storage of 19.6 cm on 4/8/2009, 4/13/2009, and 4/20/2009.

Figure A30 shows the differences in soil water content at different depths in the soil profile, along with the field capacity and wilting point water contents at the site. The shallowest (2 cm bgs) and deepest (48-57 cm bgs) were generally the driest portions of the profile, while the 15 and 30 cm depths tended to be the wettest. Mean standard deviation over the profile was 0.01 for water content and 0.66°C for temperature. The bottom of the profile exceeded the field capacity water content of 0.170 for 218 days during the winter and spring. **The soil-bedrock interface wetted up in mid-November 2008, remained wet through winter, and responded to large rain events in spring and summer.**

MHN: Mid-high Elevation, North Aspect Site

Site MHN represents the mid-high elevation, north-facing slope in this study. It is located at an elevation of 1472 m a.s.l., on a slope of approximately 28° and an aspect due approximately 5° east of north. Figure A31 shows the time series of soil water content and soil temperature with timing of precipitation and snow cover at site MHN (blue). Table A7 summarizes the dates and values given here. Snow covered the site intermittently from 12/5/2008 to 4/6/2009. Mean soil water content at the site over shared period was 0.16. The soil profile reached a maximum water content of 0.24 on 3/19/2009, 3/22/2009. The minimum observed water content was 0.03 on 8/24/2008 and 9/30/2009. The profile dropped below the wilting point water content of 0.10 on 7/19/2009. Mean profile-averaged soil temperature over the shared period was 7.2°C, with a maximum of 17.9°C on 8/3/2009 and 8/5/2009, and a minimum of 1.2°C on 3/1/2009. The mean depth of water stored in the soil profile was 14.6 cm, with storage minima of 2.9 cm on 9/18/2008 and 3.0 cm on 10/3/2009, and maximum storage of 21.7 cm on 3/19/2009.

Figure A32 shows the differences in soil water content at different depths in the soil profile, along with field capacity and wilting point water contents at the site. The shallowest (2 cm bgs) and deepest (50-60 cm bgs) were generally the driest portions of the profile, while the 15 and 30 cm depths tended to be the wettest. Mean standard deviation over the profile was 0.03 and 0.96°C. The bottom of the profile exceeded the field capacity water content of 0.165 for 162 days during the winter and spring. **The soil-**

bedrock interface wetted up in January 2008, remained wet through winter, and responded to a large rain event in June. Summer rain (August) did not appear to reach the bottom of the soil profile.

MHS: Mid-high Elevation, South Aspect Site

Site MHS represents the mid-high elevation, south-facing slope in this study. It is located at an elevation of 1457 m a.s.l., on a slope of approximately 33° and an aspect due approximately 10° east of south. Figure A31 shows the time series of soil water content and soil temperature with timing of precipitation and snow cover at site MHS (red). Table A7 summarizes the dates and values given here. Snow covered the site intermittently from 12/11/2008 to 3/13/2009. Mean water content at the site over the shared period was 0.13. The soil profile reached a maximum water content of 0.20 on 3/16/2009. The minimum observed water content was 0.02 on 10/28/2008 and 9/22/2009. The profile dropped below the wilting point water content of 0.06 on 5/27/2009. Mean profile-averaged soil temperature over the shared period was 11.9°C, with a maximum of 28.7°C on 8/4/2009 and a minimum of 1.8°C on 2/13/2009 and 2/15/2009. The mean depth of water stored in the soil profile was 9.8 cm, with storage minima of 1.26 cm on 11/1/2008 and 1.57 cm on 10/2/2009, and maximum storage of 15.6 cm on 3/16/2009.

Figure A33 shows the differences in soil water content at different depths in the soil profile, along with field capacity and wilting point water contents at the site. The shallowest (2 cm bgs) and deepest (71-97 cm bgs) portions of the profile were generally

the driest, while the 15 and 30 cm depths were generally the wettest. The mean standard deviation over the profile was 0.04 water content and 1.8[°] C. The bottom of the soil profile exceeded the field capacity water content of 0.145 for 137 days during the winter and spring. **The soil-bedrock interface wetted up from mid-November through December, remained wet through winter, and responded to a large rain event in June. Summer rain (August) did not appear to reach the bottom of the soil profile.**

MLN: Mid-low Elevation, North Aspect Site

Site MLN represents the mid-low elevation, north-facing slope in this study. It is located at an elevation of 1288 m a.s.l., on a slope of approximately 33° and an aspect due approximately 3° east of north. Figure A34 shows the time series of soil water content and temperature with timing of precipitation and snow cover at site MLN (blue). Table A7 summarizes the dates and values given here. Snow covered the site intermittently from approximately 12/4/2008 to 4/1/2009. Mean soil water content at the site over the shared period was 0.18. The soil profile reached a maximum water content of 0.28 on 3/16/2009. The minimum observed water content was 0.03 on 9/1/2008 and 10/2/2009. The profile dropped below the wilting point water content of 0.1 on 7/7/2009. Mean profile-averaged soil temperature over the shared period was 8.9°C, with a maximum of 20.8°C on 8/3/2009 and a minimum of 0.68°C on 3/16/2009. The mean depth of water stored in the soil profile was 15.4 cm, with storage minima of 2.6 cm on 9/18/2008 and 3.0 cm on 10/3/2009, and maximum storage of 24.8 cm on 3/16/2009.

Figure A35 shows the differences in soil water content at different depths in the soil profile, along with field capacity and wilting point water contents at the site. The shallowest (2 cm bgs) and deepest (61-89 cm bgs) portions of the profile were generally the driest, while the 15 and 30 cm depths were generally the wettest. The mean standard deviation over the profile was 0.05 water content and 1.6°C. The bottom of the profile exceeded the field capacity water content of 0.190 for at least 56 days during winter and spring (data gaps prevent a conclusive total). **The soil-bedrock interface wetted up in late December through January, remained wet through winter, and did not respond to summer rain (August).**

MLS: Mid-low Elevation, South Aspect Site

Site MLS represents the mid-low elevation, south-facing slope in this study. It is located at an elevation of 1298 m a.s.l., on a slope of approximately 25° and an aspect due approximately 2° east of south. Due to a series of malfunctions, the time series at MLS contains several data gaps (from 9/30/2008 to 10/15/2008, 11/14/2008-12/22/2008, 2/2/2009-3/9/2009, 3/14/2009 to 3/24/2009, 4/6/2009 to 4/18/2009, 9/16/2009 to 9/17/2009), therefore the following discussion is based largely on observed data; data gaps were filled by linear interpolation to calculate days of potential deep drainage. Also, the soil profile was only deep enough at only one soil pit to add a sensor below the 30 cm depth, so the deep soil conditions reported here for 52 cm bgs result from only one sensor, rather than a mean of four deep sensors as at most other sites.

Figure A34 shows the time series of soil water content and temperature with timing of precipitation and snow cover at site MLS (red). Table A7 summarizes the dates and values given here. Snow covered the site intermittently from approximately 12/4/2008 to 1/26/2009. Mean profile-averaged soil water content at the site over the shared period was 0.11. The soil profile reached a maximum water content of 0.21 on 4/2/2009. The minimum observed water content was 0.03 on 9/1/2008 and 10/1/2009. The profile dropped below the wilting point water content of 0.06 on 5/22/2009. Mean profile-averaged soil temperature over the shared period was 16.3°C, with a maximum of 31.0°C on 8/3/2009 and a minimum of 1.1°C on 2/1/2009. The mean depth of water stored in the soil profile was 4.2 cm, with storage minima of 0.99 cm on 9/13/2008 and 1.1 cm on 10/3/2009, and maximum storage of 7.9 cm on 4/2/2009.

Figure A36 shows the differences in soil water content at different depths in the soil profile, along with field capacity and wilting point water contents at the site. The shallowest (2 cm bgs) and deepest (52 cm bgs) portions of the profile were typically the driest, while the 15 and 30 cm depths were generally the wettest. The mean standard deviation over the profile was 0.05 water content and 1.6°C. The bottom of the profile exceeded the field capacity water content of 0.16 for at least 48 days during spring (data gaps prevent a conclusive total). **The soil-bedrock interface wetted up in January and responded to large rain events in spring and summer.**

LN: Low Elevation, North Aspect Site

Site LN represents the low elevation, north-facing slope in this study. It is located at an elevation of 1120 m a.s.l., on a slope of approximately 24° and an aspect due approximately 9° east of north. Figure A37 shows the time series of soil water content and soil temperature with timing of precipitation and snow cover at site LN (blue). Table A7 summarizes the dates and values given here. Snow covered the site intermittently from approximately 12/4/2008 to 3/13/2009. Mean soil water content over the shared period was 0.20. The soil profile reached a maximum water content of 0.28 on 3/15/2009. The minimum observed water content was 0.04 on 9/12/2008 (2009 minimum uncertain due to failure). The profile dropped below the wilting point water content of 0.14 on 7/9/2009. Mean profile-averaged soil temperature over the shared period was 9.0°C, with a maximum of 22.0°C on 8/3/2009 and a minimum of 1.1°C on 2/21/2009. The mean depth of water stored in the soil profile was 13.1 cm, with storage minima of 2.95 cm on 9/15/2008 and 5.61 cm on 8/5/2009, and maximum storage of 18.6 cm on 3/16/2009.

Figure A38 shows the differences in soil water content at different depths in the soil profile, along with field capacity and wilting point water contents at the site. The shallowest (2 cm bgs) and deepest (62-64 cm bgs) portions of the profile were generally the driest, while the 15 and 30 cm depths were generally the wettest. The mean standard deviation over the profile was 0.05 water content and 1.6°C. The bottom of the profile exceeded the field capacity water content at of 0.175 for 125 days during winter and spring. **The soil-bedrock interface wetted up in late December through January**

2008, remained wet through winter, and responded slightly to a large rain event in June. Summer rain (August) did not appear to reach the bottom of the profile.

LS: Low Elevation, South Aspect Site

Site LS represents the low elevation south-facing slope in this study. It is located at an elevation of 1139 m a.s.l., on a slope of approximately 27° and an aspect due approximately 8° west of south. Figure A37 shows the time series of soil water content and temperature with timing of precipitation and snow cover at site LS (red). Table A7 summarizes the dates and values given here. Snow covered the site continuously from 12/13/2008 to 1/18/2009. Mean soil water content over the shared period was 0.14. The soil profile reached a maximum water content of 0.21 on 4/2/2009. The minimum observed water content was 0.07 on 5/21/2009. Mean profile-averaged soil temperature over the shared period was 16.0°C, with a maximum of 34.6°C on 8/3/2009 and a minimum of 1.4°C on 1/27/2009. The mean depth of water stored in the soil profile was 4.7 cm, with a minimum storage of 2.1 cm on 6/1/2009, and maximum storage of 7.1 cm on 4/3/2009.

Figure A39 shows the differences in soil moisture at different depths in the soil profile, along with field capacity and wilting point water contents at the site. The shallowest (2 cm bgs) and deepest (30 cm bgs) portions of the profile were generally the driest, while the 15 cm depth was generally the wettest. The mean standard deviation over the profile was 0.07 water content and 1.2°C. The bottom of the profile exceeded the

field capacity water content of 0.17 for 175 days during winter, spring, and summer. **The soil-bedrock interface wetted up in December 2008, remained wet through winter, and responded to large rain events in spring and summer.**

Comparing North and South Aspects at the Highest Elevation Sites

The amount and timing of soil water and the soil temperature were all similar during the growing season at both of the highest elevation sites, HN and HS (Figure B.27, Table A.7). A priori means comparisons at the $\alpha = 0.0001$ level demonstrated that soil water storage at the high elevation sites over March through July 2009 did not differ significantly with aspect ($n = 153$ for each site; $F = 8.10$; $p < 0.0045$). Similarly, soil temperature did not differ between sites ($n = 153$ for each site; $F = 0.57$; $p = 0.4513$) (Table A.8). Soil moisture reached higher values slightly later into the spring on the north aspect relative to the south aspect (0.33 on 4/22/2009 versus 0.27 on 3/21/2009-4/20/2009), and soil water content reached higher values on the north aspect (Figure B.27 and Table A.7). Minimum observed moisture was similar on both aspects (0.02 on south aspect, 0.03 on north aspect). Overall, temperature tended to be slightly higher on the south aspect, but profile-averaged temperatures generally differed between the aspects by only around 1°C over the year (Figure B.27).

Daily time series of soil water content at different depths indicate the soil-bedrock interface at both sites wetted up in mid-November 2008, remained wet through winter, and responded to large rain events in spring (June) and summer (August) (Figures B.28

and B.29). Field capacity at the base of the profile was exceeded on 225 days at the north aspect, and on 218 days on the south aspect. **The initiation and duration of growing conditions were very similar at the highest elevation sites.** Water content was slightly higher on the north face during the dry down period, indicating that slightly more water was present later into the growing season on the north aspect than on the south aspect (Figure B.27). Snow disappeared about 5 days earlier on the south aspect than the north. The surface soil temperature warmed above 5°C on the same date at both aspects. The south aspect dried below the wilting point 4 days earlier than the north aspect.

Comparing North and South Aspects at the Mid-High Elevation Sites

At the mid-high elevation sites MLN and MLS, soils on the north aspect were significantly more wet and cool and soil moisture lasted longer during the growing season relative to the south aspect (Figure B.30, Table A.7). A priori means comparisons at the $\alpha = 0.0001$ level showed that over March – July 2009, soil water storage at the mid-high elevation sites was significantly higher ($n = 153$ for each site; $F = 298.14$; $p < 0.0001$) and profile-averaged soil temperature was significantly lower ($n = 153$ for each site; $F = 61.27$; $p < 0.0001$) on the north aspect. Maximum depth- averaged soil water content was higher and occurred at approximately the same time on the north aspect (0.24 on 3/19/2009 and 3/22/2009) relative to the south aspect (0.20 on 3/16/2009). Minimum water content was lower and occurred about 7 days earlier on the south aspect (0.02 on 9/22/2009) relative to the north aspect (0.03 on 9/30/2009). A similar pattern was

observed in the previous dry season, when the south aspect reached minimum water content of 0.00 before the earliest record on 8/16/2008, while the north aspect reached a minimum water content of 0.03 on 8/24/2008. Average annual soil temperature was about 5°C higher on the south aspect than the north, and soil temperature on the south aspect began rising about 45 days earlier than on the north aspect (Figure B.30). Daily time series of soil water content at different depths indicate that the soil-bedrock interface wetted up about 1 month earlier on the north aspect, remained wet through winter, responded to rains in June on both aspects, and did not respond to August rains on either aspect (Figures B.31 and B.32). Field capacity at the base of the profile was exceeded on 162 days at the north aspect, and on 137 days on the south aspect.

Growing conditions initiated earlier on the south aspect, but lasted longer into the growing season on the north aspect, resulting in a longer growing season on the north aspect. Snow disappeared 24 days earlier on the south aspect than on the north. The surface soil temperature warmed above 5°C 28 days earlier on the south aspect. Water content was higher on the north aspect during the dry down period, indicating that more water was present later into the growing season on the north aspect. The north aspect remained above the wilting point for 53 days longer into the growing season than the south aspect.

Comparing North and South Aspects at Mid-Low Elevation Sites

At the mid-low elevation sites MLN and MLS, north-facing soils were significantly more wet and cool and soil moisture lasted longer during the growing season relative to the south aspect (Figure B.33, Table A.7). A priori means comparisons at the $\alpha = 0.0001$ level revealed that soil water storage over March through July 2009 was significantly higher ($n = 153$ for each site; $F = 748.38$; $p < 0.0001$), and profile-averaged soil temperature was significantly lower ($n = 153$ for each site; $F = 55.89$; $p < 0.0001$) on the north aspect. Although data gaps prevent comparison of the timing of maximum moisture, the maximum moisture value observed on the south aspect was lower (0.21) than on the north (0.28). The minimum water content of 0.03 was reached almost simultaneously on both aspects. Average annual soil temperature was about 7°C higher on the south aspect than on the north. Daily time series of soil water content at different depths indicate that the soil-bedrock interface wetted up very slightly earlier on the north aspect, responded to rains in June on both aspects, and responded to August rains only on the south aspect (Figures B.34 and B.35). Data gaps prevented determination of the number of days field capacity was exceeded at the base of the profile.

Growing conditions initiated slightly earlier on the south aspect, and lasted longer into the summer on the north aspect, resulting in a longer growing season on the north aspect. Soil water content was higher on the north aspect relative to the south aspect (Figure B.33) during the dry down period. Snow disappeared about 66 days earlier on the south aspect than on the north. Surface soils warmed above 5°C three days earlier

on the south aspect than on the north. The north aspect remained above the wilting point for 46 days longer into the growing season than the south aspect.

Comparing North and South Aspects at the Lowest Elevation Sites

At the lowest elevation sites LN and LS, north-facing soils were significantly more wet and cool and soil moisture lasted longer during the growing season relative to the south aspect (Figure B.36, Table A.7). A priori means comparisons at the $\alpha = 0.0001$ level revealed that soil water storage over March through July 2009 showed that soil water storage was significantly higher ($n = 153$ for each site; $F = 444.48$; $p < 0.0001$), and profile-averaged soil temperature was significantly lower ($n = 153$ for each site; $F = 97.13$; $p < 0.0001$) on the north aspect. Maximum soil moisture was higher and occurred 18 days earlier on the north aspect (0.28 on 3/15/2009) than on the south aspect (0.21 on 4/2/2009). Minimum moisture on the south aspect was lower and occurred 60 days earlier (0.06 on 6/1/2009) than the minimum moisture on the north aspect (0.08 on 7/31/2009). Mean soil temperature is 7°C warmer on the south aspect. Soil temperature became increasingly different on north and south aspects as the summer progressed, with south aspect increasing from 0 to 13°C warmer than the north aspect between late January and late August. Daily time series of soil water content at different depths indicate that the soil-bedrock interface wetted up very slightly earlier on the south aspect, remained wet through winter, responded to rains in June on both aspects, and responded to August rains

only on the south aspect (Figures B.37 and B.38). Field capacity was exceeded at the base of the soil profile for 125 days on the north aspect and for 175 days on the south aspect.

Growing conditions initiated earlier on the south aspect, but lasted longer into the growing season on the north aspect, resulting in a longer growing season on the north aspect. Moisture was almost consistently lower on the south aspect from January in to summer, indicating that more soil water was present later into the growing season on the north aspect than on the south. One exception occurred when the heavy (37 mm) summer storm on August 7, 2009 wetted the soils sufficiently that the south aspect became temporarily more wet than the north, after which the south aspect moisture declined more steeply, again becoming the drier slope. Snow left the south aspect 55 days earlier than the north aspect. Surface soils warmed to 5°C 27 days earlier on the south aspect than on the north. The north aspect remained above the wilting point water content for 49 days longer into the growing season than the south aspect.

Comparing Sites Over the Elevation Gradient

Soil moisture shows a weak relationship with elevation, while soil temperature shows a consistent relationship with elevation. Figure B.39 shows the mean soil water content and soil temperature plotted against elevation for north and south aspects, with a trend line fitted to each group. The low coefficient of determination ($R^2 = 0.42$) and low slope on the north aspects are evidence of a weak relationship between elevation and soil moisture; on the south aspects, the R^2 value (0.69) and slope are

somewhat higher. In contrast, soil temperature shows a consistently strong negative relationship with elevation at both aspects ($R^2 = 0.99$ and 1.00), but the greater slope of the trend line fitting south aspect sites indicates a greater effect of elevation on soil temperature compared to the north aspects. In Figure B.40, the mean values of soil water storage over March through July 2009 have been plotted against elevation. Soil water storage accounts for the different soil depths at different sites; except for the highest elevation sites, soil depth increases with increasing elevation (Figure B.24). Soil water storage shows a stronger relationship with elevation on south aspects than did soil water content, although the relationship is still weak on the north aspects. When north-south aspect pairs at each elevation are grouped, a priori means comparisons indicate that soil water storage and soil temperature differ significantly at the highest elevation sites versus the mid-high elevation sites ($n = 153$ for each site; $F = 88.76$; $p < 0.0001$), and at the mid low elevation sites versus the lowest elevation sites ($n = 153$ for each site; $F = 16.25$; $p < 0.0001$). The length of the potential growing season increases consistently with decreasing elevations on north aspects, and does not relate consistently with elevation on the south aspects.